CHEMICAL REVIEWS

REVIEW

pubs.acs.org/CR

Update 1 of: Mass Accommodation and Chemical Reactions at Gas−Liquid Interfaces

Paul Davidovits*

Chemistry Department, 2609 Beacon Street, Boston College, Chestnut Hill, Massachusetts 02467, United States

Charles E. Kolb, Leah R. Williams, John T. Jayne, and Douglas R. Worsnop

Center for Aerosol and Cloud Chemistry, Aerodyne Research, Inc., 45 Manning Road, Billerica, Massachusetts 01821, United States

This is a *Chemical Reviews* Perennial Review. The root paper of this title was published in *Chem. Rev.* **2006**, *106* (4), 1323−1354, DOI: 10.1021.cr040366k; Published (Web) March 16, 2006. Updates to the text appear in red type.

CONTENTS

1. INTRODUCTION

Interactions between gas-phase molecules and liquids play an important role in a wide range of natural and industrial processes. In photosynthesis, gas-phase CO_2 diffuses into the aqueous medium within the cell to begin the transformations to carbohydrates. Respiration entails transfer of air, in this case through

Received: October 27, 2010

surfactants on thin films of water. A wide range of industrial processes likewise depend on transfer of gases into liquids, followed by chemical reactions. For example, in the manufacture of $BaCO_3$, CO_2 is absorbed into an aqueous solution of barium sulfide with subsequent reaction to yield the desired product. Much of the current experimental and theoretical work on gas−liquid heterogeneous interactions is also motivated by their importance in the atmosphere, where such processes play a central role in acid deposition, stratospheric ozone depletion, photochemical smog formation, aerosol-induced haze, and regional climate change (see, for example, ref 1).

Although the amount of condensed phase in the atmosphere is small, the collision rate of gas-phase pollutants with atmospheric condensed-phase particles can be relatively rapid. In polluted urban air, where the condensed-phase volume ratio may be typically 10^{-11} with particle diameter on the average about 0.2 μm, the collision rate is about 10^{-2} s^{-1}. That is, under such polluted conditions, within a few minutes, every gas molecule undergoes a collision with an aerosol particle. In cleaner air, the collision time is, of course, correspondingly longer. In tropospheric clouds where the droplet-to-air volume ratio is about 10^{-7} and the diameter of the droplets is about 5 μm the collision time is about 1 s. Processing of gases within clouds can be very efficient depending on the gas uptake rate.

The collision of the gas molecule with the liquid surface is only the first step in a heterogeneous interaction. The outcome of a collision between a gas molecule and a liquid is a transformation of the gas-phase species that may include incorporation of the species into the condensed phase, formation of a surface complex, and reaction at the aerosol surface or in the solvated phase. The product molecule may return into the gas phase or stay in the condensed phase. The kinetics of such transformations determine their importance in atmospheric processes.

Both gas-phase and liquid-phase chemical kinetics have been studied in their separated states for over a century. A validated theoretical framework for homogeneous reactions has been formulated, and extensive databases of kinetic parameters are available.[2,3] However, the study of the two phases in interaction with each other is relatively recent and not nearly as well developed. Such heterogeneous studies are significantly more complex both theoretically and experimentally.

In the 1950s, Danckwerts presented analytical expressions describing uptake of gas-phase species by liquids in terms of measurable parameters.[4] These expressions, based on earlier equations of heat conduction, include the effect of Henry's law solubility on gas uptake, liquid-phase reactions of the solvated molecules, and the mass accommodation coefficient α (defined as the probability that a molecule striking the liquid surface enters the liquid). The Danckwerts equations serve as the foundation for the resistor model that decouples the factors affecting gas−liquid interactions and allows inclusion of effects that cannot be incorporated into the standard analytical formulation. The resistor model allows one to calculate easily the overall uptake coefficient (probability) and the rate for the transformative gas−liquid collisions.

The experimental side of the gas−liquid interaction studies lagged significantly behind the mathematical formulations. In a well-known chemical engineering text published in 1975, Sherwood et al. state: "Not only is there no useful theory to employ in predicting α, there is no way to experimentally measure it."[5] The situation had not changed for another 10 years except that the need in atmospheric chemistry for kinetic parameters governing heterogeneous gas−liquid interactions became more evident. In a 1984 publication, Chameides calculated the role of SO_2 oxidation in clouds.[6] In this calculation, α is a key parameter and Chameides had to treat it as a variable in the range 10^{-6} to 1. He concluded: "...until controlled laboratory experiments are carried out to measure α, for the species of importance to S_{IV} oxidation, the exact values of these parameters will remain uncertain thus implying an uncertainty in our understanding of the rate at which SO_2 is oxidized in clouds."

The following 20 years were a period of increased activity in the study of heterogeneous gas−liquid interactions. A range of experimental laboratory techniques was developed that collectively allows measurement of uptake coefficients ranging over 7 orders of magnitude. The experiments yielded kinetics parameters for a large number of reactive and nonreactive gas−liquid interactions. Many of these results have been used in the modeling of atmospheric processes.

The kinetics studies revealed unexpected features of gas−liquid interactions. Interesting patterns were observed in the measured values of α that could not be explained by earlier views of the process. In several cases, enhanced reactivity was observed at the gas−liquid interface, indicating the presence of surface complexes, and in salt solutions, enhanced anion concentration was observed at the interface. These observations motivated molecular simulation studies of the interface and phenomenological treatments of the mass accommodation process. The kinetics studies together with molecular simulations, molecular beam experiments, and surface spectroscopic studies are providing an increasingly detailed and accurate molecular-level understanding of gas−liquid interfaces.[7−12]

Several review articles have been written on heterogeneous gas−liquid interactions.[7−9,11,13] The present review focuses on the kinetics of interactions at aqueous interfaces. It summarizes previously reviewed work and stresses results not included in the earlier reviews. Equilibrium thermodynamic aspects of gas−liquid interactions, such as solubility, are treated in detail in a recent text edited by Fogg and Sangster,[10] and are excluded from this review. Likewise excluded are interactions with large water surfaces such as lakes and oceans that are governed by convective and turbulent transport. (For a detailed treatment of this subject, see ref 14.) Organic surfaces that have more recently become an important field of study (see, for example, ref 15) are not in the scope of the present article. We will, however, discuss the uptake of gas-phase hydrogen halides on ethylene glycol and on octanol, where adsorbed water was found to have a significant effect on the mass accommodation of the gas-phase species.

Two highly relevant new reviews on the uptake of gas phase species have been published recently: one by Kolb et al.[13b] and a data evaluation sponsored by NASA.[13c] The article by Kolb et al. has its origin in a workshop focused on atmospherically important interactions of trace gases with aerosols and clouds. The review presents a detailed survey of the field and provides a thorough coverage of the literature up to 2010. The NASA publication is focused on heterogeneous chemistry important in the stratosphere and upper troposphere. The report, completed in 2006, is currently posted on the Web. The 2010 update will be posted in the near future.

In section 2, we review the basic phenomena governing interactions of gases with liquids and present the resistor model for gas−liquid interactions. Experimental techniques for the study of gas−liquid interactions are described in section 3. Results of experiments with both reactive and nonreactive gas-phase species are presented in section4. Phenomenological treatments of mass accommodation are briefly described in section 5. In section

6, molecular simulations of interfacial processes related to experimentally observed mass accommodation results are briefly discussed. More detailed discussions of molecular simulations are presented in other articles found in the Structure and Chemistry at Aqueous Interfaces thematic issue of *Chemical Reviews* (issue 4 of 2006). Specifically, the review by Garrett et al.[15b] discusses the relationship between experimental results and molecular simulations from the viewpoint of computational scientists. Section 7 contains some concluding remarks.

2. FORMULATION OF THE GAS UPTAKE PROCESS

The uptake of gases by surfaces is a complex interaction that is governed by gas- and condensed-phase parameters and processes. In this article, we will consider the interaction of a trace gas species (i.e., present as a small fraction of the total gas-phase concentration) with a liquid surface. Figure 1 shows a schematic of the various processes that may influence uptake: (1) diffusion of the trace species through the gas phase to the surface, (2) adsorption and desorption at the surface, (3) reaction at the surface, (4) solvation of the trace species and incorporation into the bulk liquid, (5) diffusion of the trace species in the bulk liquid, and (6) reaction in the bulk liquid. Some of these factors may not play a role in the uptake of a given species.

From an atmospheric modeling perspective, the quantities of interest are the gas- and condensed-phase concentrations of the trace species and reaction products, if any. These concentrations are described by a set of coupled differential equations that incorporate the various diffusion, collision, and reaction pathways, with appropriate boundary conditions at the interface. Analytical solutions exist for a few limited cases,[16] but, in general, the coupled differential equations must be solved numerically.

An alternative formulation initially developed by Schwartz and co-workers,[17] called the resistor model, uses steady-state solutions that decouple the differential equations for each process.[17,18] Each process is formulated in terms of a resistance which is the inverse of an uptake coefficient (defined as the heterogeneous rate for the process normalized to the rate of gas/surface collisions). The utility of the resistor model is that the various processes may be combined in series or in parallel to obtain the rate of the overall heterogeneous process, by analogy to electrical circuits. (See ref 7 for more details on the analogy.) The resistor model has been shown to provide a good approximation (within a few percent) to the numerical solution of the coupled differential equations.[19,20]

The interaction of gases with liquids is described by a net uptake coefficient, γ, in which the mass-transfer rate of molecules to the condensed phase is normalized to the gas kinetic collision rate with the surface:

$$\gamma = \frac{4J}{n_g \bar{c}} \tag{1}$$

where J (cm^{-2} s^{-1}) is the flux into the condensed phase, n_g (cm^{-3}) is the concentration of gas-phase molecules far from the surface, and c (cm s^{-1}) is the average molecular speed. The uptake coefficient is the probability that the gas-phase molecule will be taken up by the liquid. The uptake can be limited by gas-phase diffusion and solubility constraints or enhanced by chemical reaction, as described below in sections 2.1 and 2.2. In experiments subject to these effects, the measured flux into the surface is expressed in terms of a measured uptake coefficient, γ_{meas}. Experimental conditions may be quite different from typical atmospheric conditions, and experimentally measured uptake coefficients may have to be corrected when used in atmospheric models. The following sections outline a kinetic model for gas uptake by liquids and describe each of the decoupled processes in the resistor model for γ.

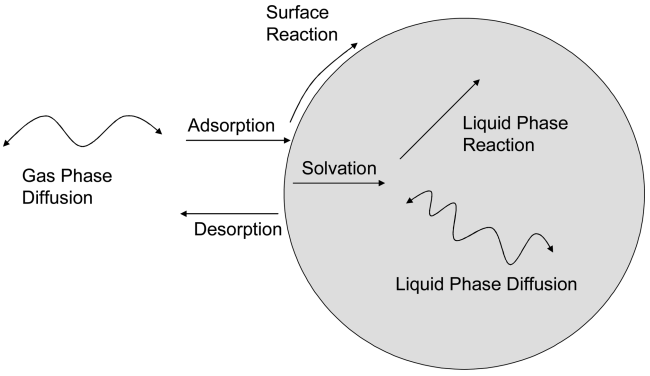

Figure 1. Schematic of transport and reactive processes which determine the net uptake in gas−liquid interactions.

2.1. Case 1. Nonreactive Gas Uptake

In the case of a nonreactive gas interacting with a liquid droplet, the overall flux of gas into the liquid is determined by transport of the trace gas molecules through the gas phase to the surface, the relative rates of adsorption and desorption at the surface, and the rates of transfer of trace molecules into the bulk of the liquid and back to the surface. The kinetic scheme describing these interactions is

$$G \underset{k_{des}}{\overset{k_{ads}}{\rightleftharpoons}} S \underset{k_{l_{to}s}}{\overset{k_{sol}}{\rightleftharpoons}} L \tag{2}$$

where G is the gas-phase molecule, S is the molecule adsorbed to the surface, L is the molecule in the bulk liquid, k_{ads} (cm s^{-1}) is the rate of adsorption, k_{des} (cm s^{-1}) is the rate of desorption, k_{sol} (s^{-1}) is the rate of transfer of molecules from the surface into the bulk liquid (solvation), and $k_{l\_to\_s}$ (s^{-1}) is the rate of transfer of molecules from the bulk to the surface.

The gas-phase flux to the surface is determined by the local gas-phase concentration just above the surface and the gas-kinetic collision rate. In situations where the uptake at the surface is high, the gas-phase concentration near the surface can become depleted if diffusion in the gas phase is too slow to replenish the molecules. This in turn limits the gas uptake by the liquid. The gas-phase diffusion limitation is described by the gas transport coefficient, Γ_{diff}. Note that the symbol Γ is used for rates (normalized to collision rates) and can be larger than 1, while the symbol γ is used for probabilities and is always less than or equal to 1.

An empirical formulation of isothermal diffusive transport[21] that is in good agreement with experimental data[22] can be written as the resistance $1/\Gamma_{diff}$[23]

$$\frac{1}{\Gamma_{diff}} = \frac{0.75 + 0.238Kn}{Kn(1 + Kn)} \tag{3}$$

where Kn is the Knudsen number, defined as λ/a, λ (cm) is the gas-phase mean free path, and a (cm) is the radius of the particle. The mean free path is expressed as

$$\lambda = 3D_g/\bar{c} \tag{4}$$

dx.doi.org/10.1021/cr100360b | *Chem. Rev.* 2011, 111, PR76 - PR109

where D_g ($cm^2\ s^{-1}$) is the gas-phase diffusion coefficient of the trace species and c ($cm\ s^{-1}$) is the average molecular speed. For a more detailed discussion of Γ_{diff}, see ref 24.

The inverse of the net uptake coefficient, γ, can now be expressed as the sum of the gas-phase diffusion resistance and the inverse of the uptake coefficient, γ_0, due to gas−liquid interactions in the limit of "zero pressure", i.e., under conditions where gas-phase diffusion does not limit the flux across the interface. That is,

$$\frac{1}{\gamma} = \frac{1}{\Gamma_{diff}} + \frac{1}{\gamma_0} \tag{5}$$

In the atmosphere, for typical submicrometer-sized aerosol particles, gas-phase diffusion does not usually limit uptake coefficients unless the uptake coefficient is large. For example, for 0.1 μm diameter droplets at 1 atm, $Kn = 1.5$ (assuming a gas-phase diffusion coefficient (D_g) of 0.1 atm $cm^2\ s^{-1}$ and $c = 4 \times 10^4$ cm s^{-1}), giving $1/\Gamma_{diff} = 0.3$. If γ_0 is less than 0.1, the gas-phase diffusion contribution is negligible, while if γ_0 is close to 1, γ is reduced by 25%. For larger atmospheric particles, such as cloud droplets, gas-phase diffusion can limit gas uptake.

In many laboratory experiments, conditions are such that gas-phase diffusion limitations need to be taken into account when analyzing experimental uptake data. For example, in the droplet train reactor experiment discussed below in section 3.1, droplets are on the order of 100 μm in diameter and the total pressure is 5 Torr. For these conditions, $Kn = 0.23$ and a γ_0 of 0.01 is reduced by 3%, while a γ_0 of 1 is reduced by 75%.

Mass accommodation occurs when a gas molecule strikes the liquid surface and enters the liquid. The mass accommodation coefficient, α, is the probability that a molecule that strikes the liquid surface enters the bulk liquid. As such, in the absence of chemical reactions, α determines the maximum possible flux, J ($cm^{-2}\ s^{-1}$), of gas molecules into the liquid:

$$J = \frac{n_g \bar{c} \alpha}{4} \tag{6}$$

where n_g (cm^{-3}) is the concentration of gas-phase molecules far from the surface. This maximum flux occurs only in the absence of gas-phase diffusion and solubility limitations.

An expression for α can be derived in terms of the rates of adsorption, desorption, and solvation shown in eq 2. The adsorption rate constant, or deposition velocity, is $k_{ads} = S\bar{c}/4$, where S is the adsorption coefficient, i.e., the fraction of collisions that results in thermal accommodation of the trace gas to the surface. The difference between the incoming and outgoing gas-phase fluxes at the surface gives the net incoming flux and provides a definition of α:[25]

$$\alpha n_g \bar{c}/4 = n_g S\bar{c}/4 - n_s k_{des} \tag{7}$$

where n_s (cm^{-2}) is the concentration of surface adsorbed trace molecules. Setting the net incoming flux from the gas phase equal to the net flux into the liquid gives

$$\alpha n_g \bar{c}/4 = n_s k_{sol} \tag{8}$$

Combining eqs 7 and 8 leads to

$$\frac{1}{\alpha} + \frac{1}{S} + \frac{k_{des}}{S k_{sol}} \tag{9}$$

S is typically close to unity for gas−liquid collisions occurring at near room temperature thermal speeds.[12,24] (This expression assumes that uptake is not limited by surface site saturation.[24]) With $S = 1$, α can be written as

$$\alpha = \frac{k_{sol}}{k_{des} + k_{sol}} \tag{10}$$

After the molecule enters the liquid, it diffuses away from the surface into the bulk liquid. However, the capacity of the liquid to absorb gas molecules is limited by the capacity of the liquid to solvate the trace gas molecules (solubility). With time, the trace molecules in the liquid-phase equilibrate with the gas phase. At equilibrium, the rate of molecules transferring to the surface ($k_{l\_to\_s}$ in eq 2) and desorbing is equal to the rate of molecules accommodating at the surface, yielding a net uptake of zero. The resistance due to solubility limitation (liquid-phase saturation) is given by[4,20]

$$\frac{1}{\Gamma_{sat}} = \frac{\bar{c}}{4HRT}\sqrt{\frac{t\pi}{D_l}} \tag{11}$$

where R (atm l $mol^{-1}\ K^{-1}$) is the gas constant, T (K) is the gas-phase temperature, H (M atm^{-1}) is the Henry's law coefficient describing the solubility of the gas-phase species in the liquid, t (s) is the gas−liquid interaction time, and D_l ($cm^2\ s^{-1}$) is the liquid-phase diffusion coefficient for the trace species. The expression for Γ_{sat} is derived by calculating the gas flux across the interface produced by a concentration gradient in the liquid imposed by liquid-phase diffusion of the species. Note that $1/\Gamma_{sat}$ increases with increasing exposure time of the gas to the liquid, reflecting the increasing rate of evaporation of dissolved molecules back into the gas phase as the trace species concentration in the liquid, n_l (cm^{-3}), approaches the solubility limit, $HRTn_g$ (i.e., equilibrium). This increasing resistance causes the overall net uptake to decrease with time. Combining the three effects described so far, the resistor model for the uptake coefficient is

$$\frac{1}{\gamma} = \frac{1}{\Gamma_{diff}} + \frac{1}{\alpha} + \frac{1}{\Gamma_{sat}} \tag{12}$$

The schematic for this combination of resistors is shown in Figure 2a.

Laboratory experiments can be designed to measure the time dependence for γ, from which the value of $H(D_l)^{1/2}$ can be obtained via eq 11. Equation 11 is applicable when the diffusion depth, $(\pi D_l t)^{1/2}$ for a planar surface, is much smaller than the size (depth) of the condensed phase. With $D_l = 10^{-5}$ $cm^2\ s^{-1}$, and typical experimental exposure times between 10^{-3} and 100 s, the diffusion depths are 10^{-4} to 10^{-1} cm, respectively. In the atmosphere, the diffusion depth often exceeds the dimensions of the condensed-phase particles, in which case the particles are saturated with the gas-phase species.

2.2. Case 2. Reactive Gas Uptake

In addition to mass accommodation and diffusion into the bulk, the trace gas molecule may undergo chemical reaction at the surface of the liquid or (after diffusion) in the bulk liquid. Reaction can occur with the liquid molecules themselves or with another trace species present in the liquid or at the surface. Loss of the trace species due to chemical reaction provides a sink for the trace species. In this way, saturation (i.e., re-evaporation of accommodated gas molecules) is reduced and uptake is enhanced. The overall

dx.doi.org/10.1021/cr100360b | Chem. Rev. 2011, 111, PR76 - PR109

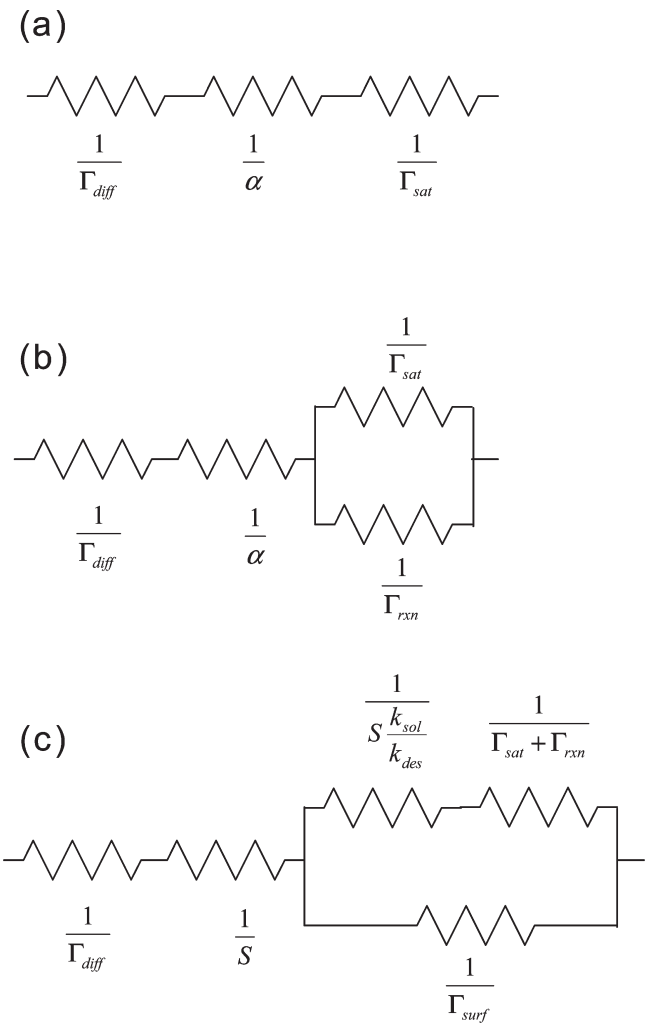

Figure 2. Schematic of the resistor model for (a) gas-phase diffusion, mass accommodation, and solubility limited uptake; (b) part a plus liquid-phase reaction; and (c) part b plus surface reaction.

kinetic scheme including both surface and liquid-phase reactions is

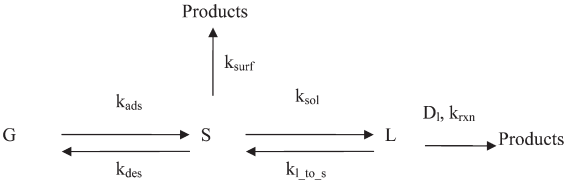

(13)

where k_{surf} (s^{-1}) is the rate of the surface reaction and k_{rxn} (s^{-1}) is the rate of the reaction in the bulk liquid phase.[26]

The resistance to uptake due to liquid-phase reactions is given by[4,16]

$$\frac{1}{\Gamma_{rxn}} = \frac{\bar{c}}{4HRT}\sqrt{\frac{1}{D_l k_{rxn}}} \tag{14}$$

Equation 14 is derived assuming that the reaction is first order and that the rate of the reverse reaction is negligible or zero. When the trace gas molecule reacts with the molecules constituting the liquid phase, the liquid molecules are in great excess and k_{rxn} (s^{-1}) is a true first-order reaction rate. In the case of a bimolecular reaction in solution, k_{rxn} (s^{-1}) is a pseudo-first-order rate constant expressed as $k_{rxn} = k_l[Y]$, where k_l (L mol^{-1} s^{-1}) is the second-order rate constant for the liquid-phase reaction and [Y] (mol L^{-1}) is the concentration of the second reacting species, assumed to be in adequate excess. In laboratory experiments, [Y] is often varied and $1/\gamma$ is plotted versus $([Y])^{1/2}$ to yield $H(k_l D_l)^{1/2}$, or k_l if H and D_l are known. Uptake coefficients for true second-order reactions can also be formulated; however, the expressions are significantly more complex.[27]

In the absence of surface reactions, the resistor model description of uptake includes the liquid-phase reaction and solubility processes as parallel resistances shown in Figure 2b. The uptake coefficient is expressed as

$$\frac{1}{\gamma} = \frac{1}{\Gamma_{diff}} + \frac{1}{\alpha} + \frac{1}{\Gamma_{sat} + \Gamma_{rxn}} \tag{15}$$

In many cases, either reaction or solubility dominates the uptake process. When there is no significant reactive loss, $\Gamma_{rxn} \ll \Gamma_{sat}$ and eq 15 reduces to eq 12. For a given H and exposure time (t) the net uptake can be time dependent, as indicated by eq 11 for $1/\Gamma_{sat}$.

When chemical reaction is fast and solubility is low, i.e., $\Gamma_{sat} \ll \Gamma_{rxn}$, eq 15 reduces to eq 16:

$$\frac{1}{\gamma} = \frac{1}{\Gamma_{diff}} + \frac{1}{\alpha} + \frac{1}{\Gamma_{rxn}} \tag{16}$$

In this case, the net uptake is time independent. For intermediate cases, where slow reaction and relatively low solubility both limit the net uptake, reaction and solubility are not decoupled processes. Equation 15 assumes that the two processes are decoupled and is valid only for limited cases, when $(k_{rxn}t)^{1/2} < 1$.[7] Note that, in the case of fast reaction and high solubility (or short exposure times), the last term in eq 15 is small and the net uptake is governed by mass accommodation and gas-phase diffusion.

The thickness of the liquid layer in which a liquid-phase reaction occurs is determined by the relative values of D_l and k_{rxn} and is given by the reacto-diffusive length, l (cm)

$$l = \sqrt{\frac{D_l}{k_{rxn}}} \tag{17}$$

In laboratory experiments that use bulk quantities of liquid, the reacto-diffusive length is typically small compared to the depth of the liquid. However, for experiments with submicrometer aerosol particles and for atmospheric particles, the reacto-diffusive length can be on the order of or larger than the particle diameter. In that case, reaction occurs throughout the volume of the particle. The lack of a concentration gradient reduces the diffusive driving force, and the net reactive uptake is smaller than expected from laboratory measurements on relatively thick liquid layers. A more general expression for Γ_{rxn} that includes a correction factor for this effect has been presented by Hanson and Lovejoy.[28]

The expression for $1/\gamma$ in eq 16 assumes that the concentration of the liquid-phase molecules is uniform. In cases of fast reaction and viscous liquids, the concentration of liquid reactant molecules may be depleted within the reacto-diffusive length. For these cases, Worsnop et al.[27] introduced an additional resistance term that takes into account the diffusion of the liquid species from the interior of the particle to the surface. Smith et al.[29] introduced a further refinement that takes into account the effect

dx.doi.org/10.1021/cr100360b | Chem. Rev. 2011, 111, PR76 - PR109

of the diffusion of the liquid molecules on the diffusion of the trace gas molecules beyond the diffusion effects already incorporated via D_l in the expression for Γ_{rxn}.

When chemical reactions occur in the interfacial region, reactive loss at the surface competes with mass accommodation and subsequent reaction in the liquid phase. The trace gas molecule is thermally accommodated at the surface and then can undergo either reaction at the surface or solvation and incorporation into the liquid. The resistor model for uptake including surface reactions is[19,26]

$$\frac{1}{\gamma} = \frac{1}{\Gamma_{diff}} + \frac{1}{S} + \frac{1}{\frac{1}{\frac{1}{S\frac{k_{sol}}{k_{des}}} + \frac{1}{\Gamma_b}} + \frac{1}{\Gamma_{surf}}} \quad (18)$$

where Γ_b refers to bulk-phase processes, such as reaction or solubility limitations. Equation 18 is represented with resistors in Figure 2c, where $1/\Gamma_b$ is expressed as the more general $1/\Gamma_{sat} + 1/\Gamma_{rxn}$. Note that α has been split into the two parts shown in eq 9 because the surface reaction, represented by Γ_{surf}, occurs after thermal accommodation but before solvation. As pointed out by Hanson,[26] the definition of the mass accommodation coefficient as the fraction of collisions that leads to incorporation into the liquid may not be a meaningful parameter for describing uptake when surface reactions are significant because the number of molecules accommodated into the liquid is strongly impacted by the number of molecules lost via surface reactions. In other words, α is only well-defined in the absence of surface reactions.

The surface reaction term can be expressed as[26]

$$\frac{1}{\Gamma_{surf}} = \frac{\bar{c}}{4k_{surf}b'} \quad (19)$$

where b' (cm) is a surface adsorption equilibrium constant such that, in the absence of reaction, the surface concentration of the trace species is proportional to the gas-phase concentration through b'. Note that the expression for Γ_{surf} is proportional to k_{surf}, in contrast to the case of eq 14 for liquid-phase reactions, where Γ_{rxn} is proportional to the square root of k_{rxn}. Experimentally, surface reactions can be distinguished from liquid-phase reactions by the dependence of the uptake coefficient on the concentration of the second reactant in a bimolecular reaction. Surface reactions exhibit a linear dependence on reactant concentration, while liquid-phase reactions vary as the square root.[30,31]

Surface reactions may have a significant effect on the uptake (1) because of the formation of a surface complex (e.g., the uptake of SO_2[32]), (2) because of enhancement of reactant concentration at the interface due to surface excess or electric double layer formation (e.g., the reaction rate of Cl^- in sea-salt aerosol[33]), or (3) because the reaction rate is so fast that the reacto-diffusive length is only a few molecular diameters (e.g., for D/H isotope exchange[34]).

Pöschl et al.[24] have recently developed a kinetic model framework for gas-surface interactions that uses multiple layers to allow for possible gradients in physical properties. Flux-based equations for mass balance and reaction rates lead to master equations that separate mass transport from chemical reactions and distinguish between gas-phase, gas-surface, surface layer, and bulk liquid processes. These master equations provide a consistent framework for describing interactions with different types of surfaces (liquids and solids) over a wide range of reaction rates and time scales. They can be reduced to include only the species and processes relevant to a particular type of interaction.[35] In the case of many gas−liquid interactions, Pöschl et al.[24] show that their equations are equivalent to the resistor model expressions presented above.

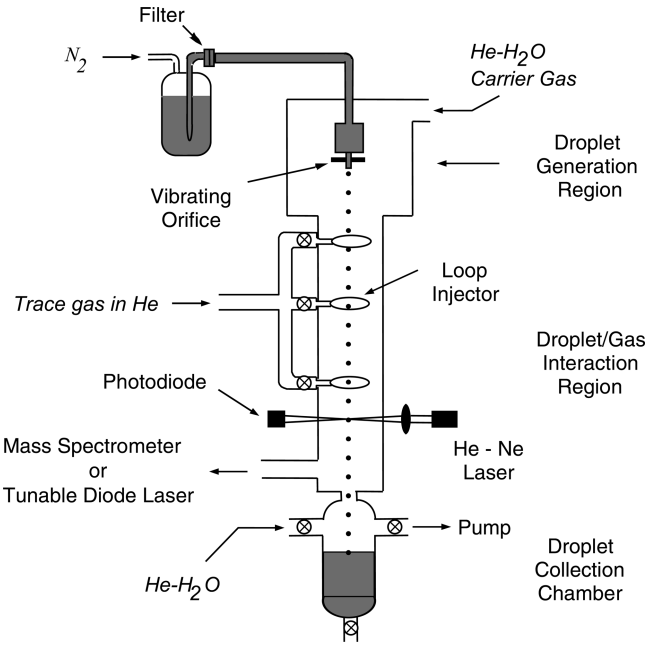

Figure 3. Schematic of a droplet train flow reactor. (Reprinted with permission from ref 19. Copyright 1999 American Chemical Society.)

3. EXPERIMENTAL TECHNIQUES

Over the past 20 years, many experimental techniques have been developed to measure the magnitudes and rates of gas−liquid interactions. The basic principle of such measurements is simple. Gas molecules of interest are brought into contact with the liquid of a known surface area, and after a controlled period of gas−liquid interaction time, the amount of gas that entered the liquid or was depleted from the gas phase is determined. The liquid phase can be in the form of a planar surface, a jet, a droplet, or small aerosol particles. In most techniques, the loss (or production) of the gas-phase species is monitored. Less common are techniques that interrogate the liquid phase for the appearance or disappearance of species. For small aerosol particles, changes in size can be used to monitor absorption of gas-phase species. Finally, in a few cases, surface specific spectroscopic techniques interrogate the gas−liquid interface itself. These spectroscopic techniques are covered in other articles in the Structure and Chemistry at Aqueous Interfaces thematic issue of *Chemical Reviews* (issue 4 of 2006). In this section, we give a brief overview of the most common experimental techniques used to study gas−liquid interactions.

3.1. Droplet Train Flow Reactor

In the droplet train flow reactor, gas−liquid interactions are studied by monitoring the gas-phase concentration of a trace species in contact with a stream of droplets on the order of 100 μm diameter entrained in a vertical flow tube.[18] A schematic diagram of the droplet train apparatus is shown in Figure 3. A monodisperse, spatially collimated train of droplets is produced

dx.doi.org/10.1021/cr100360b | *Chem. Rev.* 2011, 111, PR76 - PR109

by forcing a liquid through a vibrating orifice, driven by an electrically pulsed piezoelectric ceramic. The droplet train passes through a vertical low pressure (5−20 Torr) flow tube which contains the trace gas species entrained in a flowing mixture of an inert carrier gas (usually helium) and vapor of the liquid being studied. The trace gas is introduced through one of three loop injectors located along the flow tube. By selecting the gas inlet port and the droplet velocity, the gas−droplet interaction time can be varied between 2 and 20 ms, allowing solubility effects to be investigated.

The liquid vapor entrained in the carrier gas is maintained at a partial pressure in equilibrium with the chosen surface temperature of the liquid droplets. As a result, there is no significant droplet growth or evaporative loss as the droplets transit the flow reactor. Control of the vapor pressure associated with the droplet liquid is especially important because the surface temperature of the droplets is determined by the partial pressure of this vapor both in the droplet generation chamber and in the flow tube.[18]

The liquid surface area exposed to the trace gas is determined by the diameter and number of droplets, and is changed in a stepwise fashion by changing the driving frequency applied to the piezoelectric ceramic in contact with the droplet-forming orifice. The concentration (number density) of the trace gas is monitored after the gas exits the flow tube, either with a quadrupole mass spectrometer or with a tunable infrared diode laser. The uptake coefficient, γ_{meas}, as defined by eq 1 is calculated from the measured change in trace gas signal as

$$\gamma_{meas} = \frac{4F_g}{\bar{c}\Delta A} \ln \frac{n_g}{n'g} \qquad (20)$$

where F_g ($cm^3\ s^{-1}$) is the carrier-gas volume rate of flow through the system, $\Delta A = A' - A$ (cm^2) is the change in the total droplet surface area in contact with the trace gas, and n_g and n_g' (cm^{-3}) are the trace gas densities at the outlet of the flow tube after exposure to droplet trains of total surface area A and A', respectively.[18,25]

The pressure and droplet diameter in the droplet train flow reactor are such that gas-phase diffusion limitations often affect the measured uptake coefficient and a correction needs to be applied to extract the mass accommodation coefficient or reactive uptake coefficient. The expression for Γ_{diff} presented in eq 3 was developed for uptake on stationary droplets. However, experiments have shown that the same expression applies in the droplet train flow reactor if the droplet diameter, d, used to calculate Kn is replaced with an effective diameter related to the diameter of the droplet-forming orifice.[36−38]

In a recent publication, Morita et al.[39] presented results of a computational fluid dynamics simulation of the droplet train flow reactor experiments performed by the Boston College/Aerodyne Research, Inc. (BC/ARI) group. This work is an important contribution to understanding gas-phase diffusive transport to a train of moving droplets. These simulations confirm the key experimental findings of the BC/ARI group used to analyze the experimental results. However, based on their fluid dynamics simulation, Morita et al. suggest that in the BC/ARI measurements the effect of gas-phase diffusion may be underestimated, yielding a smaller value of α. Thus, for example, Morita et al. suggest that the BC/ARI measurement of α = 0.2 (such as obtained for $H_2O(g)$ at 273 K) is consistent with values of α between 0.2 and 1. In a Comment,[40] the BC/ARI group pointed out that, in the presentation of the fluid dynamic simulation results of the BC/ARI experimental technique, Morita et al. did not take into account key experimental results that support the values of α as quoted in the BC/ARI publications. Morita et al. published a Reply to the Comment.[41] The fluid dynamics simulation of the droplet train flow reactor experiments is further described by Garret et al.[15b]

Table 1. Characteristics of Experimental Techniques

	droplet train flow reactor	bubble train reactor	wetted wall flow reactor	Knudsen cell	aerosol flow reactor
surface area ratio ($cm^2\ cm^{-3}$)	10^{-3}	5	2	$\sim10^{-2}$	$\sim10^{-5}$
factor for gas-phase diffusion correction to γ_{meas}	1−20	∼1	1−10	1	∼1
detection limit (γ)	10^{-3}	10^{-7}	10^{-6}	10^{-4}	10^{-4}
exposure time (s)	10^{-2} to 10^{-3}	10	∼1	10−1000	10−100

The lower limit of the uptake coefficient that can be measured by a specific experimental technique depends on the ratio of the liquid surface area to the gas-phase volume and the signal-to-noise characteristics of the detection system. A comparison of the detection limits for the first five techniques discussed in this section is given in Table 1. In the droplet train flow reactor, the surface area-to-volume ratio is roughly 10^{-3} cm^2 cm^{-3}, allowing measurement of uptake coefficients down to about 1×10^{-3}, although this limit can be lowered by a factor of 5 by detecting reaction products in the liquid phase.[42] When the uptake is limited by solubility, the observation of a time dependent γ_{meas} depends on the relative values of H and the gas−liquid interaction time. In the droplet train flow reactor, the maximum interaction time of about 20 ms allows measurement of H values above 1×10^4 M atm^{-1}.

Optical spectroscopic techniques have been used to monitor changes in the droplets themselves in a droplet train flow reactor. For example, cavity-enhanced Raman scattering has been used to measure the changing size of water droplets when exposed to a trace species,[43] and laser-induced fluorescence of droplets seeded with an appropriate dye molecule has been used to measure the pH of the droplets.[44]

3.2. Bubble Train Reactor

In the bubble train reactor, the trace gas is contained in bubbles that pass through a column of liquid.[45,46] The bubble train reactor was developed to obtain longer gas−liquid interaction times in the 1−100 s range and to increase the surface area-to-volume ratio to around 5 cm^2 cm^{-3}. In the bubble train reactor, the range of measurable uptake coefficients is 1×10^{-3} to 1×10^{-7}, while the range of measurable Henry's law coefficients is 10^{-3} to 3 M atm^{-1}.

A schematic of the bubble train reactor is shown in Figure 4. Gas bubbles containing the trace species and an inert carrier gas are injected into the flowing column of liquid with a movable injector so that the gas−liquid interaction time can be varied. After the bubbles burst, the amount of trace gas remaining is measured using a mass spectrometer.

Because the bubbles change shape and size as they travel through the liquid column, this technique requires significantly more complex analysis than the resistor model presented in

dx.doi.org/10.1021/cr100360b | Chem. Rev. 2011, 111, PR76 - PR109

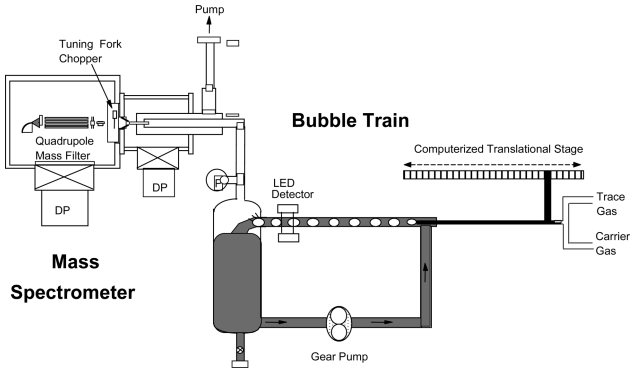

Figure 4. Schematic of a horizontal bubble train reactor. Adapted from ref 45.

section 2. In addition, convective mixing can occur in the liquid layer next to the bubble as the bubbles move through the column, further complicating the extraction of H and/or k from the measured uptake data. The system is modeled using numerical techniques that couple the gas density to the liquid diffusion and reaction processes and incorporate the changing shape of the bubbles. Empirical parameters in the model are calibrated by making measurements for species with known Henry's law solubilities and reaction rates.

A closely related experimental technique is the bubble column in which the trace species is dissolved in the liquid phase.[47,48] Nitrogen gas is bubbled through the liquid and causes a decrease in trace species concentration as a function of time. The first-order decay of the concentration is monitored in both the gas and liquid phases and yields a value for the Henry's law solubility.

3.3. Wetted Wall Flow Reactor

In a wetted wall flow reactor, uptake is measured on a layer of liquid coating the inside surface of a flow tube.[16] In one version, the liquid flows down the inner surface of a vertical flow tube.[49] The flow tube has an annular lip at the top over which the liquid spills to create a thin, uniform film over the entire surface. Care must be taken to ensure that the liquid flow is laminar. If the liquid flow rate is too high, rippling of the liquid occurs and can cause turbulence in the gas flow.[16] Turbulence enhances the mass transport of the trace gas to the liquid and increases the measured uptake coefficient.[50]

In another version, the flow tube is horizontal.[31,51,52] A schematic of a typical horizontal flow tube apparatus is shown in Figure 5. The liquid can be contained in a holder in the flow tube, or it can coat the walls. If the liquid is sufficiently viscous, the coating stays in place during the course of an experiment. Alternately, the flow tube can be rotated to keep the coating uniform as in Figure 5.[52]

The trace gas is introduced into the flow tube through a movable injector so that the exposure time of the gas to the liquid can be varied. Loss of the trace gas is measured with a mass spectrometer or an optical technique. The measured loss of the trace gas as a function of exposure time is plotted to give a first-order loss rate to the coated walls

$$\frac{d[X]}{dt} = -k_w[X] \qquad (21)$$

where $[X]$ (cm^{-3}) is the concentration of the gas-phase species, k_w (s^{-1}) is the first-order loss rate, and t (s) is the exposure time.

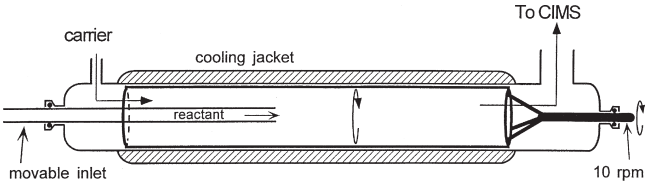

Figure 5. Schematic of a wetted wall flow reactor. (Reprinted with permission from ref 52. Copyright 1995 American Geophysical Union.)

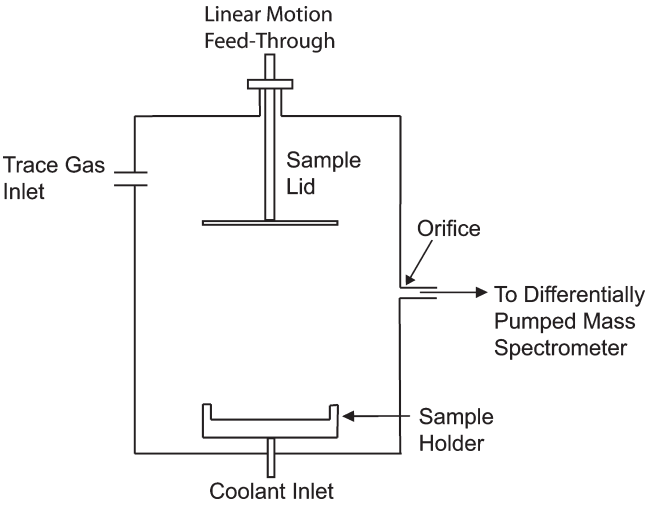

Figure 6. Schematic of a Knudsen cell reactor.

The uptake coefficient is calculated from k_w via

$$\gamma_{meas} = \frac{2rk_w}{\bar{c}} \qquad (22)$$

where r (cm) is the radius of the flow tube.

Flow tubes are usually operated at a pressure of a few Torr, and gas-phase diffusion limitations often apply. Values of k_w are corrected for gas-phase diffusion effects using an algorithm developed by Brown.[53] Typical surface area-to-volume ratios for wetted wall flow tubes are 2 cm^2 cm^{-3}, and typical exposure times are 0.01 to 1 s, giving a lower limit for measurable uptake coefficients of 10^{-6}. Values for γ above 10^{-1} are difficult to measure accurately in a wetted wall flow reactor because of gas-phase diffusion limitations. In a 2008 publication Davis[53b] reviewed the literature on flow reactor analysis methods and presented a detailed analysis of data interpretation from flow reactor gas uptake measurements, consolidating data obtained in earlier flow tube studies.

3.4. Knudsen Cell Reactor

Knudsen cell reactors operate at relatively low pressures, less than 10 mTorr, ensuring that gas-phase diffusion does not limit the interaction of the gas with the surface.[54] A typical Knudsen cell apparatus consists of two chambers separated by a valve. The schematic in Figure 6 shows a version of the Knudsen cell in which one chamber is a sample holder with a lid that can be raised or lowered and the second chamber surrounds the first chamber. The liquid of interest is placed in the sample holding chamber. The trace gas flows through the other chamber, which has a small

dx.doi.org/10.1021/cr100360b | Chem. Rev. 2011, 111, PR76 - PR109

escape aperture leading to a low pressure detection system, usually a mass spectrometer. The concentration in the chamber is kept low enough so that the flow is in the free molecular regime and the residence time in the chamber is determined by the size of the escape aperture. When the sample holder lid is raised, loss of the gas-phase species to the surface competes with escape through the aperture and is observed as a decrease in the mass spectrometer signal. The number of molecules lost to the surface is measured by the change in flux through the escape aperture, while the number of gas-surface collisions is calculated from gas kinetic theory. The expression for the uptake coefficient is

$$\gamma_{meas} = \frac{A_h}{A_s}\frac{F_0 - F}{F} \quad (23)$$

where A_h (cm^2) is the area of the escape aperture, A_s (cm^2) is the area of the surface, F_0 (molecules s^{-1}) is the flux through the escape aperture with the valve closed, and F (molecules s^{-1}) is the flux through the escape aperture with the surface exposed. By varying the relative sizes of A_h and A_s, uptake coefficients in the range between 1 and 1×10^{-4} can be measured accurately. The exposure time in the Knudsen cell reactor is on the order of a few seconds to hundreds of seconds. Measurements at shorter exposure times are usually precluded by the time needed to physically open the valve and the time needed for the pressure to equilibrate between the two chambers. Fenter et al.[55] have extended measurements to shorter exposure times (a few tenths of seconds) by injecting the trace gas with a pulsed valve and carefully modeling the initial expansion of the vapor.

The requirement that the pressure be in the molecular flow regime makes Knudsen cells unsuitable for many liquids of atmospheric interest. However, Knudsen cell reactors have been used successfully for low vapor pressure liquids such as low temperature sulfuric acid.[56−58]

3.5. Aerosol Flow Reactors and Aerosol Chambers

In several experimental techniques, gas−liquid interactions are measured on small aerosol particles, i.e., < 10 μm diameter, rather than the bulk liquid layers or droplets used in the techniques described above. Performing experiments on aerosol particles makes the gas-phase diffusion correction negligible and more closely simulates actual atmospheric aerosols. However, because the overall particle area in the reaction zone is small, reactions on the reactor walls can be a significant problem. In addition, the generation of a well-characterized and stable aerosol population can be difficult for some condensed-phase materials. The total particle surface area in the reaction zone is particularly important for determining the uptake coefficient and can be a source of uncertainty in these experiments.

In an aerosol flow reactor, aerosol particles are introduced into a laminar flow tube similar to the ones used for wetted wall flow reactor experiments (e.g., Lovejoy and Hanson,[59] Kane et al.,[60] Hu and Abbatt,[61] Mozurkewich et al.,[62] and McMurry et al.[63]). Figure 7 shows a typical aerosol flow reactor system. Particle concentrations and size distributions are measured with an optical particle counter or with a differential mobility analyzer/condensation particle counter combination in order to determine the condensed-phase surface area exposed to the trace gas species. The chemical composition of the aerosol particles before and after exposure can be measured with an aerosol mass spectrometer (e.g., Morris et al.[64] and Tolocka et al.[65]) to yield information about condensed-phase reaction products. The trace gas species is introduced through a movable injector so that the exposure time can be varied. The density of the trace gas can be monitored with mass or optical spectrometric techniques.

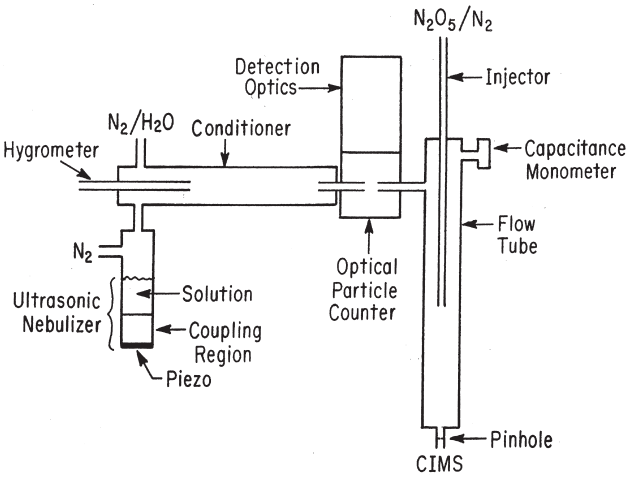

Figure 7. Schematic of an aerosol flow reactor. Reprinted with permission from ref 61. Copyright 1997 American Chemical Society.

Table 1 gives a comparison of the experimental characteristics of surface area-to-volume ratio, gas-phase diffusion correction, detection limit, and typical exposure time for the five techniques discussed above. With the various techniques, it is possible to span a range of 7 orders of magnitude in the value of the uptake coefficient.

In an aerosol chamber experiment, the aerosol particles are introduced into a static chamber with relatively unreactive walls (e.g., Mentel et al.[66] and Hunt et al.[67]). The potentially long residence time of up to many hours enables the study of slower gas−liquid interactions. However, during long residence times, the aerosol particle size distribution can change due to settling and coagulation. The trace gas species can be introduced into the chamber or generated in situ via chemical or photochemical reactions. Trace gas density is often monitored in situ with Fourier transform infrared spectroscopy.

3.6. Expansion Chamber

For some systems, mass and thermal accommodation coefficients can be obtained from growth rates of droplets in an expansion chamber.[68] For example, Winkler et al.[69a,b] introduced a well-defined mixture of water vapor and seed particles in air into an expansion chamber at near atmospheric pressure. Fast adiabatic expansion of the water vapor−air mixture in the chamber produces a controlled vapor supersaturation (saturation ratio 1.3 to 1.45). Subsequent condensation on the pre-existing nanometer-scale particles leads to growth of monodisperse liquid droplets. Droplet growth is monitored on a time scale of 6−200 ms by laser light scattering. The mass and thermal accommodation coefficients are obtained by fitting the measured droplet growth rates to numerical solutions of the differential equations describing the coupled mass and heat fluxes in the vicinity of the droplets.

3.7. Liquid Jet Techniques

In a coaxial liquid jet reactor, shown in Figure 8, liquid is forced through a capillary to form a jet with a diameter on the order of 100 μm.[70,71] The uptake of trace species from a coflowing gas stream is measured. The length of the liquid jet is on the order of 1 mm, leading to a short gas−liquid interaction time of 0.1−1 ms.

dx.doi.org/10.1021/cr100360b | Chem. Rev. 2011, 111, PR76 - PR109

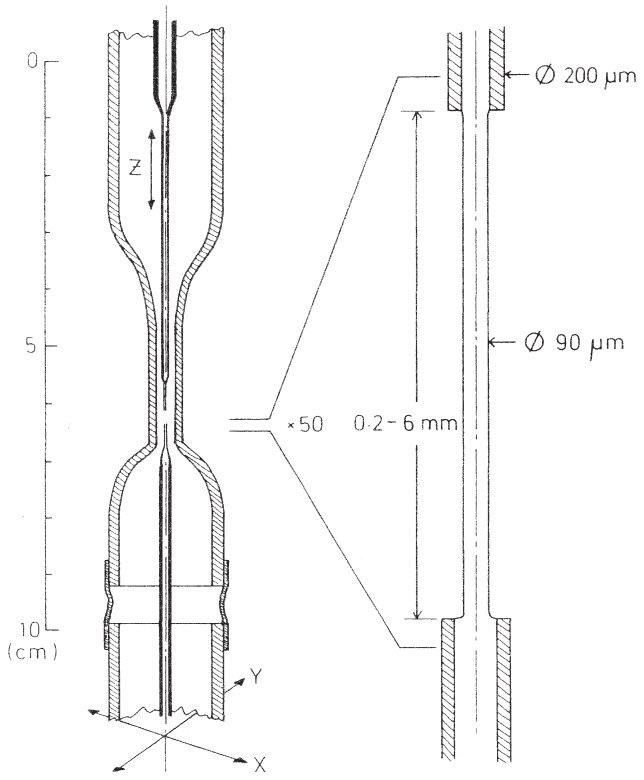

Figure 8. Schematic of a coaxial liquid jet reactor. (Reprinted with permission from ref 70. Copyright 1990 Springer Science and Business Media.)

The interaction time can be varied by varying the length of the liquid jet exposed to the gas. In addition, the short length of the jet prevents it from breaking up into droplets. The liquid is collected and analyzed to yield the gas uptake rate. Data analysis requires a detailed mass-transfer model that incorporates gas- and liquid-phase diffusion processes, chemical reactions in the liquid, and mass transfer at the interface.

Liquid jets, or beams, can be introduced into a vacuum chamber where high vacuum analysis techniques can be used to interrogate molecules at the liquid surface.[72] A review by Kondow and Mafuné[72] discusses the use of ultraviolet photoelectron spectroscopy and multiphoton ionization-mass spectrometry to study the structure of the liquid beam surface and ion−molecule reactions at the surface in high vacuum.

3.8. Single-Droplet Techniques

Several techniques have been developed that measure gas−liquid interactions on an individual droplet. In the electrodynamic trap technique, a slightly charged droplet (5−20 μm in diameter) is held in the null point of an electric field generated by a series of electrodes. The trace gas species is introduced into the trap, and relative changes in the mass of the droplet are detected by changes in the dc potential required to keep the droplet in the null point.[73] Changes in droplet size can also be detected with Mie scattering.[74] For example, in one experiment, Shaw and Lamb[75] injected individual water droplets into a controlled subsaturated environment. They observed changes in droplet size and the time for a droplet to freeze via optical scattering. By modeling the evaporation kinetics, mass and thermal accommodation coefficients were determined.

Optical levitation of liquid droplets has been reported by King et al.[76] In this technique, 5−9 μm droplets are trapped in the focused beam of an Ar-ion laser and held in place for up to 30 min. Raman scattered laser light is analyzed with a spectrometer to give the chemical composition of the droplet before, during, and after exposure to a trace gas species. Droplet size is recorded with a camera.

In the suspended droplet flow reactor technique, developed by Schütze and Herrmann, uptake measurements are performed on a droplet several millimeters in diameter suspended at the tip of a pipet inside a flow reactor.[77,78] The trace gas species introduced into the flow tube changes the composition of the droplet. The droplet composition and the gas-phase species concentration are monitored with UV−visible absorption spectroscopy.

3.9. Impinging Flow Technique

In the impinging flow technique, a gas flow containing the trace species is directed coaxially from above onto a continuously renewed liquid surface generated by the liquid flowing upward through an open-ended tube.[79,80] The spatial distribution of the gas-phase trace species is measured with laser-induced fluorescence. The uptake coefficient is determined from the gradient in the trace species concentration above the liquid surface. The exposure time is varied by changing the liquid flow rate. This technique makes measurements on a continuously refreshed surface, thus avoiding saturation effects, but is limited to species that exhibit laser-induced fluorescence.

3.10. Molecular Beam/Liquid Surface Technique

The detailed molecular dynamics of gas−liquid surface interactions can be determined by monitoring the fate of a beam of gas-phase molecules directed onto a liquid surface. Because molecular beam techniques require fairly high vacuum conditions, most aqueous liquid surfaces cannot be investigated with this method. However, Nathanson and co-workers have performed experiments on concentrated sulfuric acid and other low vapor pressure liquid surfaces. A description of the technique and its application to sulfuric acid surfaces is presented in a recent review by Nathanson.[81]

3.11. Aqueous Microjet Electrospray Mass Spectrometry Technique

In this technique, recently developed by Colussi, Hoffmann, and co-workers, gas−liquid interactions can be characterized on the surface of microjets injected through an electrically grounded nozzle into the spraying chamber of an electrospray ionization mass spectrometer (ESI/MS) that contains dilute concentrations of the trace gases of interest. While this technique has not yielded quantitative heterogeneous uptake coefficients, because the surface areas of the mircojets and/or the mirodroplets they produce are not well characterized, valuable information about the mechanisms and product branching ratios of heterogeneous processes can be obtatined. Published studies include the reactions of surface active trace negative ions[81b,c] and organic compounds[81d,e] with ozone, as well as the reaction of trimethylamine with interfacial hydronium ions.[81f]

4. TRACE GAS UPTAKE: EXPERIMENTAL RESULTS

As noted in the Introduction, over the past two decades most heterogeneous kinetics studies involving gas−liquid surface interactions have been driven by interest in atmospheric processes. The chemical complexity of atmospheric gas−liquid heterogeneous processes varies widely. The simplest, as detailed

dx.doi.org/10.1021/cr100360b Chem. Rev. 2011, 111, PR76 - PR109

in section 2, is mass accommodation (interfacial mass transport) of soluble, nonreactive vapor molecules into pure water, simulating fog or cloud droplets. More chemically complex processes include (1) trace gas mass accommodation into aqueous acid or aqueous salt solutions simulating stratospheric or tropospheric liquid aerosol particles; (2) uptake of gaseous species where Henry's law solubility constraints may impede uptake; (3) reactive uptake of trace gases subject to reversible neutral or ionic hydrolysis reactions in aqueous solutions, where the rate of hydrolysis may depend on the activity of water and thus on the acid or salt concentration; and (4) irreversible reactive uptake by aqueous solutions, where, for relatively insoluble gases, the reaction rate, controlled by the water activity or the concentration of a dissolved reactant, might control the rate of uptake. Further complexity arises when fast surface reactions occur in parallel with mass accommodation followed by bulk liquid-phase reactions, or when organic surfactants on aqueous surfaces impede mass accommodation or influence surface reactions. Finally, liquid water on the surface of organic particles may change the mass accommodation or surface reaction rates for trace gases on organic liquids. Examples of each of these types of gas−liquid surface heterogeneous processes are presented below.

4.1. Mass Accommodation on Water Surfaces

The mass accommodation kinetics of trace vapor species on liquid water surfaces have been extensively investigated in about a dozen laboratories, using complementary experimental techniques. As discussed in section 3, to avoid contamination of the water surface and to avoid near surface Henry's law solubility constraints (in the case of all but the most soluble gases), it is important to use a technique that constantly refreshes the water surface. For gases with lower Henry's law solubility, it is also helpful to use a technique with short (subsecond) and variable gas−liquid interaction times to experimentally test for saturation effects, which are indicated by lower apparent uptake rates at longer interaction times. It has also been important to study trace gas uptake kinetics as a function of water surface temperature. Mass accommodation coefficients have been shown to vary significantly with temperature, and the atmosphere contains liquid water from ~300 K down to supercooled temperatures as low as ~250 K. Given liquid water's high vapor pressure at atmospheric temperatures and large heats of vaporization and condensation, it is also important to maintain equilibrium water vapor pressures over experimental liquid water surfaces if the liquid surface is to be maintained at a constant temperature and, for droplets, a constant surface area.

Given these experimental constraints, a few techniques have produced most of the reliable trace gas mass accommodation measurements on liquid water. These include the wetted wall flow reactor, the droplet train flow reactor, and the coaxial liquid jet reactor, all described in section 3. Results from these experimental techniques demonstrate that measured mass accommodation coefficients vary inversely with temperature. An example is shown in Figure 9, which displays the temperature dependence of the mass accommodation coefficient for ethanol vapor on liquid water, as measured with a droplet train flow reactor.

As shown in section 2, eq 10, assuming a thermal accommodation coefficient of one, the mass accommodation coefficient can be expressed as a ratio of the rate constant for the thermally accommodated gas surface species to be solvated by the bulk liquid, k_{sol}, divided by the sum of $k_{sol} + k_{des}$, where k_{des} is the rate constant for desorption of the trace species back into the gas phase:

$$\alpha = \frac{k_{sol}}{k_{des} + k_{sol}} \tag{10}$$

which can be rearranged to

$$\frac{\alpha}{1-\alpha} = \frac{k_{sol}}{k_{des}} \tag{24}$$

To represent the experimental mass accommodation data, such as that shown in Figure 9, the temperature dependence of this expression can be represented as an exponential function:

$$\frac{\alpha}{1-\alpha} = \frac{k_{sol}}{k_{des}} = \exp\left(\frac{-\Delta G_{obs}}{RT}\right) \tag{25}$$

The parameter $\Delta G_{obs} = \Delta H_{obs} - T\Delta S_{obs}$ is in the form of a free energy. Its meaning will be discussed in section 5. The values for ΔH_{obs} and ΔS_{obs} can be obtained from the experimental results by plotting the natural log of $\alpha/(1-\alpha)$ as a function of $1/T$. The slope of such a plot is $-\Delta H_{obs}/R$, and its intercept is $\Delta S_{obs}/R$. The functional form of ΔG_{obs} depends on the theoretical formulation of the uptake process. Therefore, as will be discussed in section 5, the parameter ΔG_{obs} serves as a bridge between experiment and theory. The form of eq 25 is consistent with transition state kinetic theory, in which both k_{sol} and k_{des} are expressed with an Arrhenius exponential temperature dependence.

The values of α at 273 K (or the closest temperature measured, shown in parentheses) and values for ΔH_{obs} and ΔS_{obs} obtained from temperature dependent experimental studies for over three dozen vapor species on water are listed in Table 2. Most of the measurements were performed with the droplet train flow reactor, but available results from wetted wall flow reactor and coaxial liquid jet reactor studies are also tabulated. Table 2 lists only data for mass accommodation on liquid water obtained under near equilibrium water vapor conditions. The special case of water vapor accommodation by liquid water surfaces will be discussed in more detail below.

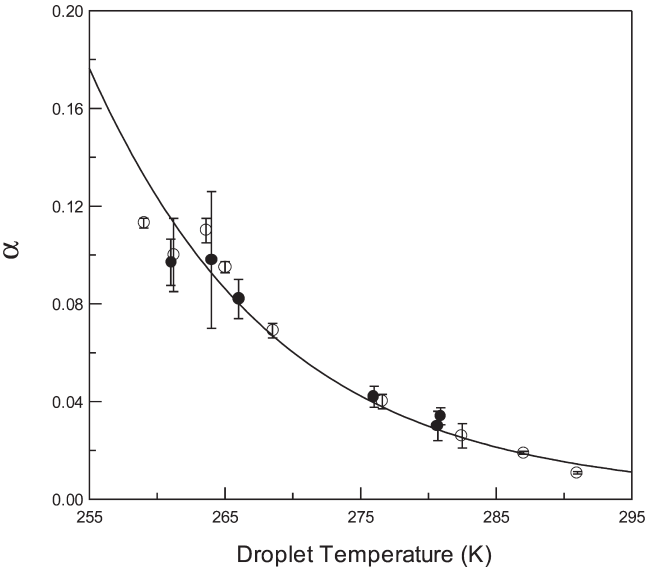

Figure 9. Temperature dependence of α for ethanol on liquid water. The solid line is an exponential fit of eq 25 to the data. The open and filled symbols are obtained from two sets of measurements using different ways of taking Henry's law saturation into account. (Reprinted with permission from ref 25. Copyright 1991 American Chemical Society.)

dx.doi.org/10.1021/cr100360b Chem. Rev. 2011, 111, PR76 - PR109

Table 2. Measured ΔH_{obs}, ΔS_{obs}, and α (273 K) on Water Surfaces

gas-phase species	ΔH_{obs} (kcal/mol)	ΔS_{obs} (cal/(mol K))	α (273 K)	exp method[a]
$C_{10}H_8$	−29.4	−115.2	0.00022 (296 K)	DTFR[b]
$(C_2H_5O)_2C(O)$	−36	−137	0.018	DTFR[c]
$(CH_3O)_2C(O)$	−26	−99	0.09	DTFR[c]
4-$CH_3C_6H_4OH$	−25.9	−100.3	0.012 (283 K)	WWFR[d]
3-$CH_3C_6H_4OH$	−5.7	−29.4	0.010 (278 K)	WWFR[94]
	−25.1	−98.6	0.012 (278 K)	WWFR[d]
2-$CH_3C_6H_4OH$	−23.5	−94.9	0.0050 (278 K)	WWFR[d]
2-$NO_2C_6H_4OH$	−14.8	−84.6	0.012 (278 K)	WWFR[94]
	−21.9	−82.5	0.0052 (283 K)	WWFR[d]
C_6H_5OH	−14.8	−59.3	0.037 (278 K)	WWFR[94]
$CH_3C(O)CH_3$	−12.7	−53.7	0.026	DTFR[95]
$(CH_3)_3COH$	−8.2	−35.8	0.052	DTFR[25]
$CH_3CH(OH)CH_3$	−9.9	−43.0	0.033	DTFR[25]
$CH_3CH_2CH_2OH$	−9.2	−40.9	0.026	DTFR[25]
CH_3CH_2OH	−11.0	−46.2	0.049	DTFR[25]
	−4.8	−21.9	0.100	DTFR[34]
	−5.6	−27.4	0.030	DTFR[86]
CH_3OH	−8.0	−34.9	0.056	DTFR[25]
IH_2CCH_2OH	−8.2	−34.4	0.10	DTFR[25]
BrH_2CCH_2OH	−8.4	−35.9	0.070	DTFR[25]
ClH_2CCH_2OH	−7.3	−32.3	0.057	DTFR[25]
$CH_3C(O)OH$	−8.1	−34.9	0.067	DTFR[25]
$HC(O)OH$	−7.9	−34.9	0.047	DTFR[25]
$CClH_2C(O)OH$	−8.4	−34.4	0.14	DTFR[e]
$CCl_2HC(O)OH$	−8.0	−33.0	0.14	DTFR[e]
$CCl_3C(O)OH$	−9.9	−40.0	0.13	DTFR[e]
$CF_2ClC(O)OH$	−7.1	−29.4	0.15	DTFR[e]
$CF_3C(O)OH$	−4.5	−20.1	0.14	DTFR[e]
HI	−10.6	−43.4	0.091	DTFR[83]
HBr	−10.0	−41.5	0.079	DTFR[83]
	−11.8	−45.3	0.26	DTFR[87]
HCl	−7.2	−29.4	0.18	DTFR[83]
	−8.8	−34.6	0.23	DTFR[82]
$(CH_3)_2SO_2$	−10.7	−43.0	0.13	DTFR[84]
$(CH_3)_2SO$	−5.1	−23.1	0.098	DTFR[84]
NH_3	−9.3	−36.8	0.20	DTFR[19]
	−7.2	30.1	0.12 (275 K)	CLJR[89]
SO_2	−7.6	−29.2	0.34	DTFR[32]
HNO_3	−6.6	−27.6	0.15	DTFR[82]
CH_3OOH	−6.5	−32.5	0.012	DTFR[109]
$HOCH_2CH_2OH$	−5.3	−24.5	0.072	DTFR[25]
H_2O_2	−5.5	−22.5	0.23	DTFR[18]
H_2O	−4.8	−20.3	0.22	DTFR[99]
$(CH_3OC(O))_2(CH_2)$	−3.1	−16.8	0.06	DTFR[f]
$(CH_3OC(O))_2(CH_2CH_2)$	−3.4	−19.0	0.04	DTFR[f]
CH_3SO_3H	−3.5	−16.7	0.12	DTFR[84]
	−2.7	−14.0	0.11	DTFR[85]

[a] DTFR = droplet train flow reactor. WWFR = wetted wall flow reactor. CLJR = coaxial liquid jet reactor. [b] Raja, S.; Valsaraj, K. T. *Environ. Sci. Technol.* **2004**, *38*, 763. [c] Katrib, Y.; Deiber, G.; Mirabel, P.; Le Calvé, S.; George, C.; Mellouki, A.; Le Bras, G. *J. Atmos. Chem.* **2002**, *43*, 151. [d] Leyssens, G.; Louis, F.; Sawerysyn, J.-P. *J. Phys. Chem. A* **2005**, *109*, 1864. [e] Hu, J.; Shorter, J. A.; Davidovits, P.; Worsnop, D. R.; Zahniser, M. S.; Kolb, C. E. *J. Phys. Chem.* **1993**, *97*, 11037. [f] Katrib, Y.; Le Calvé, S.; Mirabel, P. *J. Phys. Chem. A* **2003**, *107*, 11433.

Several vapor species listed in Table 2 have been studied in more than one laboratory. Since experimental heterogeneous kinetics for liquid surfaces is still a relatively young field and the experimental techniques and data analyses are complex (see sections 2 and 3), the level of agreement between experiments conducted on what are nominally the same systems is not as good

dx.doi.org/10.1021/cr100360b *Chem. Rev.* 2011, 111, PR76 - PR109

as that often achieved in either gas-phase or bulk liquid-phase kinetic studies. When uptake coefficients are compared from studies using either similar or differing experimental techniques, values within a factor of 2 or 3 are often judged to be in reasonable agreement given the challenges of identifying, quantifying, and reducing systematic errors. However, for some experimental systems studied in different laboratories, the agreement is good.

Droplet train studies performed in the Boston College/Aerodyne Research Inc. (BC/ARI) laboratories and at the Université Louis Pasteur (LP) for hydrogen chloride[82,83] and methane sulfonic acid[84,85] produced data that overlap within one standard deviation (~±20%) and yield very similar values for ΔH_{obs} and ΔS_{obs}. On the other hand, for three droplet train flow reactor studies on ethanol uptake, two from the BC/ARI group and one from the LP group, the agreement is not as good. The most recent study from the BC/ARI group[34] obtained a similar temperature dependence for α to that measured by the LP group,[86] but the BC/ARI mass accommodation values are about a factor of 3 higher. The BC/ARI initial ethanol study[25] obtained α values that are consistent with the lower LP values[86] at higher temperatures and the higher values obtained in the BC/ARI later study[34] at lower temperatures, while the initial BC/ARI ethanol α values fall between those of refs 34 and 86 at intermediate temperatures, thus displaying a much steeper temperature dependence, as indicated in Table 2. The three data sets are plotted together in ref 86. While this level of disagreement is worse than typical levels of precision for the droplet train flow reactor technique, indicating some systematic error in at least two of these experiments, the agreement is still acceptable given the difficulty of the experiments. Also, while the agreement for HCl α values measured by the LP group and the BC/ARI group is excellent (as shown in Table 2), agreement for HBr values is not as good. Similar temperature dependencies were obtained, but the BC/ARI mass accommodation values[87,88] exceed those of the LP group[83] by about a factor of 3. In addition, the BC/ARI group has not measured a temperature dependence for HI uptake on water, but the BC/ARI value at 273 K[88] is about a factor of 2 higher than the LP group value at that temperature.[83] The LP group measured significantly smaller α values for HBr and HI compared to HCl,[83] while the BC/ARI values were similar for all three hydrogen halides.[82,87,88] Further work will be required to resolve the discrepancy for the higher weight hydrogen halides.

It is also instructive to compare α values measured for NH_3 by the BC/ARI group[19] and the LP group,[42] using the droplet train flow reactor technique, and by the Schurath group, using the coaxial liquid jet method.[71,89] Figure 10, reprinted from ref 90, shows data from all three groups, along with exponential fits to the droplet train[19,42] and coaxial liquid jet[71,89] results, and a fit to the combined data. Given that the reported data where taken by two independent techniques in three laboratories in four distinct time periods, the agreement is encouraging.

While comparable temperature dependent studies as presented above are relatively sparse, additional single temperature measurements can be compared to the corresponding points from temperature dependent studies. For example, room temperature droplet train flow reactor results for SO_2 and HNO_3 uptake obtained by Ponche et al.[42] are in fair to good agreement with the BC/ARI temperature dependent studies,[32,82] as are room temperature coaxial liquid jet measurements for SO_2, HC(O)OH, and $CH_3C(O)OH$ by Schurath et al.[91] Shimono and Koda used a novel impinging flow method to measure a 293 K value of α = 0.2 for SO_2,[92] in reasonable agreement with the

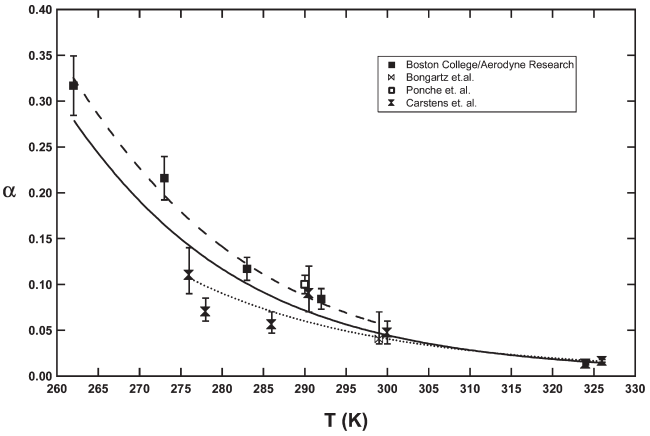

Figure 10. Mass accommodation coefficient α for $NH_3(g)$ on water as a function of temperature. Data points are from the following studies: Boston College/Aerodyne Research, Inc.,[19] Ponche et al.,[42] Bongartz et al.,[71] Carstens et al.[89] In replotting the data of Carstens et al.,[89] we combined and averaged experimental points taken near the same temperature. Dashed lines are fits to the droplet train and coaxial liquid jet data, respectively. The solid line in the figure is the fit to all of the data. (Reprinted with permission from ref 90. Copyright 2004 American Chemical Society.)

droplet train flow reactor results. Similarly, a droplet train flow reactor measurement for phenol at 283 K yielding α = 0.027 ± 0.005[93] is in excellent agreement with the temperature dependent wetted wall flow reactor data of Müller and Heal[94] that yielded values of 0.037 at 278 K and 0.012 at 288 K. Heal et al.[93] also measured α = 0.018 ± 0.005 for aniline at 283 K and reported an upper limit of 0.001 for toluene. Schütze and Herrmann used a suspended droplet flow reactor technique to measure uptake coefficients at 293 K for acetone, 2-butanone, 2,3-butanedione, and 2-oxypropanal;[78] their modeled value of α = 0.0021 (+0.0009/-0.0008) for acetone agrees well with the temperature dependent values measured by Duan et al.[95] shown in Table 2.

More recently, Diévart et al.[95b] measured the temperature dependent uptake between 279 and 293 K of 2,5-dimethylphenol and 2,6-dimethylphenol on aqueous surfaces, using the wetted-wall flow tube technique coupled with UV absorption. At 279 K the value of α for the two molecules was measured to be 1.1×10^{-3} and 5.4×10^{-4}, respectively. The temperature dependence was in good agreement with the critical cluster model of mass accommodation described in section 5.1.

However, not all single temperature measurements are consistent with the data presented in Table 2. For example, Guimbaud et al.[96] have used an innovative technique using radioactive isotopes to prepare gaseous species that can be precisely tracked in aerosol flow reactor studies. They used this method to measure uptake of ^{13}N-labeled HNO_3 on deliquescent NaCl particles, yielding α = 0.5 ± 0.2 at 300 K. This value is several times higher than those for HNO_3 on pure water in the droplet train flow experiments noted above. Whether mass accommodation coefficients on deliquescent salts or other high ionic strength aqueous surfaces can be expected to be equal to those on pure water is discussed further below.

4.2. Mass Accommodation of Water Vapor on Water

The accommodation of water vapor to liquid water surfaces is a critical atmospheric process, playing an important role in the

dx.doi.org/10.1021/cr100360b Chem. Rev. 2011, 111, PR76 - PR109

growth of cloud condensation nuclei into cloud droplets. Because of its importance in cloud physics as well as its fundamental nature, a large number of experimental investigations have been published. The most recent review by Marek and Straub[97] includes 25 published experimental studies of the water condensation (mass accommodation) coefficient and 30 studies of the evaporation coefficient, which is related to the condensation coefficient by microscopic reversibility. An earlier review by Mozurkewich[98] includes studies published prior to 1983. Marek and Straub note that values of α deduced from these experiments range from ~0.001 to 1.0, with experiments involving growing water drops tending to higher values.

Recently, results from several new experiments have been published supporting values nearer the higher end of the range. Shaw and Lamb[75] used an electrodynamic droplet levitation cell to make simultaneous ice nucleation/water droplet evaporation rate observations that yielded a range of $0.04 < \alpha < 0.1$ at ~237 K. Li et al.[99] used a droplet train flow reactor to measure the uptake of $H_2{}^{17}O$ (in small excess) on water droplets that were in equilibrium with the surrounding normal water vapor, yielding a value of 0.17 ± 0.03 at 280 K which increased to 0.32 ± 0.04 at 258 K (see Table 2). In ref 69, the University of Vienna/University of Helsinki collaboration lead by Wagner and Kulmala used precise Mie scattering analyses of the growth of freshly nucleated droplets in an expansion chamber to deduce $0.4 < \alpha < 1.0$ over the temperature range 250−290 K. Results from these two latter studies are shown in Figure 11. Given the precision of these two experiments, it seems clear that mass accommodation values of water vapor on liquid water for temperatures below 290 K must exceed 0.1.

Li et al.[99] and Winkler et al.[69] experiments are further discussed in a collaborative paper between the Vienna/Helsinki group and the BC/ARI group[100] which notes that the differences in deduced values of α may reflect the different state of the water surface in the very near equilibrium saturation droplet train experiments versus the highly supersaturated vapor regimes used in the expansion chamber experiments. The surface of a rapidly growing water droplet under highly supersaturated conditions may be significantly more disordered, enhancing the number of dangling bonds available to interact with incoming species. This effect may also account for the high nitric acid vapor accommodation coefficients ($0.3 \leq \alpha \leq 1.0$) obtained by the Vienna/Helsinki group from expansion chamber experiments on water vapor/nitric acid codeposition.[68]

In a recent Comment, Winkler and co-workers[101] have argued that their higher value for water vapor of $\alpha \approx 1$ should be used in cloud modeling studies, since the same coupled heat- and mass-transfer equations used to deduce α from their droplet growth experiments are used in many cloud physics models. However, this assertion relies on the supposition that the accommodation properties of water droplets at the saturation ratios of 1.3−1.5 used in their experiments[69] are the same as those of water droplets formed at saturation ratios of ~1.01, typical of atmospheric cloud formation.

The tendency for experiments with quasi-static surfaces to yield lower α values than those for dynamically renewed surfaces as noted by Marek and Straub[97] may be due to the accumulation of contaminant surfactant molecules that impede interfacial mass transport. However, there is no guarantee that dynamically renewing the surface by rapid condensation produces the same surface at the molecular scale as flow refreshed surfaces with water vapor pressures maintained very near equilibrium, such as those used in the droplet train flow reactor, wetted wall flow reactor, and coaxial liquid jet techniques.

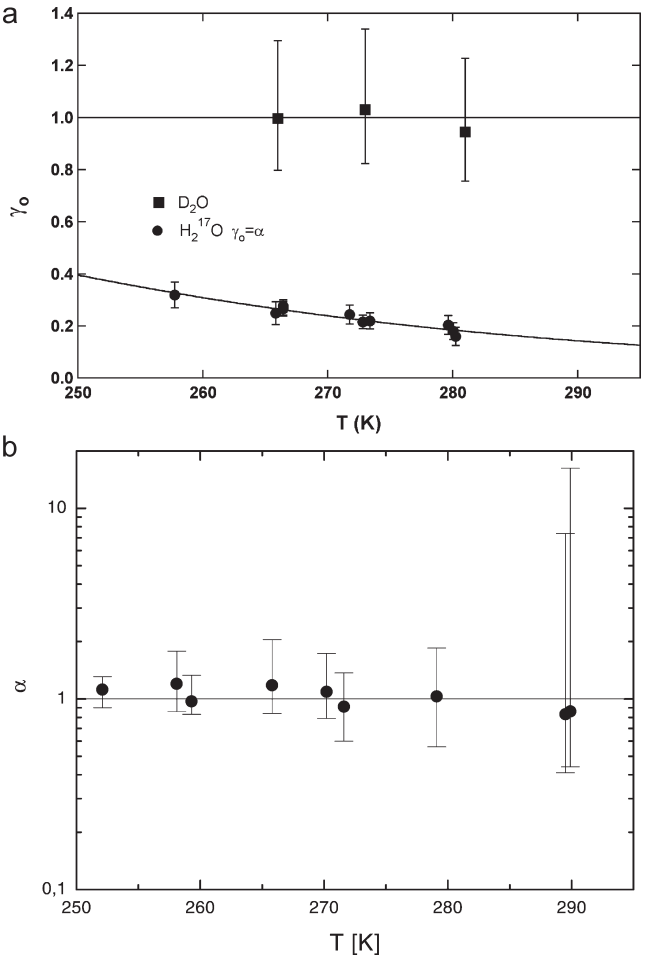

Figure 11. (a) Uptake coefficient γ_o for $H_2O(g)$ and $D_2O(g)$ as a function of temperature obtained by the BC/ARI group. For $H_2O(g)$, γ_o is the mass accommodation coefficient α. For $D_2O(g)$, γ_o is the surface accommodation coefficient S. (Reprinted with permission from ref 99. Copyright 2001 American Chemical Society. (b) Mass accommodation coefficient α for $H_2O(g)$ as a function of droplet temperature obtained by the University of Vienna/University of Helsinki group. For details, see ref 69. (Reprinted with permission from ref 100. Copyright 2004 American Geophysical Union.)

In a recent set of experiments, Cappa et al. measured isotope fractionation occurring during free molecular evaporation from liquid microjets.[102] They found that the isotope ratios of evaporating molecules were significantly different from equilibrium vapor values. These results were interpreted to indicate that there is an energetic barrier to evaporation and that the evaporation coefficient of water (and therefore also the mass accommodation coefficient) is significantly less than unity.[102]

Since the completion of the 2006 review, several new studies of the water vapor mass accommodation on water have been published. In their first set of measurements, the Berkeley group of Saykally and Cohen (Cappa et al.[102]) measured the H/D isotope ratio of evaporating molecules with a mass spectrometer. In subsequent more definitive studies, the Berkeley group measured the evaporative cooling rate of a train of water droplets

dx.doi.org/10.1021/cr100360b Chem. Rev. 2011, 111, PR76 - PR109

formed by the breakup of a water jet injected into vacuum, using Raman thermometry (Smith et al.[102b] and Drisdell et al.[102c]). The Smith et al. experiment reported weak temperature dependence between 245 and 298 K with an average evaporation coefficient value of 0.62 ± 0.09. (By microscopic reversibility the evaporation coefficient and α are equal to each other.) The same method was applied to D_2O by Drisdell et al.,[102c] yielding an evaporation coefficient of 0.57 ± 0.06 for approximately the same temperature range. Drisdel at al.[102d] also measured the evaporation coefficient of a 3 M ammonium sulfate solution, obtaining an evaporation coefficient of 0.58 ± 0.05. Thus, the Berkeley experiments point to an evaporation coefficient = mass accommodation coefficient significantly smaller than 1, indicating a barrier to evaporation and therefore by microscopic reversibility also to mass accommodation. Cappa et al.[102e] developed a theoretical construct based on transition state theory to model their experimental results.

The Vienna/Helsinki group[69b] using their expansion cloud chamber technique remeasured mass accommodation and thermal accommodation coefficients, this time varying the temperature over a range from 250 K to 290 K. With one exception, the experiments were performed at vapor saturation ratios ranging from 1.30 to 1.50. One experiment was performed at the saturation ratio 1.02, more characteristic of the troposphere. They concluded that, for all experimental conditions studied, both coefficients are likely to be unity.

Voigtländer et al.[102f] analyzed droplet growth in a laminar diffusion flow reactor using droplet growth models similar to those of Winkler et al.[69b] They obtained similar results, estimating the mass accommodation coefficient to be greater than 0.3 at 275−277 K.

Single water droplet evaporation experiments were reported by Zientara et al.[102g] in a series of papers culminating in a thorough temperature dependent study. Because the evaporation experiments were conducted at atmospheric pressure, the reported results must be derived using a continuum theory modified by incorporating an effective gas phase diffusivity and an effective thermal conductivity, which is similar to, but they suggest is more complete, than the model used by Winkler et al.,[69a,b] to analyze their expansion cloud chamber growth data. The Zientara et al. temperature dependent evaporation coefficients are in good agreement in both magnitude and temperature dependence with the droplet train mass accommodation coefficients reported by Li et al.[99]

As is evident, the new series of experiments did not resolve the original issue raised by the measurements of Li et al.[99] and Winkler et al.[69a,b] The question still remains, why do some studies yield α_{H_2O} significantly smaller than 1 while others point to a value of α =1. The suggestion has been made recently[102g,h] that the larger values of α obtained by Winkler et al. are due to incomplete representation of the heat and mass transfer in the analysis of their measurements. This suggestion requires further examination.

4.3. Mass Accommodation Measurements with Solubility Constraints

As shown in section 2, due to slow liquid-phase diffusion, gases with relatively low Henry's law constants may saturate the bulk-phase layer near the surface, impeding further uptake. This effect can be counteracted with a rapid reactive sink for the accommodated species in the bulk liquid. Examples of reactive sinks in aqueous liquids include (1) first order, reversible hydrolysis reactions, such as the dissociative ionization of hydrogen halide and nitric acid vapors,[82,83] (2) H^+ and HSO_3^- formation for SO_2,[18,103] and (3) diol formation for aldehydes.[104,105] These processes facilitated several of the measurements of species with low physical Henry's law constants listed in Table 2 by taking advantage of a higher "effective" Henry's law constant, H^*.[106]

In some cases solubility constraints can be circumvented by adding a soluble reactant to enhance second-order kinetic losses of the accommodated species. For SO_2, H_2S, and CO_2 this can be accomplished by raising the pH to scavenge H^+ created in their hydrolysis reactions, increasing their solubility.[32,103] Direct reaction of OH^- with accommodated vapor species such as BrCl[107] and I_2[108] enhances their uptake. Adding a reactive anion such as $S_2O_3^{2-}$, SO_3^{2-}, Br^-, or I^- to scavenge accommodated species such as O_3,[30,49,77,91,109,110] $ClONO_2$,[111] $BrONO_2$,[111] and HOBr[112] is also effective in enhancing uptake.

Uptake coefficient measurements for CO_2 using the coaxial liquid jet technique established a lower limit of α ≥ 0.0001,[91] consistent with bubble train flow reactor measurements using OH^- scavenging that measured a lower limit a factor of 10 smaller.[32] Both lower limits are many orders of magnitude higher than the previously published value.[108]

Katrib et al.[107] used OH^- scavenging in their droplet train flow reactor to deduce a value of α = 0.33 ± 0.18 for BrCl in the temperature range 270−285 K, and Takami et al.[108] used OH^- scavenging with their impinging flow technique to determine that α ≥ 0.1 for I_2 at 293 K.

A variety of techniques have employed $S_2O_3^{2-}$, SO_3^{2-}, or, most frequently, I^- to try to overcome ozone's very low solubility in water. These include (1) wetted wall flow reactor studies by Utter et al.[49] and Müller and Heal[110] that yielded lower limits for α of 0.002 at 276 K and 0.04 at 293 K, respectively; (2) droplet train flow reactor studies by Hu et al.[30] and, much more extensively, by Magi et al.[109] that set a lower limit for α of 0.1 for the temperature range 275−293 K; (3) coaxial liquid jet measurements by Schurath et al.[91] that obtained a value of α = 0.0045 at 298 K but that may have been affected by lower than calculated I^- concentrations;[109] and (4) a suspended droplet flow reactor study by Schütze and Herrmann[77] that measured a lower limit for α of 0.02 at 298 K.

Similarly, Dieber et al.[111] used a droplet train flow reactor to measure uptake of $ClONO_2$ and $BrONO_2$ vapor on aqueous NaBr solutions, using the reaction with Br^- to scavenge accommodated halogen nitrates. These studies yielded values for α at 274.5 K of 0.108 ± 0.011 and 0.063 ± 0.021, respectively. Wachsmuth et al.[112] used radioactively labeled HOBr to measure its uptake on deliquescent NaBr particles near 295 K in an aerosol flow reactor, obtaining α = 0.6 ± 0.2. In this case, surface saturation is not an issue, since the sensitivity of radioactive detection allows extremely small numbers of accommodated molecules to be measured; the role of the liquid-phase Br^- is to produce the labeled Br_2 used to monitor uptake.

As mentioned earlier, the degree to which these measurements of mass accommodation coefficients using high levels of anionic reactants correspond to α values for nearly pure water is uncertain. Recent experimental evidence shows that ionic constituents can change the distribution of interfacial water bonds[113] and the surface tension,[114] possibly influencing mass accommodation mechanisms. Further, as discussed below, there is now clear experimental evidence that concentrations of monovalent anions, including Br^- and I^-, can be enriched at the water/air interface where they are available to react with some trace gases

dx.doi.org/10.1021/cr100360b Chem. Rev. 2011, 111, PR76 - PR109

(see section 4.7).[113,115] As noted in section 2, these surface reactions occur in parallel with mass accommodation, so it is possible that enhanced surface reactions may be mistaken for mass accommodation.

The behavior of ions at the interface of aqueous solutions continues to be an important area of both experimental and theoretical studies. For recent reviews see, for example, Jungwirth and Tobias,[115b] Gopalakrishnan et al.,[115c] Petersen and Saykally,[115d] Jungwirth and Winter,[115e] and Allen et al.[115f] The effect of surface ions on mass accommodation and interfacial chemical reactions remains to be clarified.

4.4. Mass Accommodation of Free Radicals

A number of highly reactive free radicals, including OH, HO_2, NO_3, Cl, ClO, Br, BrO, I, and IO, play major roles in the photochemistry of the troposphere and/or the stratosphere. Because these radicals generally have small Henry's law constants in aqueous solutions[2] and because, under laboratory conditions, surface reactions may compete effectively with mass accommodation, quantifying their mass accommodation coefficients has been difficult. Accurate radical uptake coefficients are necessary to model atmospheric photochemical processes.

Hanson et al. studied OH uptake with a wetted wall flow reactor, obtaining a lower limit for α of 0.0035 at 275 K.[50] Takami et al. used their impinging flow technique to obtain a value of 0.0042 $\pm$ 0.0028 at 293 K and pH 7, measuring values 2 to 3 times higher for pH = 1 and pH = 10−13 surfaces or when benzoic acid is added to scavenge OH.[80] Their measured OH uptake coefficient increased with decreasing gas−liquid contact times, indicating that saturation was still occurring.[80] From these studies it is likely that α for OH is greater than 0.01, although how much greater is unknown. Recent experiments by Laskin et al.[80b] point to a lower limit on α of 0.1 for OH uptake onto deliquesced NaCl particles.

Hanson et al.[50] also studied HO_2 uptake with a wetted wall flow reactor, measuring a lower limit for α of 0.02 by using dissolved $CuSO_4$ to chemically scavenge dissolved HO_2. Mozurkewich et al.[62] and Thornton and Abbatt[116] have used deliquescent salt particles in aerosol flow reactors to investigate HO_2 uptake, also using dissolved Cu(II) to scavenge HO_2. Mozurkewich et al.[62] reported a room temperature lower limit of 0.2 for α on deliquescent ammonium sulfate and lithium nitrate solutions, while Thornton and Abbatt[116] reported α = 0.5 $\pm$ 0.1 for Cu(II)-doped deliquescent ammonium sulfate particles. From these studies it is clear that the mass accommodation coefficient of HO_2 on aqueous surfaces is large and that heterogeneous loss on aerosol particles and cloud droplets may be a significant atmospheric sink for this radical.[116]

In more recent experiments Taketani et al.[116b,c] measured the uptake coefficient of HO_2 as a function of relative humidity on $CuSO_4$ doped NH_4SO_4, NaCl, and KCl. At 75% RH the uptake coefficient for NH_4SO_4, NaCl, and KCl was about 0.5, decreasing significantly with humidity.

Rudich et al.[117] used the wetted wall flow reactor technique to investigate the uptake of the NO_3 radical on pure water and sodium salt solutions. Uptake with pure water was reactive, presumably producing OH and HNO_3. The low uptake coefficient (0.0002 $\pm$ 0.0001) at 273 K indicated saturation effects. Reactive uptake with sodium salt anions scaled with anion concentration, indicating electron-transfer reactions were taking place to produce NO_3^-. A detailed analysis of the uptake kinetics indicated that α at 273 K was greater than 0.04. Schütze and Herrmann used their suspended droplet flow reactor technique to study the uptake of NO_3 radicals at room temperature on aqueous solutions of the pH sensitive dye Alizarin Red S and NaCl.[118] Uptake was detected by the change in optical absorption of the dye, due to acidification from HNO_3 product formation, or by the nitrate ion absorption at 235 nm in the salt or pure water droplets. The data from both experiments were consistent, yielding a measured mass accommodation coefficient of 0.0042 (+0.002.2/−0.0017) at 293 K.[118] This value is an order of magnitude lower than the lower limit at 273 K determined by Rudich and co-workers;[111] both studies are consistent with a lower limit of 0.002 at 293 K measured by Thomas et al. using a denuder technique.[119] Some of the difference between the wetted wall flow reactor and suspended droplet flow reactor studies is probably due to the lower temperature of the former, since mass accommodation coefficients are often observed to increase with decreasing temperature and some may be due to saturation effects in the near surface layer of the suspended droplet, because the droplet surface is not continuously renewed.

Despite the strong interest in atomic halogen and halogen oxide radical reactions in the marine boundary layer and other tropospheric regions, very little is known about their interactions with aqueous surfaces. Motivated by the major role chlorine- and bromine-containing radicals play in stratospheric ozone depletion, a few studies have been reported involving halogen radical uptake by concentrated sulfuric acid surfaces.[2] However, these studies, discussed below, are less than definitive, and more thorough experiments are required to better quantify loss of these species on stratospheric aerosol surfaces.

4.5. Reactive Uptake by Liquid Water and Salt Solution Surfaces

As noted above, in a number of cases, reversible reactions of atmospheric trace gases with liquid water enhance their effective solubility. Other trace species react irreversibly with liquid water, either in the bulk liquid or at its surface. If the mass accommodation coefficient is not rate limiting, the reaction fast, and the solubility low, reactive uptake can control the gas−liquid surface interaction (see eq 16). One important example is N_2O_5, which reacts with liquid water to form two HNO_3 molecules.[120] Another case, noted above, is NO_3 uptake by relatively pure water surfaces.[117]

4.5.1. Uptake of N_2O_5. Uptake of N_2O_5 on water and aqueous salt solutions has been studied using droplet train flow reactors[120,121,122] and a suspended droplet flow reactor.[77] Uptake of N_2O_5 has also been measured on deliquescent salt particles in aerosol flow reactors[61,123,124] and in aerosol chambers.[66,125] Measured reactive uptake coefficients (γ) show mild negative temperature dependences. Higher γ values, in the range 0.1−0.04 from studies by Van Doren et al.,[120] Mozurkewich and Calvert,[123] and Hu and Abbatt,[61] are consistent with other results when temperature and relative humidity (RH) effects are factored in. Most recently, Thornton and Abbatt used an aerosol flow reactor to study uptake at 295 K on submicrometer artificial sea salt aerosols as a function of relative humidity, obtaining uptake coefficients between 0.022 and ~0.03 for RH values between 43 and 70%.[124]

The lower N_2O_5 uptake values from the LP group appear to have a much less pronounced temperature dependence and are inconsistent with other measurements.[121,122] Aerosol chamber measurements at low nitrate loadings are generally consistent

dx.doi.org/10.1021/cr100360b Chem. Rev. 2011, 111, PR76 - PR109

with the higher range of values.[66,125] The suspended droplet value was very low due to the build up of nitrate products that inhibit further reaction.[77] Uptake on alkali halide salt solution surfaces is only marginally higher than that on water, but gaseous $ClNO_2$ (for NaCl solutions), $BrNO_2$, Br_2, and HONO (for NaBr solutions), and I_2 (for NaI solutions) products were observed.[122]

Experiments with N_2O_5 continue to be central to understanding a variety of gas uptake processes. Most of the recent experiments with N_2O_5 were focused on understanding the effects of surface organics on the uptake of gas phase species by aqueous surfaces. As such, these studies are surveyed in section 4.9.

4.5.2. Uptake of HONO. Nitrous acid, HONO, is an important atmospheric free radical reservoir, photodissociating to OH + NO. Bongartz et al.[126] performed uptake measurements with two independent techniques, the coaxial liquid jet flow reactor and the droplet train flow reactor. With a surface temperature of ~245 K, the droplet train technique yielded $0.045 < \gamma < 0.09$, while the liquid jet operating at a surface temperature of 297 K yielded $0.03 < \gamma < 0.15$. Mertes and Wahner[127] used the coaxial liquid jet technique to measure $0.004 < \gamma < 0.04$ at 278 K. Harrison and Collins[128] performed aerosol flow reactor experiments on deliquescent sodium chloride and ammonium sulfate droplets at 279 K and 85% relative humidity, obtaining reactive uptake coefficients for HONO of 0.0028 ± 0.0015 and 0.0028 ± 0.0006, respectively. These measurements are probably subject to significant surface saturation. Since HONO uptake by liquid water involves hydrolysis, an increase in Henry's law solubility with decreasing temperature may be offset by a decreasing hydrolysis rate constant, leaving the uptake coefficient's temperature trend uncertain. Because of various constraints, these measured uptake coefficients do not correspond to the mass accommodation coefficient. Recent studies of HONO are focused on photochemical interactions, as discussed in Kolb et al.[13b]

4.5.3. Uptake of $ClONO_2$ and $BrONO_2$. A variety of chloro and bromo nitrogen oxide species can be formed by heterogeneous and homogeneous reactions in the marine atmosphere, and significant experimental effort has been expended to characterize their heterogeneous interactions with both dry and deliquescent salt particles. Some of the salient uptake results on alkali salt solutions simulating deliquescent salt aerosol particles are presented in the following paragraphs. More detailed discussions can be found in reviews by Rossi[129] and the NASA Atmospheric Kinetics Evaluation Panel.[2]

Deiber et al.[111] measured uptake coefficients for $ClONO_2$ and $BrONO_2$ on pure water as well as NaCl and NaBr solutions using a droplet train flow reactor. Reactive uptake coefficients for $ClONO_2$ of ~0.025 on water and 0.1 M NaCl solutions were essentially identical for temperatures in the 275−285 K range. $BrONO_2$ reactive uptake coefficients on water and 0.1 M NaCl solutions were also essentially identical, but they varied from ~0.024 at 273 K to ~0.040 at 280 K. Uptake of $ClONO_2$ on NaBr solutions produced gas-phase BrCl and Br_2, while uptake of $BrONO_2$ produced gas-phase Br_2. Uptake coefficients varied as the square root of the Br^- concentration. As noted above, these data were used to derive values for the mass accommodation coefficients.

4.5.4. Uptake of $ClNO_2$, $BrNO_2$, and ClNO. The reactive uptake of $ClNO_2$ and $BrNO_2$ on aqueous alkali halide solutions has been extensively studied using a wide range of techniques.[2] Behnke, George, and co-workers used droplet train and wetted wall flow reactor techniques to investigate the reactive uptake of $ClNO_2$ on aqueous solutions.[122,130−132] Droplet train flow reactor experiments from 268 to 279 K demonstrated that the reactive uptake coefficient on pure water is $<1 \times 10^{-5}$.[131] Wetted wall flow reactor studies from 279 to 292 K on pure water and on solutions of very low sodium halide concentrations all yielded reactive uptake coefficients in the 10^{-6} range, with typical values of $(4.84 \pm 0.13) \times 10^{-6}$ at 291 K,[130] 3.41×10^{-6} at 276.6 K, 4.27×10^{-6} at 282.2 K, and 4.48×10^{-6} at 287.4 K.[132] The uptake exhibits no significant temperature dependence. This team has also used wetted wall flow reactor techniques to investigate the reactive uptake of $BrNO_2$ on aqueous solutions from 276 to 298 K.[122,132] Measured reactive uptake coefficients range from 1 to 3.5×10^{-6} with a small positive temperature dependence.

Reactive uptake coefficients for $ClNO_2$ and $BrNO_2$ are significantly increased when NaBr and NaI are added to water, with higher uptake occurring as the concentration of NaBr and NaI is increased.[122,131−133] In contrast, adding NaCl actually decreases uptake.[130] Uptake coefficients measured for $ClNO_2$ on NaBr solutions are of order 10^{-5}, rising to the 10^{-3} range for NaI solutions. $BrNO_2$ uptake coefficients on NaBr solutions range from $\sim 10^{-5}$ to $\sim 10^{-4}$, while uptake by NaI solutions ranges up to $\sim 4 \times 10^{-3}$.[122,133]

Scheer et al.[134] used droplet train and wetted wall flow reactor measurements to determine reactive uptake of ClNO by water and NaCl solutions as a function of pH over the temperature range 273−293 K. Measured uptake coefficients show a weak negative temperature dependence ranging from 0.012 at 273 K to 0.0058 at 293 K. The reaction was determined to be base catalyzed, producing HONO.

4.5.5. Uptake of Halocarbonyls. Another class of gaseous compounds where solubility constraints are encountered and reactive uptake is important is the halocarbonyls created by atmospheric oxidation of hydrochlorocarbon solvents and hydrofluorocarbon/hydrofluorochlorocarbon replacement compounds for chlorofluorocarbon compounds (CFCs) regulated by the Montreal Protocol. The key issue here is the atmospheric fate of these halocarbonyls. The question is whether uptake by and hydrolysis in cloud and aqueous aerosol droplets is an efficient atmospheric sink. The BC/ARI group and the LP group have investigated the uptake of carbonyl halides (CCl_2O and CF_2O) and haloacetyl halides (CCl_3CClO, CF_3CClO, CF_3CFO) on water droplets using combinations of droplet train flow reactor, bubble column flow reactor, and bulk liquid kinetics techniques.

The BC/ARI group used droplet train methods to determine that the reactive uptake coefficients of these halocarbonyls were all less than 5×10^{-4} except at high pH, where OH^- effectively catalyzes their hydrolysis.[135] Using liquid-phase detection with their droplet train flow reactor, Mirabel and co-workers did detect measurable uptake for each of these species, and they derived somewhat higher uptake coefficients.[136,137] They did not study CCl_2O. Some of the uptake measured in their experiments may have been due to an artifact caused by trace halide vapor carried with the droplets into the reservoir where the liquid droplets are collected. For higher uptakes, this carry-through is small enough to be neglected, and with gas-phase detection it can be minimized and/or corrected by monitoring the loss of an insoluble tracer gas in the flow tube.[19,138] However, for liquid-phase trace species product detection, such a correction is not possible and this droplet "piston" effect may cause an overestimate of the trace gas uptake by the droplets.

dx.doi.org/10.1021/cr100360b Chem. Rev. 2011, 111, PR76 - PR109

To better study the relatively slow uptake of these less soluble gases, the BC/ARI group developed an apparatus in which a train of bubbles containing the trace gas is driven through a column of the liquid of interest, allowing much longer gas−liquid interaction times.[45,46] (See section 3.2.) The BC/ARI group used the initial vertical bubble column apparatus[46] to reinvestigate the uptake of the carbonyl halides and haloacetyl halides originally studied with the droplet train technique.[139] Since the Henry's law constants for these compounds are not generally known, both the Louis Pastuer group[136,137] and the BC/ARI group[135,139] reported results in terms of $H(k^{1/2})$ (see eq 14), where k is the first-order liquid-phase hydrolysis rate constant. The BC/ARI values measured with the bubble column apparatus were significantly smaller by factors ranging from about 5 to 100 than the LP group droplet train results.[139] The BC/ARI results for CCl_2O, where H and k had been previously determined by bulk techniques, were in good agreement with previous measurements.[140,141]

Even though there were quantitative differences, uptake coefficients measured by both groups indicate these organic halocarbonyl compounds will be efficiently removed from the atmosphere by cloud scavenging in the troposphere and they will not persist long enough in the atmosphere to contribute to stratospheric ozone depletion.[142] However, the haloacetic acids created by the hydrolysis of the three haloacetyl halides studied have long atmospheric lifetimes and will be deposited onto the surface, where they may cause undesirable ecosystem effects.[143]

4.6. Uptake by Aqueous Acid Solutions

Trace gas uptake on binary sulfuric acid/water and ternary sulfuric acid/nitric acid/water aerosol droplets plays an important role in stratospheric chemistry and can also be important in the polluted troposphere, where photo-oxidation of gaseous sulfur compounds can, under some conditions, produce high enough sulfuric acid vapor concentrations to trigger binary nucleation with water vapor.

In the stratosphere, acid aerosols are an important sink for HNO_3, as well as N_2O_5, which hydrolyzes to produce HNO_3

$$N_2O_5 + H_2O \rightarrow 2HNO_3 \quad (26)$$

The uptake of these nitrogen oxide reservoir species lowers the amount of gas-phase reactive nitrogen oxide species (NO, NO_2, NO_3) and produces ternary acid solutions. The uptake of chlorine and bromine reservior species such as HCl, HOCl, HBr, and HOBr can reduce the level of reactive halogen radicals, and the uptake of the mixed reservoir species, $ClONO_2$ and $BrONO_2$, reduces the level of both reactive halogen species and nitrogen oxide species. On the other hand, second-order, bulk-phase heteogeneous reactions between reservoir species, such as

$$ClONO_2 + HCl \rightarrow Cl_2(g) + HNO_3 \quad (27)$$

$$HOCl + HCl \rightarrow Cl_2(g) + H_2O \quad (28)$$

$$HOBr + HCl \rightarrow BrCl(g) + H_2O \quad (29)$$

$$BrONO_2 + HCl \rightarrow BrCl(g) + HNO_3 \quad (30)$$

produce easily photolyzed halogen molecules that quickly transform into ozone-destroying atomic halogen and halogen oxide radicals. These reactions are generally mediated in the stratosphere by the uptake of the non-HCl reactant, except for the HOCl reaction, which is driven by the hydrolysis of $ClONO_2$ noted below. Furthermore, hydrolysis reactions of some reservoir compounds with water in acid aerosols produce much more labile halogen compounds:

$$ClONO_2 + H_2O \rightarrow HOCl(g) + HNO_3 \quad (31)$$

$$BrONO_2 + H_2O \rightarrow HOBr(g) + HNO_3 \quad (32)$$

In the troposphere, interactions of sulfuric acid and acid sulfate aerosol droplets with neutralizing NH_3 and some volatile organic species, such as HCHO, are important. The mass accommodation of water vapor on sulfuric acid aerosols may also impact the growth rate of cloud condesation nuclei in the troposphere and sufuric acid droplets in the stratosphere. Uptake data for the processes described above will be summarized in this subsection.

4.6.1. Uptake of HNO_3 and HCl. The uptake kinetics of the gaseous acid species HNO_3 and HCl on aqueous sulfuric acid are dependent on the H_2SO_4 concentration. As the H_2SO_4 concentration increases toward the normal stratospheric concentrations of 60−80 wt %, the activity of the remaining water decreases rapidly and the ability of the weaker gaseous acids to dissociatively dissolve falls sharply. This results in effective Henry's law constants for acid gases that are sharply reduced with increased H_2SO_4 concentration.

A droplet train uptake study of HNO_3 on 73 wt % sulfuric acid yielded a mass accommodation coefficient of 0.11 ± 0.01,[120] illustrating that HNO_3 uptake on most stratospheric sulfuric acid particles will be relatively efficient, especially since colder surfaces can be expected to have higher accommodation rates. Knudsen cell uptake studies on 97 wt % sulfuric acid at room temperature and 75 wt % sulfuric acid at 220 K obtained only lower limits due to saturation effects.[2]

Uptake of HNO_3 by submicrometer deliquescent sea salt or NaCl particles was studied by Guimbaud et al.[120b] and more recently by Saul et al.[120c] Measured uptake coefficients are in the range 0.1−0.5.

Droplet train experiments by the BC/ARI group yielded uptake coefficients for HCl on sulfuric acid over the concentration range 39−69 wt % and the temperature range 330−283 K.[138,144] Measurements on acid solutions with concentrations less than 50 wt % were anlyzed to yield a mass accommodation coefficient for HCl and combined with the BC/ARI pure water results[82] to produce a plot of α on relatively dilute aqueous sulfuric acid solutions and water as a function of temperature. These data are reproduced in Figure 12 and show a smoothly varying curve that increases from less than 0.2 at 287 K as the temperature decreases, reaching a plateau of 1.0 near 240 K. However, Hanson and Lovejoy[145] assigned a value of α = 0.75 ± 0.2 on 26 wt % sulfuric acid at 272 K from an aerosol flow reactor study where HCl was scavenged by reaction with excess HOCl. This value is shown in Figure 12 as a solid triangle. Since the other data in Figure 12 predict a value of α = 0.3 ± 0.1 at this concentration, there is a disagreement between the two results. The difference might be due to a fast surface reaction between HCl and HOCl. While it is difficult to distinguish between mass accommodation and surface reactions, since both scale with droplet surface area, Hanson and Lovejoy state that their experiment does distinguish the two processes. They present uptake data as a function of particle radius, from which they conclude that, for particles <0.5 μm, the HCl uptake is volume limited and surface specific reactions do not need to be taken into account. (See section 2 and the discussion below.)

dx.doi.org/10.1021/cr100360b Chem. Rev. 2011, 111, PR76 - PR109

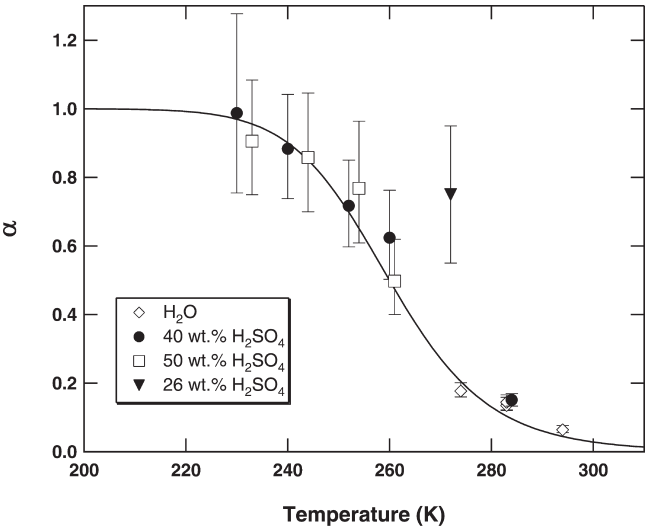

Figure 12. Mass accommodation coefficient, α, for HCl on water and dilute aqueous acid solutions as a function of temperature: (open diamonds) water from refs 82 and 144; (filled circles) 40 wt % sulfuric acid and (open squares) 50 wt % sulfuric acid from ref 138; (filled triangle) 26 wt % sulfuric acid from ref 145.

The solubility of HCl in sulfuric acid droplets under stratospheric conditions is a critical parameter in determining the effectiveness of the activation reactions for the halogen reservior species listed above (reactions 27−30).[2,146] Robinson et al.[138] also present data on the Henry's law constant for HCl in sulfuric acid derived from analysis of the time dependence of HCl uptake measurements as a function of acid concentration and temperature. These data are shown to be fully consistent with a variety of other measurements of HCl solubility in sulfuric acid, except at the highest acid concentration studied (69 wt %), where the BC/ARI group measured uptake in excess of that predicted from extrapolation of *H* from lower acid concentrations. The BC/ARI group suggested that the additional HCl uptake observed is due to the reaction of HCl with sulfuric acid at very high ionic strengths to form cholorosulfonic acid, HSO_3Cl.[138]

The detailed dynamics of HCl (and HBr) interactions with 52.5−70.5 wt % D_2SO_4 at 213 K have been investigated by Nathanson and co-workers using molecular beam scattering techniques.[81] The H/D exchange fraction, which they equate to the aproximate HCl fraction that dissolves in the acid, falls steadily as the acid concentration increases. Their derived solubility also falls with increasing acid concentration, until ∼65 wt %, where it starts to rise. This is consistent with the rise in solubility for 69 wt % acid detected in the droplet train experiments.

4.6.2. Uptake of N_2O_5, $ClONO_2$, and $BrONO_2$. Reactive uptake on sulfuric acid solutions can be sensitive to the mass accommodation coefficient, the Henry's law constant, and the bulk reaction rate, all of which generally vary with both temperature and acid concentration. The hydrolysis uptake reactions for N_2O_5 and $ClONO_2$ on sulfuric acid (eqs 26 and 31) have also been studied by the BC/ARI group as a function of temperature for acid concentrations between 39 and 69 wt % using the droplet train flow reactor method.[147] The results obtained were generally consistent with studies using other techniques, including wetted wall flow reactors, aerosol flow reactors, and Knudsen cell reactors, in other laboratories (see ref 147 for references and data plots). The N_2O_5 hydrolysis reactive uptake coefficient remains relatively large (∼0.05−0.15) over the full range of temperatures and acid concentrations studied, while γ for $ClONO_2$ reactive uptake starts at ∼0.2 for 40 wt % acid at lower temperatures and decreases to as low as ∼0.0001 for 75 wt % acid. These combined data sets were used to produce a phenomenological model of these key hydrolysis reactions that can be used to predict their rates for the full range of stratospheric conditions.[2,146] Most recently, Wagner et al. presented results from an aerosol chamber study designed to determine the uptake coefficient of N_2O_5 on supercooled ternary $H_2SO_4/H_2O/HNO_3$ solutions at 193.6 K, characteristic of polar winter stratospheric conditions.[148] They deduced uptake coefficients of ∼0.04 for nitric acid/sulfuric acid concentrations of 14:28, 18:25, and 31:17 wt %, respectively, with measured values falling off to 0.016 at 45:6 wt %, as expected from saturation due to the common (nitrate) ion effect.[148]

Hanson and co-workers have studied the very important hydrolysis reaction of the reservoir species $BrONO_2$ on sulfuric acid surfaces using both wetted wall and aerosol flow reactor techniques,[23,149,150] demonstrating that, unlike $ClONO_2$ reactive uptake, γ for $BrONO_2$ remains very large (∼0.8) up to acid concentrations of over 70 wt % before falling off at higher acid concentrations. Hanson has fit the data from these studies to a model based on eq 16 in section 2, obtaining a value of $\alpha = 0.80$. This model can be used to predict the value of γ over the range of stratospheric conditions.[2,150] Hanson et al.[149] also obtained data on the reactive uptake of $BrONO_2$ with HCl, but given the rapidity of the $BrONO_2$ hydrolysis reaction which produces HOBr, the halogen activation reaction, HOBr + HCl, is the more atmospherically important process.

4.6.3. Reaction of HOBr + HCl in Sulfuric Acid. The second-order heterogeneous reaction of HOBr + HCl in sulfuric acid solutions is difficult to represent by a single reactive uptake coefficient because, depending on the specific stratospheric conditions, either HOBr or HCl might be in excess in the acid solution. Thus, reactive uptake studies with one or the other species in excess will not necessarily represent stratospheric reality. Flow reactor uptake studies by Hanson and Ravishankara,[149] Hanson et al.,[23] and Waschewsky and Abbatt[151] have yielded valuable data on the bulk second-order rate constant for the reaction of HOBr and HCl for part of the relevant range of stratospheric conditions. However, significant disagreement remains between the different measurements, particularly on the Henry's law solubility of HOBr. Therefore, unlike the cases of $ClONO_2$ + HCl and HOCl + HCl,[2,146] no definitive model currently exists that can be used to reliably predict uptake coefficients for this important process.

4.6.4. Uptake of Ammonia. The reactive uptake of ammonia by sulfuric acid solutions to produce NH_4^+ and HSO_4^- or SO_4^{2-} is the major neutralization process for atmopheric acid aerosols. The reaction has been studied in a droplet train flow reactor by the BC/ARI group[19,156] and using aerosol flow reactors by Robbins and Cadle,[152] Huntziker et al.,[153] McMurry et al.,[63] Daumer et al.,[154] and, most recently, Hanson and Kosciuch.[155] The most recent measurements[156,157] agree that the reactive uptake coefficient reaches unity at acid concentrations above ∼50 wt %. The aerosol flow reactor data of Hanson and Kosciuch[155] find that $\gamma \approx 1$ down to their lowest acid concentration of 16 wt %, while the droplet train data show a smooth falloff from ∼50 wt % acid to the pure water values of α shown in Figure 10.[90] This disagreement between aerosol and droplet train

dx.doi.org/10.1021/cr100360b *Chem. Rev.* 2011, 111, PR76 - PR109

flow reactor studies is similar to that noted in connection with the HCl studies from the same researchers. The possible causes for this discrepancy at lower acid concentrations have been the subject of recent literature debate;[90,155,157] a clear resolution will require further investigation.

4.6.5. Uptake of Water Vapor. Acid sulfate aerosols can grow by the uptake of water vapor, sulfuric acid vapor, or sulfur trioxide, SO_3, which is the anhydride of sulfuric acid vapor. The BC/ARI group investigated the uptake of water vapor as a function of temperature on 50, 70, and 82 wt % sulfuric acids solutions, using the droplet train technique to monitor the uptake of isotopically labeled $H_2{}^{17}O$.[158] Measured mass accommodation coefficients ranged from 0.4 to 0.9, increasing with acid concentration and decreasing at higher temperatures.

4.6.6. Uptake of Sulfuric Acid Vapor and Related Compounds. In a collaboration between the ARI group and the Molina group at the Massachusetts Institute of Technology (MIT), the uptake of sulfuric acid vapor on liquid sulfuric acid was measured using a wetted wall flow reactor.[159] Measurements for acid concentrations between 73 and 98 wt % yielded $0.43 < \alpha < 1.0$ at 303 K. The wetted wall reactor technique is subject to gaseous diffusion restrictions at high uptake rates, so these measurement are consistent with $\alpha = 1$, yielding the upper limit quoted above. Hanson used an aerosol flow reactor with chemical ionization mass spectrometric detection to measure the mass accommodation coefficient of sulfuric acid vapor on submicrometer sulfuric acid droplets ranging between 21.6 and 65.8 wt %.[160] Uptake coefficients varying between 0.64 and 1.34 were obtained, with many values consistent with 1.0 within the assessed error bars.

The above results on liquid sulfuric acid are consistent with the very high sulfuric acid vapor mass accommodation coefficients measured by Jeffferson et al.[161] on room temperature ammonium sulfate particles in an aerosol flow reactor, but they contradict a value of $0.02 < \alpha < 0.09$ for 42.5 wt % acid obtained in a photochemical aerosol reactor by Van Dingenen and Raes.[162]

The ARI group also collaborated with the Molina group on wetted wall flow reactor studies to measure the reactive uptake coefficient of SO_3 on 78−92 wt % acid at 300 K, obtaining a lower limit, $\gamma > 0.7$.[163]

In addition to studying the uptake of sulfuric acid vapor with his aerosol flow reactor/chemical ionization mass spectrometer technique, Hanson also studied the uptake of methane sulfonic acid at room temperature on submicrometer sulfuric acid droplets.[160] Measured uptake coefficients for acid wt % values between 7.2 and 47.0 varied between 0.69 and 1.18, with most values being consistent with 1.0 within the assessed error bars. There was an apparent sharp drop-off in uptake above 50 wt % acid, with values of 0.04 (+0.06/−0.04) and 0.25 (+0.05/−0.04) measured for 56.0 and 65.0 wt %, respectively. Hanson suggests that his large uptake coefficients measured for CH_3SO_3H at low acid concentrations (7.2−20 wt %) are not compatible with those of the two temperature dependent studies on pure water obtained in the droplet train flow reactor studies[78,79] described above and shown in Table 2.

4.6.7. Uptake of Formaldehyde. The uptake of formaldehyde, an oxidation product of methane and other volatile organic compounds, on acid surfaces has been of interest for stratospheric and upper tropospheric photochemistry.[164] This process has been studied using Knudsen call techniques by Tolbert and co-workers[56,164] and by the BC/ARI group using the droplet train technique.[104,105] Droplet train studies by Jayne et al.[105] report uptake measurements for single acid/water and ternary solutions (0−85 wt % H_2SO_4 and 0−54 wt % HNO_3) over the temperature range 241−300 K. Measured uptake coefficients vary from 0.0027 to 0.027, increasing with H^+ activity[105,164] and with increasing pH above 7.[104]

Reversible uptake is solubility limited through reaction to form $H_2C(OH)_2$ and CH_3O^+. A model of the uptake kinetics developed by Jayne et al.[105] is consistent with $\alpha = 0.04 \pm 0.01$ for all compositions. A chemisorbed surface complex dominates uptake at 10−20 wt % H_2SO_4, and CH_3O^+ formation dominates above 20 wt % according to Tolbert et al.,[164] Jayne et al.,[105] and Iraci and Tolbert.[56] The formation of a surface complex allows γ to greatly exceed α for strong acidic and basic solutions. Low temperature (197−214 K) uptake studies by Iraci and Tolbert[56] confirm that uptake is solubility limited with uptake coefficients in the 10^{-3} to 10^{-2} range even at low temperatures. The uptake model for acid solutions presented by Jayne et al.[105] can be used for predictions over a wide range of atmospheric conditions.

4.6.8. Uptake of Reactive Radicals. Reactive radicals can also be scavenged by acid aerosol particles. Hanson et al.[50] used a wetted wall flow reactor to determine a lower limit of $\gamma > 0.07$ for OH on 28 wt % sulfuric acid at 275 K, while Cooper and Abbatt[165] used similar techniques to obtain $\gamma > 0.2$ for 45−65 wt % acid between 220 and 230 K and for 96 wt % acid at 230 and 298 K. Gershenzon et al.[166] used a coated insert flow reactor to measure $\gamma \approx 1$ on ∼96 wt % acid at 298 K. The hypothesized uptake reaction is

$$OH + HSO_4{}^- \rightarrow H_2O + SO_4{}^{2-} \qquad (33)$$

Cooper and Abbatt[165] reported what they assumed to be a self-reaction uptake coefficient for HO_2 of $\gamma = 0.025 \pm 0.005$ on 55 wt % sulfuric acid at 223 K, while, in more recent work, Thornton and Abbatt[116] used an aerosol flow reactor with sensitive chemical ionization mass spectrometric detection to determine a lower limit for the mass accommodation coefficient of $\alpha > 0.8 \pm 0.3$ for room temperature, 35 wt % sulfuric acid by doping the acid with Cu(II) to scavenge accommodated HO_2. For undoped acid, they measured a reactive uptake coefficient of $\gamma < 0.01$. Gershenzon et al.[167] measured a lower limit for HO_2 uptake of 0.2 on 80 and 96 wt % sulfuric acid at 243 K, while Hanson et al.[50] obtained a lower limit of 0.07 on 28 wt % acid at 275 K.

Martin et al.[168] investigated the uptake of Cl and ClO on sulfuric acid in a flow reactor between 221 and 296 K, measuring Cl uptake coefficients between 0.00003 and 0.0007 and ClO uptake coefficients between 0.00002 and 0.0002. Both coefficients varied as the temperature and acid concentration changed. HCl was detected as a product of both reactions. However, Abbatt[169] measured an upper limit of γ for ClO of 0.00001 for 60 and 70 wt % sulfuric acid at 213 K. Both studies indicate that ClO uptake on sulfuric acid is slow and, therefore, probably not an important stratospheric loss mechanism for this radical.

4.7. Trace Gas-Surface Reactions in the Aqueous and Aqueous Acid Interface

Reactions in the interfacial surface layer compete with mass accommodation and subsequent bulk liquid-phase reaction,[26] as illustrated by eq 18 in section 2. In bulk experiments, it is difficult to resolve accommodation from enhanced surface reactivity, since surface diffusion and subsequent surface reaction must be fast to compete with the very rapid desorption of thermally accommodated molecules. The millisecond time resolution of the droplet train technique has proven to be fast enough to

dx.doi.org/10.1021/cr100360b Chem. Rev. 2011, 111, PR76 - PR109

separate uptake driven by fast interfacial reactions from slower bulk-phase controlled processes. Examples for several types of surface reactions are described below.

4.7.1. Reversible Chemisorption. In the early BC/ARI uptake studies of SO_2, uptake on aqueous surfaces was observed at low pH that was significantly larger than that expected from bulk processes limited by solubility restrictions. This observation, coupled with time-resolved uptake studies and uptake measurements as a function of SO_2 gas-phase density, led the BC/ARI group to attribute the uptake to formation of a chemisorbed interfacial HSO_3^- species.[103,170] Subsequent nonlinear spectroscopic studies also detected a surface adsorbed species.[171]

The BC/ARI droplet train flow reactor studies of CH_2O[105] and NH_3[156] uptake by sulfuric acid solutions also revealed chemisorbed CH_3O^+ and NH_4^+ species at the vapor/aqueous acid interface. Similarly, droplet train uptake studies of glyoxal by the LP group indicate that a $CHOCHOH^+$ species may explain the increased rate of uptake they observed in experiments with acidic solutions.[85]

4.7.2. Reactive Chemisorption. The BC/ARI group observed fast surface adsorption, followed by irreversible reaction, in the interaction of Cl_2 with aqueous surfaces containing Br^- or I^- and of Br_2 with aqueous solutions containing I^-.[30] The fast initial uptake observed in these systems was attributed to the formation of a trihalide anion, e.g., $ClCII^-$, at the gas−water interface. This surface complex presumably reacts, just as it does in the bulk, to form the diatomic interhalide, e.g. ICl, plus a lighter halide ion, e.g. Cl^-.

The LP group observed a very similar fast surface adsorption/reaction in the interaction of $ClNO_2$ with aqueous I^-.[131] They also observed a fast surface reaction between BrCl and I^-; however, they did not observe measurable surface complex formation when BrCl interacts with aqueous Br^- or OH^-.[107]

Finlayson-Pitts and co-workers invoked efficient surface reactions between OH and Cl^- at the surface of deliquescent salt particles to explain aerosol chamber production of Cl_2.[33] This same group also demonstrated that the level of Br_2 produced in aerosol chamber studies of the reaction of O_3 with deliquescent NaBr particles is an order of magnitude larger than can be explained by known gas-phase and bulk liquid reactions, again suggesting the participation of fast liquid surface reactions.[67]

The possibility of fast interfacial reactions involving halide anions is supported by recent experimental observations of excess I^-[115] and Br^-[115] at the interface of aqueous alkali halide solutions. These spectroscopic studies qualitatively confirm molecular dynamics studies that show significant enhancement of I^- and Br^- in simulations of the air−water interface.[67,173,174]

4.7.3. Surface Isotopic Exchange. Droplet train flow reactor studies in the BC/ARI laboratories have also demonstrated that D/H isotopic exchange can take place rapidly on aqueous surfaces. Uptake studies with deuterated ethanol and acetic acid clearly indicate that for both molecules the observed uptake/conversion rate of the deuterated species is significantly higher than the uptake (mass accommodation) rate for the nondeuterated species.[34] Since it is expected that the mass accommodation rate is relatively insensitive to isotopic composition, it follows that the enhanced uptake for the deuterated species is due to isotopic exchange reactions at the interface. The results indicate that a weakly adsorbed near surface state interacts with near surface ions to achieve D/H exchange. In the case of acetic acid, the 273 K uptake coefficient increases from about 0.07 to 1.0. The enhancement of the ethanol uptake rate is modest at near neutral pH but grows by a factor of 2 at high and low pH values where higher H^+ or OH^- activities drive the isotope exchange process.[34]

This same rapid interfacial D/H exchange occurs for D_2O interacting with water[99] and sulfuric acid surfaces.[158] For uptake on liquid water, the BC/ARI group observed that the D_2O uptake coefficient is unity over the experimental temperature range, while the $H_2{}^{17}O$ uptake, representing the mass accommodation coefficient, varies from 0.32 to 0.17.[99] On 70 wt % sulfuric acid, uptake of $H_2{}^{17}O$ at 285 K due to mass accommodation is 0.65 ± 0.06, while the uptake coefficient for D_2O is 0.94 ± 0.10. These results indicate that, in the case of concentrated sulfuric acid, D/H surface isotopic exchange competes effectively with a very fast mass accommodation process. Even on near neutral pH water, D/H exchange in the interfacial region is proceeding on a surprisingly fast time scale.

Hanson et al. have argued that wall loss of D_2O is a possible explanation for the larger uptake coefficients measured for this species compared to $H_2{}^{17}O$.[175] However, great care was taken to keep the flow reactor walls clean and dry, and significant wall loss was seldom measured in these experiments.[40,158] Sulfuric acid is a sticky substance and would be expected to tend to stick to the walls, binding water vapor and providing many charged surface proton exchange sites, leading to the potential for fast D/H exchange. The fact that no significant wall-induced D/H exchange was observed in experiments employing sulfuric acid droplets[158] is strong evidence that, by heating the walls and carefully controlling the droplet train to eliminate splash wetting of the walls, significant wall loss of deuterated species can be avoided in droplet train experiments and that wall loss of D_2O does not explain its more effective uptake. Quantitative details of the wall loss studies are provided in ref 158, where it is also pointed out that, in the $H_2{}^{17}O$ on water experiments,[99] wall loss was below the detection limit.

Surface charges on the droplets produced by a vibrating orifice (as used in the droplet train flow reactor) may provide an explanation for the observed rapid D/H exchange. The density of such charges, most likely in the form of surface ions, may be significant.[176] The BC/ARI group has previously shown that the charge density has no effect on the uptake of SO_2.[176] However, it may enhance the rate of an ion-catalyzed reaction such as D/H exchange.

Further, ions in the interfacial region have fewer surrounding coordinated water molecules than in bulk water due to lower water density and the distortion of the hydrogen bonding network. Recent molecular dynamics simulations demonstrate that excess protons form hydronium ions with a marked preference for the interface, with their lone pair pointing outward, away from the surface.[172a,b,c] Experimental results by Enami et al. indicate that interfacial hydronium ions react rapidly with impinging gaseous trimethylamine.[81f] The fact that interfacial ions may have low water coordination numbers could be very significant. $H^+(H_2O)_n + D_2O$ cluster ion kinetics experiments have shown that D/H isotopic exchange for deuterated water molecules occurs up to 4 orders of magnitude faster for H^+ ions with only two coordinated water molecules compared to the same ion surrounded by six to eleven water molecules. The latter situation is more representative of the H^+ coordination shell characteristic of bulk water.[177]

4.8. Effect of Surface Water on Trace Gas Uptake on Liquid Organic Surfaces

Tropospheric aerosols were initially envisioned as consisting mainly of mineral particles and inorganic salts that were

deliquescent at moderate to high relative humidity. Recent field studies have shown that their composition is far more complex. It is now clear that organic aerosols are abundant in many regions of the troposphere and represent a significant mass fraction of tropospheric aerosols.[178,179] It is also becoming increasingly clear that organic aerosol particles undergo significant heterogeneous processing in the atmosphere; a recent review by Rudich illustrates the range of heterogeneous processes being explored in laboratory studies of vapor uptake by model organic aerosol surfaces.[15]

Since water vapor is a ubiquitous atmospheric component, it can be expected to play an important role in the heterogeneous processing of organic aerosol particles. In fact, hydrophilic organic aerosols can serve as cloud condensation nuclei, often as effectively as inorganic sulfate aerosols.[179,180] Several groups have recently investigated the wetting of model organic surfaces,[15,181−187] illustrating that many organic surfaces can effectively collect water, especially as atmospheric oxidation processes create surface species with higher oxidation states.

To investigate the heterogeneous chemistry of organic aerosols, including the role of condensing water, a series of droplet train flow reactor studies were performed on liquid organic surfaces selected as models of organic atmospheric particles with various oxidation states. Organic aerosols are known to contain hundreds of compounds with a large fraction still unidentified.[178,179,188] To obtain basic kinetic information about the heterogeneous reactions of organics in the face of such complexity, one must study surrogate compounds representing classes of organic species found in aerosols.[15,181,189] To date, the BC/ARI group has studied uptake on ethylene glycol,[87] 1-octanol,[88,190] and 1-methylnaphthalene.[191] Below, the focus is on results where water had a significant effect on trace gas uptake.

4.8.1. Uptake on Ethylene Glycol Surfaces. In the initial BC/ARI organic surface study,[87] the uptake of gas-phase HCl and HBr was measured on pure ethylene glycol surfaces as a function of temperature (T = 258−303 K for HCl and 262−293 K for HBr). The BC/ARI group then investigated ethylene glycol/water mixture surfaces as a function of water mole fraction (0 to 1) and temperature (273 and 283 K for HBr and 273 and 293 K for HCl). The uptake of DCl on an ethylene glycol surface was also measured. While ethylene glycol is not an important component of atmospheric aerosol particles, it is a convenient surrogate for hydrophilic organic compounds. The HCl and HBr uptake studies probe the nature of hydrophilic organic surfaces as a function of relative humidity. The uptake studies yielded the mass accommodation coefficient (α) and the thermal accommodation coefficient (S).

The mass accommodation coefficient (α) for HCl on dry ethylene glycol increases from 0.40 ± 0.06 at 303 K to 0.79 ± 0.12 at 258 K. This negative temperature dependence for α is similar to that observed in studies of gas uptake by aqueous surfaces. The HBr mass accommodation coefficient on ethylene glycol is near unity, independent of temperature in the range studied. The D/H isotope exchange probability of DCl at the gas−liquid interface of ethylene glycol was also studied and was measured to be 1. As discussed by Li et al.,[87] this implies that the thermal accommodation coefficient is also 1.

The most interesting results of these studies are the values of α measured as a function of liquid mole fraction of water. (In these experiments the water vapor pressure was set at its appropriate equilibrium value.) In general, these values of α on mixed ethylene glycol/water surfaces follow the expected pattern. At zero mole fraction of water (X_w = 0) the α values are those measured on pure ethylene glycol, decreasing to the measured value of α on pure water at X_w = 1. In between, α follows a composition-weighted sum of the individual α values for ethylene glycol and water. Since the decrease between the two end points is not a straight line, the weighting factor is not simply the liquid mole fraction of the mixture. This is not surprising since mass accommodation is a surface, rather than a bulk-phase, phenomenon. Therefore, it is reasonable to expect that the mass accommodation coefficient on the ethylene glycol/water solution is weighted by the fractional surface coverage $X(s)_{H_2O}$ as

$$\alpha = \alpha_{H_2O} X(s)_{H_2O} + \alpha_{EG}(1 - X(s)_{H_2O}) \qquad (34)$$

where α is the mass accommodation coefficient of HCl(g) or HBr(g) on the ethylene glycol/water solution and the α's with subscripts attached are the mass accommodation coefficients on pure water and pure ethylene glycol.

4.8.2. Uptake on 1-Octanol Surfaces. Droplet train uptake studies were also performed on 1-octanol surfaces for hydrogen halides, HCl, HBr, and HI, and the organic species, acetic acid,[88] as well as α-pinene, γ-terpinene, p-cymene, and 2-methyl-2-hexanol.[190] Mass accommodation coefficients for the gas-phase organic compounds including acetic acid were fairly large, with ~265 K values of 0.4 for acetic acid, 0.25 for 2-methyl-2-hexanol, 0.20 for p-cymene, and 0.12 for γ-terpinene, falling off gradually with increasing temperature;[88,190] the uptake of α-pinene was solubility limited, but it exhibited an uptake coefficient >0.1 at the shortest gas/droplet contact times, setting a lower limit for its α. None of the measured mass accommodation coefficients for the organic compounds showed any significant change as the relative humidity was varied between 0 and >100%.

In contrast, the influence of water vapor on the uptake behavior of the hydrogen halides was unexpected. The measured mass accommodation coefficients for HBr and HI on dry 1-octanol at 273 K were 1.01 ± 0.11 and 0.98 ± 0.10, respectively, and showed no significant temperature dependence. The mass accommodation coefficient for HCl was much smaller, 0.008 ± 0.001 at 273 K, and exhibited a negative temperature dependence. The effect of water vapor was dramatic. At 100% relative humidity (which corresponds to a less than 10% liquid water surface coverage), the 273 K mass accommodation coefficients for HBr and HCl had fallen to 0.21 ± 0.03 and 0.18 ± 0.05, respectively, while that for HCl had risen to 0.17 ± 0.03.[88] All of the 100% relative humidity values are equal, within measurement error, to their values on pure water.[88] The measured uptake coefficients at 273 K are show in Figure 13. The figure also shows that surface water has no effect on acetic acid mass accommodation.

To explain these results, the BC/ARI group formulated a Langmuir−Hinshelwood model where the surface mobility of the thermally accommodated hydrogen halide molecule is sufficient to allow it to find and cluster to surface water. Since both the evaporation and the mass accommodation rate constants of the water−hydrogen halide cluster can be expected to differ from those rate parameters for the hydrogen halide monomers, the BC/ARI group derived a parametrized total mass accommodation coefficient based on the mass accommodation coefficient of the complex, the unclustered hydrogen halide solvation and desorption rate constants, the surface density of water molecules, and the rate constant for hydrogen halide−surface water cluster formation. This formulation, detailed by Zhang et al.,[88] was used

dx.doi.org/10.1021/cr100360b Chem. Rev. 2011, 111, PR76 - PR109

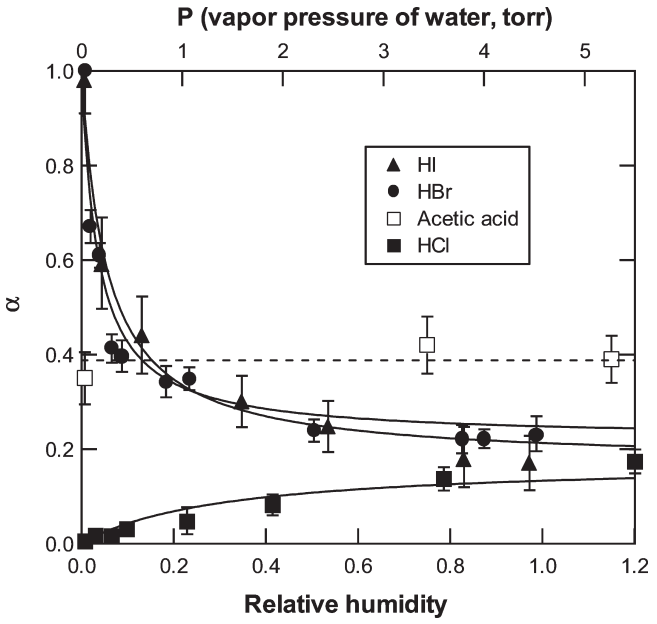

Figure 13. Mass accommodation coefficients, α, on 1-octanol droplets as a function of relative humidity (RH) for HCl at 273 K, HBr at 273 K, HI at 273 K, and acetic acid at 266 K on 1-octanol surfaces. Solid lines are best fits to a model discussed in ref 88. (Reprinted with permission from ref 88. Copyright 2003 American Chemical Society.)

to fit the hydrogen halide mass accommodation data shown in Figure 13, with the best fit shown as the solid lines. The surface rate constants derived from fitting the data are physically reasonable and reproduce the measured uptake data well. Of course, confirmation of the model will require additional experiments, possibly molecular beam/liquid surface scattering of the type pioneered by Nathanson.[81]

4.9. Effect of Surface Organics on Uptake by Aqueous Surfaces

The possibility that organic molecules adsorbed on the surface of aqueous aerosol particles may influence heterogeneous chemical processes has long been recognized.[192,193] Levitated acid droplet[194,195] and acid aerosol flow reactor studies of NH_3 uptake[154] have demonstrated that organic coatings can have significant effects on trace gas interfacial mass transfer.

Recent aerosol flow reactor studies of N_2O_5 reactive uptake on submicrometer sea salt aerosols by Thornton and Abbatt demonstrated that millimolar levels of hexanoic acid in the bulk aerosol reduced the uptake coefficient by a factor of 3−4 for 70% relative humidity (deliquesced) particles.[124] This result is probably the strongest evidence to date that a monolayer of organic molecules at the surface of an aqueous droplet can significantly impede trace gas uptake. Additional direct measurements of the impact of surface adsorbed organics are presented by Lawrence and co-workers, who used mass spectrometric techniques and supercooled deuterated sulfuric acid surfaces doped with 1-butanol to study the impact of the organic surface film on water (D_2O) evaporation[196] and D−H isotopic exchange of impinging HCl and HBr molecular beams.[197] Even though they determined that at 0.18 M the butanol film covers ∼80% of the acid's surface, the 0.18 M butanol bulk concentration had no effect on D_2O evaporation from 60, 64, or 68 wt % D_2SO_4 at 213 K,[196] and the butanol actually enhances the isotopic exchange of gaseous HCl or HBr, probably due to the alcohol OH group contributing to an increase in surface protonation sites.[197] It would appear that the nature of the organic film coating aqueous surfaces may have a strong effect on its ability to influence trace gas interfacial transport.

Recently, Donaldson and co-workers developed a laser fluorescence method to monitor the uptake of polycyclic aromatic hydrocarbon (PAH) compounds such as anthracene and pyrene to water surfaces[198] and their subsequent reactions.[199−201] They investigated the uptake of anthracene and pyrene both on pure water and on water coated with 1-octanol or hexanoic acid, observing that uptake coefficients for the octanol-coated surface are 2−3 times higher than the pure water uptake coefficient of $\sim 10^{-5}$. The uptake enhancements are much smaller on a hexanoic acid-coated water surface.[198] They also studied the oxidation of the PAH compounds anthracene and pyrene by ozone on both pure water and coated water surfaces.[199,201] Reactions followed a Langmuir−Hinshelwood mechanism, with O_3 first adsorbing to the surface and then reacting with the PAH. The reaction on the pure water and octanol-coated water surfaces displayed nearly identical surface second-order rate constants for the ozone/PAH reaction for both PAHs, with the anthracene rates about a factor of 5 higher than those for pyrene,[201] while the rate on hexanoic acid-coated water was less than that on pure water.[200] The major product of the anthracene reaction is 9,10-anthraquinone.[200]

In a recent droplet train flow reactor study, Raja and Valsaraj investigated the heterogeneous oxidation of naphthalene absorbed on water droplets.[202] They demonstrated that the first-order rate constant increased with decreasing droplet size. They were able to fit their data to a Langmuir−Hinshelwood mechanism and determine that the ozone/naphthalene reaction rate constant at the water interface was ∼15 times faster than the corresponding gas-phase rate constant.

Studies such as these are yielding valuable insights into the atmospheric fates of an important class of semivolatile air-toxic compounds.

The effect of surface organics on uptake of gas phase molecules by the aqueous surfaces continues to be an active area of research. The subject was reviewed by Donaldson and Vaida[202b] and more recently by Donaldson and Valsaraj.[202c] The latter review presents methods of assessing experimental and theoretical values of thermodynamic air water partition functions and adsorption isotherms for atmospherically important organic molecules.

Recent experiments continue to show that organic coatings on aqueous surfaces diminish evaporation of water[202d] and reduce uptake of trace gases. Badger et al.[202e] showed that uptake of N_2O_5 by sulfate aerosol was reduced by humic acid coatings. Uptake coefficients decreased by an order of magnitude as the humic acid mass fraction was increased over the range 0−50%. McNeil et al.[202f] found that a monolayer coating of sodium dodecyl sulfate is sufficient to inhibit N_2O_5 uptake. The uptake coefficient was reduced by an order of magnitude from 0.02 to 0.001 as the organic acid mass content was increased over the range 0.05−3% by weight. Above 3 wt % organic acid, no further decrease in uptake coefficient was observed.

Molecular beam studies by Nathanson and co-workers[202g] showed that on concentrated sulfuric acid surfaces the conversion efficiency of N_2O_5 into nitric acid was reduced by films of butanol and hexanol. The uptake coefficient decreased linearly from 0.12 to 0.05 with increasing surface coverage over the range 0.2−0.6 monolayers.

dx.doi.org/10.1021/cr100360b Chem. Rev. 2011, 111, PR76 - PR109

Using a molecular fluorescent pH probe, Clifford et al.[202h] showed that compared to a clean air−water interface, monolayer and submonolayer coatings of 1-octanol suppress hydrolysis in the interfacial region. This is in accord with subsequent molecular dynamics simulations[202i] indicating that acid hydrolysis occurs in the near surface region and requires the initial formation of a surface "critical cluster".

5. PHENOMENOLOGICAL TREATMENT OF MASS ACCOMMODATION

In section 4, eq 25, it was shown that, assuming the thermal accommodation coefficient $S = 1$, the mass accommodation coefficient can be expressed as[25]

$$\frac{\alpha}{1-\alpha} = \exp\left(\frac{-\Delta G_{obs}}{RT}\right) \qquad (25)$$

As was pointed out, the parameter $\Delta G_{obs} = \Delta H_{obs} - T\Delta S_{obs}$ is the Gibbs energy of the transition state between the species in the gas phase and in its solvated aqueous phase. The functional form of ΔG_{obs} depends on the theoretical formulation of the uptake process. Therefore, the parameter ΔG_{obs} can serve as a bridge between experiment and theory. Parts of the discussion in this section follow closely the presentations by Nathanson et al.[12] and Kolb et al.[9]

Several features are evident in the experimentally determined parameters ΔH_{obs} and ΔS_{obs} listed in Table 2. (1) For all species the mass accommodation coefficient exhibits a negative temperature dependence (i.e., ΔH_{obs} is negative in all cases). (2) The magnitudes of ΔH_{obs} are ordered approximately as diols < acids < halo-ethanols < alkyl alcohols < acetone < esters. This arrangement seems to be inversely proportional to the expected hydrogen bonding ability of the species. (3) The magnitudes of ΔH_{obs} and ΔS_{obs} do not depend strongly on the size or shape of the molecule. This is evident from a comparison of the results for methanol and *tert*-butyl alcohol. The hydrophobic component of *tert*-butyl alcohol is significantly larger than that of methanol. Specifically, the molar volume of *tert*-butyl alcohol is larger by a factor of 2.3, yet ΔH_{obs} and ΔS_{obs} are, within experimental error, the same for the two species. (4) There is a nearly linear relationship between ΔH_{obs} and ΔS_{obs}, as is shown in Figure 14. In this figure, ΔH_{obs} vs ΔS_{obs} values are plotted for all the data listed in Table 2. (Smaller sets of data are plotted by Davidovits et al.[203] and Kolb et al.[9]) The crossed squares in the figure are calculated ΔH_{obs} and ΔS_{obs} values based on the critical cluster model of mass accommodation described below.

Almost all of the experimentally measured values fall on a straight line. There is no such generally corresponding relationship in the solvation parameters for the species. For example, as shown by Davidovits et al.[203] and Kolb et al.,[9] the magnitude of ΔH_{sol} for H_2O_2 is relatively high yet the magnitude of its ΔS_{sol} is the lowest in a listing of hydrophilic molecules. At present, no *ab initio* theory exists to predict the mass accommodation of gaseous species on liquid surfaces.

Prior to the mid-1980s very little experimental information was available to aid in the formulation of a model describing the uptake of gases by liquids. In a prevalent conceptualization of the process,[204] it was assumed that since the impinging gas molecule does not have sufficient kinetic energy to displace solvent molecules, the molecule could enter the liquid only if a microscopic cavity of appropriate size forms at the surface near its location. As is discussed by Davidovits et al.,[205] predictions based on this model are not in accord with experimental observations. Here we describe two phenomenological models that present a picture of mass accommodation consistent with experimental results. Both models are based on similar views of the water−vapor interface.

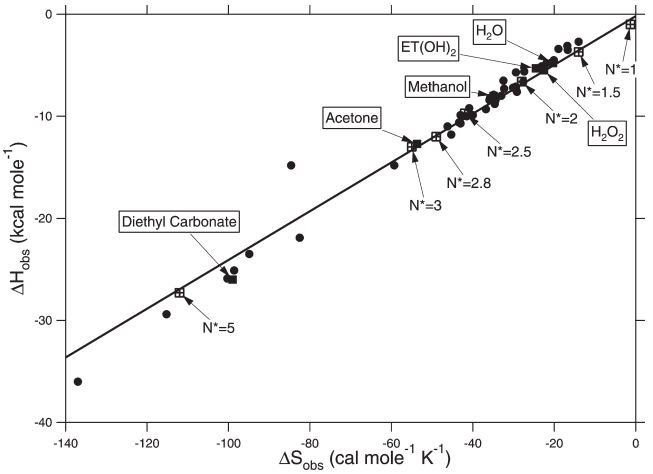

Figure 14. Experimental (circles) and calculated (crosses in squares) values of ΔH_{obs} and ΔS_{obs}.

Experimental[206−209] and modeling studies[210−215] show that the surface of water is a sharp but finite transition region several molecular diameters in thickness. On a molecular scale, the surface is rough due to uneven distribution of the surface molecules. A "snapshot" view obtained via molecular simulation shows molecules protruding out of the bulk phase singly or in clusters of two or three. Thus, the size of peaks and valleys is on the average two or three molecular diameters. The snapshot view is short-lived. The surface is a zone of rapid fluctuations with molecules continually arriving and departing and bonds forming and dissociating.

Vibrational sum-frequency generation (VSFG) spectroscopy studies of the water vapor−liquid water interface indicate that at least 20% of the water molecules have one free OH projecting into the vapor[216] and, thus, are available to form hydrogen bonds. Soft X-ray absorption studies of liquid water microjets imply that O−O distances for surface water molecules are longer than those for the gaseous water dimer, indicating that the equilibrium water surface is dominated by weakly bonded water interacting at longer distances than those in bulk water and suggesting "an interfacial 'phase' of relatively more mobile molecules."[217] This is consistent with molecular dynamics simulations predicting significantly larger interfacial diffusion constants than bulk water values.[212,218]

5.1. Critical Cluster Model of Mass Accommodation

In the critical cluster (sometimes called surface nucleation) model of mass accommodation, dynamic interactions of surface molecules are viewed from the perspective of nucleation theory. The bonding of the surface molecules may assume various configurations and aggregations. Some molecules may be only weakly bound, perhaps connected only by one bond, while other molecules may be more tightly interconnected. In other words, within the interface there are density fluctuations or local tightening of bond configurations, forming clusters. The tightly bound clusters are more liquid-like than the loosely bound molecules.

dx.doi.org/10.1021/cr100360b Chem. Rev. 2011, 111, PR76 - PR109

In this dynamic interfacial region, clusters are expected to be continually forming, falling apart, and re-forming. Nucleation theory, which describes the formation of a new phase, is perhaps a viable description of such surface dynamics. In this context, the formation of the new phase can be thought of as the formation of a more liquid-like cluster from the more loosely bound surface species.

The equilibrium density of surface clusters is proportional to $\exp(-\Delta G_N/RT)$, where ΔG_N is the molar free energy for the formation of a cluster with N molecules. Classical nucleation theory shows that ΔG_N first increases with cluster size, reaches a maximum, and then decreases. The initial resistance to cluster growth (formation of the new phase) is due to a surface free energy barrier associated with the phase boundary. The barrier is entropic in nature. The driving force is such that clusters smaller than a critical size (N^*) fall apart, whereas clusters larger than the critical size serve as centers for further condensation and grow in size until they merge into the adjacent bulk liquid.

The critical cluster model assumes that gas uptake proceeds via growth of critical clusters as described above. The incoming gas molecule (solute) of interest (here called the trace molecule) becomes a loosely bound surface species (n_s) upon striking the surface that participates in the nucleation process. If such a molecule becomes part of a critical sized cluster, it will be incorporated into the bulk liquid via aggregation.

In this model, the ease with which an incoming solute gas molecule can be incorporated into bulk water depends on its ability to enter the nucleation or aggregation process with water molecules at the interface. The critical cluster consists of a specific number of molecules, N^*, that is the sum of the number of trace molecules plus the additional number of water molecules required to form the critical cluster or aggregate leading to growth and subsequent uptake by the bulk liquid. The number N^* required to form a critical cluster depends on the structure of the specific molecule undergoing the process of uptake. Thus, for example, ethylene glycol with two OH functional groups makes a larger contribution toward the formation of a critical cluster than a simple alcohol with only one OH. The critical cluster size N^* for ethylene glycol is therefore expected to be smaller than N^* for a simple alcohol. Consequently, a critical cluster is more readily formed around the former than the latter. The number of water molecules that have to aggregate with the incoming molecule to form a critical cluster is $(N^* - 1)$. Thus, a value of $N^* = 1$ implies that the molecule itself is in effect a critical cluster leading to growth by water condensation. According to this model, once a critical cluster is formed around the hydrophilic part of the molecule, the cluster continues to grow and the whole molecule is enveloped, nearly independent of its size. Therefore, in accord with experimental observations, N^* is also expected to be nearly independent of the size of the hydrophobic portion of the molecule.

The incoming molecule, once adsorbed in the interface surface region, can be found in various cluster configurations. However, since the gas-phase species under consideration consists primarily of monomers, detailed balance considerations lead to the conclusion that molecules of the trace gaseous species leave the interface primarily as monomers via the breakage of an interfacial bond associated with the most weakly bound unaggregated species, n_s. Therefore, it seems reasonable to assume that the uptake process involves primarily only two of the various interfacial configurations of the trace molecule: the most weakly

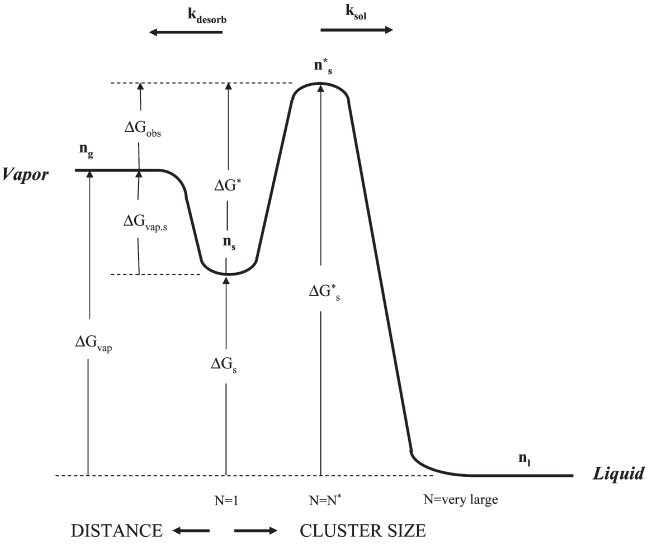

Figure 15. Postulated free energy diagram for the liquid vapor interface. Note the change in reaction coordinate at $N = 1$ (see text). The experimentally measured ΔG_{obs} corresponds to the difference in energy between the vapor (n_g) and the surface transition state (n^*_s). Negative ΔH_{obs} and ΔS_{obs} values imply that the n^*_s barrier is entropic in nature, with the barrier height determined by the critical cluster size (N^*). The mass accommodation kinetics is controlled by the relative rates k_{des} and k_{sol} (see eq 10). (Reprinted with permission from ref 12. Copyright 1996 American Chemical Society.)

interconnected species, n_s, and the species within a critical cluster, n^*_s. The free energies with respect to the bulk liquid for these two species are ΔG_s and ΔG^*_s.

A postulated free energy diagram for the relevant species in the region between liquid and gas is shown in Figure 15. To take into account the clustering process, we rewrite eq 2 to interpose the critical cluster n^*_s between n_s and n_l:

$$n_g \underset{k_{des}}{\overset{k_{ads}}{\rightleftharpoons}} n_s \xrightarrow{k_s} n_s^* \xrightarrow{k_{sol}} n_l \qquad (35)$$

Evidence for such a chemically adsorbed surface state, as postulated in Figure 15, was first observed in the BC/ARI SO_2 uptake experiments.[103,170] More recently, using second harmonic generation (SHG), Donaldson et al.[171] directly detected and characterized the surface state of SO_2. Donaldson and co-workers used surface tension measurements to characterize surface absorption of ammonia,[219] small organic acids, alcohols, and acetone,[220] and methylamines.[221] Several groups have also characterized dimethyl sulfoxide (DMSO) adsorption on water surfaces, using surface tension,[222] SHG,[223] and VSFG[224] techniques, respectively. The adsorption of methane sulfonic acid (MSA) has also been characterized using VSFG techniques.[225] Thus, the concept that small molecules, including many of those listed in Table 2, actively bond to liquid water surfaces is now well established.

One has to be careful in interpreting the reaction coordinate in Figure 15. To the left of the n_s minimum, the reaction coordinate represents the distance between the trace gas molecule and the interface. However, to the right of this minimum, distance is no longer a well-defined quantity. The trace molecule is now within the interface. Here the appropriate reaction coordinate is the number size (N) of the aggregate containing the trace molecule.

dx.doi.org/10.1021/cr100360b Chem. Rev. 2011, 111, PR76 - PR109

Thus, at the n_s minimum $N = 1$. As N increases, the free energy first increases and then, past the critical size (i.e., $N = N^*$), the free energy decreases and the cluster grows until it merges with the bulk liquid.

In Figure 15, ΔG_{obs}, the experimentally measured free energy governing mass accommodation, corresponds to the difference between ΔG_{vap} and ΔG^*_s, the free energies (with respect to the liquid state) of the vapor (n_g) and the critical cluster (n^*_s), respectively. The model formulation of critical cluster nucleation invokes transition state theory to account for the barrier at n^*_s that controls observed accommodation kinetics. We note that, since ΔH_{obs} and ΔS_{obs} are both always negative, the free energy barrier at n^*_s is entropic in nature. Formation of the critical cluster is always favored enthalpically; the negative entropic term reflects dissolution of the vapor into the liquid with a large contribution due to the surface tension of small clusters. The barrier to mass accommodation implies that, in the transition of the surface species n_s to a critical cluster, the decrease in entropy is greater than the decrease in enthalpy. The relatively greater change in entropy is consistent with simulation results showing a more rapid translational diffusion at the interface that becomes restricted as the surface molecule becomes confined by the cluster.[212,218]

Note that the kinetics within the interface, represented in Figure 15, serves as a bridge between the vapor and the liquid phases. Interfacial transport, characterized by α, is distinct from bulk-phase transport that is controlled by solubility and diffusion.

An appropriate expression for k_{sol}/k_{des} can be derived in terms of the critical cluster model. Such an expression in turn yields values for ΔH_{obs} and ΔS_{obs} via eq 25, to be compared with the experimentally measured parameters listed in Table 2. The first formulation and calculations are found in refs 203 and 205. The calculations are based on a highly simplified approach of using bulk liquid-phase parameters to estimate the properties of the small clusters found at the gas−liquid interface. For example, this formulation assumes a constant liquid-phase diffusion coefficient across the interface in order to simplify the equations. A more detailed description of the assumptions and approximations used in the calculations is presented by Nathanson et al.[12] The formulation results in expressions for ΔH_{obs} and ΔS_{obs} in terms of the critical cluster size N^*. Calculated values of ΔH_{obs} and ΔS_{obs} for selected values of N^* are shown in Figure 14 together with the experimentally derived values.

Clearly, individual critical clusters must contain an integer number of molecules. However, for a given trace molecule, the number of water molecules required to form a critical cluster ($N^* - 1$) may depend on the orientation of the trace molecule with respect to the bulk liquid and its penetration into the interfacial region. We interpret noninteger N^* values as representing an average number of molecules in a critical cluster or aggregate in the interfacial region. For example, in the case of 2-propanol, where the measured values of ΔH_{obs} and ΔS_{obs} are best matched with $N^* = 2.5$, the critical-sized cluster consists of the molecule itself with either one or two water molecules aggregated with it, depending on its position and orientation within the interfacial region.

Figure 14 shows that the formulations for ΔH_{obs} and ΔS_{obs} as outlined above and presented by Nathanson et al.[12] are in accord with the measurements. The values of ΔH_{obs} and ΔS_{obs} are always negative. The magnitudes of the parameters do not depend strongly on the size of the gas molecule. Rather, they are a function of the number of water molecules that have to be added to the target molecule in order to form a critical-sized cluster. Finally, the monotonic relationship between ΔH_{obs} and ΔS_{obs} is quantitatively explicit in the formulation.

In summary, the key result of the observations is that an entropic barrier both controls vapor/liquid accommodation kinetics and separates the surface state, n_s, from the liquid, n_l, as shown in Figure 15. The nucleation-based theory presented here accounts for the barrier in terms of critical cluster binding energy and surface tension, based on a highly simplified approach using bulk liquid-phase parameters to estimate properties of the small clusters found at the gas−liquid interface.

Since mass accommodation (condensation) is the reverse of evaporation, balance considerations suggest the following mechanism for the evaporation of a solvated molecule. Evaporation begins with the spontaneous emergence of a critical cluster from the bulk. The species n_s is formed by the dissociation of critical clusters. This implies, as shown in Figure 15, that a barrier exists to the direct formation of species n_s from the bulk liquid. In other words, evaporation consists of a stepwise process: bulk liquid to critical aggregate n^*_s, to a weakly bound surface species n_s, to a vapor molecule.

In a recent work Remorov and Bardwell obtained an analytical formulation for the mass accommodation coefficient based on the Hertz−Knudsen equation and the critical cluster model.[226] The quantitative estimates provided by this formulation are in reasonable agreement with the experimental measurements.

5.2. Capillary Wave Model of Mass Accommodation

In this model of mass accommodation, the random motion of surface molecules is viewed from the perspective of capillary waves that are thermally excited with surface tension providing the restoring force.[227] The wavelength (λ) spectrum of the harmonic capillary waves extends from macroscopic to molecular dimensions. Because capillary wave theory is a continuum construct, it is not expected to be strictly applicable on the scale of discrete molecular structure. Still, the theory can be usefully applied to analyze motion on a single molecule scale, as is done in the model of mass accommodation formulated by Knox and Phillips.[228]

At short wavelengths, capillary wave motion is strongly damped by viscosity. On a molecular scale, surface motion can be regarded as a superposition of overdamped normal capillary wave modes forming local modes. In the words of Phillips: "Thus the typical over-damped motion resembles that of a geothermal mud pool or boiling porridge with a fast rise time and slow fall time."[229] The root-mean-square displacement of the water surface is about 3.8×10^{-8} cm at 300 K.[230] The shorter rise time (τ_1) of the local mode is $\tau_1 = \rho/2k^2\eta$, and the longer fall time (τ_2) is $\tau_2 = 2\eta/k\gamma$. The parameters ρ, η, and γ are respectively the density, the coefficient of viscosity, and the surface tension of the liquid. The parameter k is the wave vector $2\pi/\lambda$.

In this picture of mass accommodation, the solute molecule is assumed to become part of a collapsing local mode as it becomes incorporated into the bulk liquid. The mass accommodation is described in terms of coordination number N_c, defined as "the number of solvent molecules surrounding and in contact with the solute molecule".[228] In the process of uptake, N_c increases from 1 for the surface-adsorbed molecule to some maximum number corresponding to full solvation. The process is represented in Figure 16.

In a corresponding depiction of evaporation, it is assumed that the solute molecule is ejected from the tip of a high k-value (λ on

dx.doi.org/10.1021/cr100360b Chem. Rev. 2011, 111, PR76 - PR109

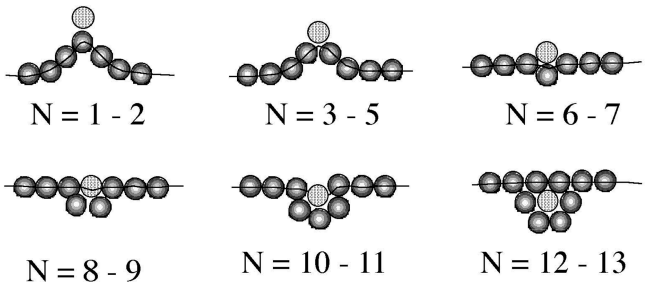

Figure 16. Coordination number N during progressive stages of solvation of a solute molecule (light sphere) by solvent molecules (dark spheres). (Reprinted with permission from ref 228. Copyright 1998 American Chemical Society.)

the order of molecular dimensions) local mode wavelet with positive displacement.[231] Phillips suggests that the normal modes (i.e., modes with wavelength much greater than molecular dimensions that extend over a wider surface area) promote mass accommodation by continually creating and destroying surface area. However, they do not have a significant effect on evaporation.[229]

The free energy diagram in Figure 15, describing mass accommodation from the perspective of surface nucleation, is also applicable for the capillary wave model of uptake if one interprets N as the coordination number. The two ways of formulating mass accommodation appear to be related. The experimentally observed near linear relationship between ΔH_{obs} and ΔS_{obs} that is predicted by the critical cluster model can also be explained within the framework of the capillary wave formulation.[228] In fact, the two models have complementary features. The critical cluster model predicts an entropic maximum on the free energy path from a surface-adsorbed molecule to solvation. Using simple nucleation theory to fit the experimental results, the model yields quantitative expressions for ΔH_{obs} and ΔS_{obs} and, therefore, also the correct temperature dependence. While a maximum on the free energy path is consistent with the capillary model, the model in its present form does not provide a quantitative formulation of the barrier. Nor does it yield the correct temperature dependence for the process.[232] On the other hand, via the intrinsic oscillatory nature of the capillary waves, the capillary wave model leads more readily to the formulation of time scales associated with mass accommodation. In a simple picture, the fall time of the local mode (τ_2) can be associated with the gas uptake and the shorter rise time (τ_1) with evaporation. Thus, for example, if we assume that the base width of the local mode is 10^{-9} m $\approx \lambda/2$ (about 3 molecular diameters), then $k \approx 3 \times 10^9$ m, and at 298 K, $\tau_2 = 8 \times 10^{-12}$ s and $\tau_1 = 6.2 \times 10^{-14}$ s. An attempt to formally merge these two models might be useful.

6. MOLECULAR DYNAMICS SIMULATIONS OF MASS ACCOMMODATION

The following brief discussion is confined to molecular dynamics (MD) simulations of mass accommodation. A more detailed discussion of MD simulations of molecular transport across the liquid−vapor interface of water is presented by Garrett et al.[15b] Several of the points in this section have also been raised in ref 40.

Molecular dynamics simulations of mass accommodation on liquid water have been performed for gas-phase ethanol,[233,234] methanol,[37,235] ethylene glycol,[234] H_2O(g),[39,235−238] HO_2,[239] O_3,[238,240] and OH.[238,240,241] With the exception of the case of O_3, the MD simulations for the above species yield values of α at room temperature close to 1, whereas the experimental values listed in Table 2 are temperature dependent and, at or near room temperature, significantly smaller than unity.

Experimentally measured temperature dependent mass accommodation coefficients were obtained for about 40 species by several research groups using three different techniques. Examination of the results led us to conclude that the experimental measurements are by and large correct. In this section we explore factors we think may be responsible for the differences between the MD simulations of α and the experimental measurements. Another perspective on molecular simulations was presented by Garrett et al.[15b]

The similarity in the results of molecular simulations performed by the various groups is not surprising since the methods used in all these simulations are closely related. The simulations are done with periodic cells each initially containing about 1000 molecules. The pairwise intermolecular potentials used are likewise similar.

Several factors may be responsible for the difference between the MD simulated values of α and experimental measurements. A number of recently published studies indicate that the currently available water interaction potentials may not fully capture liquid water properties, particularly at the liquid−vapor interface. Kathmann et al.[242] showed that the widely used Dang−Chang potentials[243] and the TIP4R potentials[244] cannot be used to reliably predict nucleation rates. Kathmann et al.[242] found that a systematic shift in the Helmholtz free energies of each cluster by 0.5 kcal/mol changes the nucleation rate by more than 10 orders of magnitude. Similarly, comparisons of Monte Carlo simulations of the critical cluster sizes and homogeneous water vapor nucleation rates with accurate experimental nucleation rate measurements showed that three popular water interaction potentials all did a poor job of reproducing experimental nucleation rates, overpredicting them by many orders of magnitude.[245] In view of the critical cluster model of mass accommodation, one might expect that the factors in the simulation procedure that overpredict nucleation rates are likely also to overpredict α.

Furthermore, there is recent evidence that both the SPC and more realistic intermolecular potential models may not provide a fully accurate simulation of the bonding in bulk water. In a recent experiment, Wernet et al.[246] used X-ray absorption spectroscopy and X-ray Raman scattering to study the first hydration shell of a water molecule in liquid water. They reported serious discrepancies with structures based on current molecular dynamics simulations. Zubavicus and Grunce[247] suggest that the disagreements of the simulation results with the water structure "snapshots" measured by Wernet et al.[246] are likely to be of major consequence for all molecular dynamics simulations of water using established computer program packages.

If molecular dynamics simulations based on SPC/E and similar model intermolecular potentials fail to adequately reproduce bonding in either bulk water or water clusters, it is unlikely that they adequately reproduce the relaxed and disordered hydrogen-bonded network known to exist at the liquid water/vapor interface[217,248] with a high level of both single donor and acceptor only surface species.[249] The modeled α values could certainly be reduced to the experimentally measured range if the surface binding energy of the incoming gas-phase species is significantly overpredicted by the model water potentials.

dx.doi.org/10.1021/cr100360b Chem. Rev. 2011, 111, PR76 - PR109

Before MD calculations of interfacial uptake coefficients can be considered definitive, it must be demonstrated that such MD calculations can reliably reproduce both interface densities and the types and abundances of surface hydrogen bonding species specified by nonlinear surface vibrational spectroscopy[216,250] and X-ray absorption spectroscopy[217,248,249,251] experiments. Using methods pioneered by Morita and Hynes,[252] an initial attempt to compare water surface vibrational spectra with molecular dynamics predictions has been published by Richmond and co-workers,[250] who note that the comparison is subject to the approximations of the H_2O−H_2O interactions provided by the SPC/E model.

The time and distance scales of the simulations raise the question of whether molecular simulations have captured the same mass accommodation process as experimental measurements. As is discussed by Davidovits et al.,[40] Vieceli et al.,[238] and Garrett et al.,[15b] current MD simulations of mass accommodation are necessarily restricted to simulating spatial scales on the order of 10 nm and time scales of less than 1 ns. Important processes that may control the mass accommodation of vapors to macroscopic liquid surfaces take place on much larger spatial and temporal scales.

It is possible that the MD simulations are capturing thermal accommodation of vapor molecules, which the BC/ARI measurements for deuterated water vapor indicate is near unity, without fully simulating mass accommodation. For example, at equilibrium the surface region of water reconstructs (exchanging vapor and "liquid" molecules), on time scales of microseconds, a time factor at least 1000 larger than that accommodated by current MD simulations. If the molecules "accommodated" in MD simulations are still in the near surface region on a microsecond time scale, microscopic reversibility would indicate that they have a high probability of evaporating, erasing their apparent uptake. Further, Knox and Phillips[228] and Phillips[253] suggest that interfacial mass transport for macroscopic gas−liquid surfaces is governed by thermally excited capillary waves. Because the capillary wave description breaks down on molecular distance scales,[230] capillary waves are not present in the MD calculations. Their absence in MD simulations may neglect a major process that returns initially accommodated molecules to the outer surface and then to the gas phase.

Several molecular dynamics simulations have been published since 2006 that model the interactions of molecules at the water interface. An extensive listing of these works is found in Kolb et al.[13b] Here we bring attention to two studies relevant to mass accommodation. Canneaux et al.[234b] modeled the mass accommodation of ethanol, acetone, and benzaldehyde by the liquid−vapor interface of water. In line with earlier similar studies, the calculations yielded $\alpha = 1$. Carignano et al.[254] modeled uptake of ammonia by the water/vapor interface. The simulation shows a minimum in the free energy at the interfacial region. However, this minimum is too small to affect significantly the mass accommodation process.

During the past few years a number of molecular dynamics calculations have been performed in an attempt to determine whether the water surface is acidic or basic (i.e., occupied by an excess of hydronium or hydroxide ions). These studies were motivated in part by the conflicting experimental results, some indicating that the water surface is basic, with others pointing to an acidic surface. E. K. Wilson succinctly summarized the studies in a recent *Chemical & Engineering News*[255] survey. At this time, molecular dynamics calculations cannot resolve the issue. Some calculations yield an acidic surface while others indicate that the surface is basic. (See, for example, Buch et al.[172b] and Beattie et al.,[256] respectively.) It seems that the modeling representation of the water interface remains incomplete. This may affect the applicability of molecular dynamics simulations of the mass accommodation process. The issue needs to be further examined.

7. SUMMARY

Over the past 20 years the uptake by aqueous solutions of a large number (more than 50) of gas-phase species has been studied. Mass accommodation coefficients (α) have been measured as a function of temperature for about 40 gas-phase species. The α coefficients display a negative temperature dependence indicating that the energy barrier to mass accommodation is entropic. The results of the experiments led to the formulation of phenomenological models for the mass accommodation process.

In cases where the uptake of gas-phase species into the pure liquid is solubility limited, the addition of a reactive species to the liquid results in increased gas uptake due to the irreversible sink for the species. In several cases the enhanced uptake is larger than one would expect from bulk-phase reactions alone. The larger uptake provides evidence for irreversible reactions occurring at the gas−liquid interface. For some species, there is also compelling experimental evidence for the formation of chemisorbed species at the interface.

The studies of mass accommodation and chemical reactions at gas−liquid interfaces have provided a large body of useful information and have elucidated important basic properties of the liquid surface. However, many questions remain unanswered. For example, why do some species react more readily at the interface than in the bulk liquid while other species do not? Are there specific photochemistry and catalytic processes at the interface? What is the mechanism for reactions at the interface and how does this depend on the identity of the gas-phase species?

At this point, our understanding of gas−liquid molecular interactions is essentially qualitative. Reasonable explanations can be provided for observed experimental results, but a theory or a model that can quantitatively predict values for mass accommodation coefficients or surface reaction rates is not available. More systems need to be investigated, with both existing and new techniques, before gas−liquid interactions will be more adequately elucidated. Interactions between the experimental and the theoretical/simulation communities are guiding and helping to prioritize ongoing work in this field.

In principle, molecular dynamics simulations should provide the most detailed molecular picture of the interface. However, as has been discussed, the simulation procedures at this stage are not adequately developed to properly reproduce kinetics at the gas−liquid interface. One of the impediments to progress in this area is the disparity in the temporal and spatial scales of the experimental measurements and the simulations. Experimental measurements are on time scales of milliseconds or longer and macroscopic spatial dimensions, whereas the time and spatial scales of simulations are of nanoseconds and nanometers, respectively. In agreement with Garrett et al.,[15b] we also conclude that more effort is needed to bridge the gap between macroscopic scale-uptake experiments and nanoscale molecular simulations. The development of experimental and theoretical techniques that can link available experimental data with molecular dynamics simulations is a challenging opportunity for the physical chemistry community.

AUTHOR INFORMATION

Corresponding Author

*Phone: 617-552-3617. Fax: 617-552-2705. E-mail: Paul.Davidovits@bc.edu.

BIOGRAPHIES

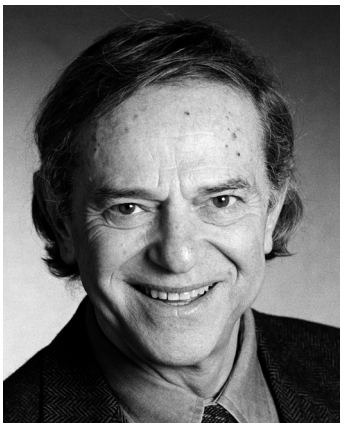

Paul Davidovits received his B.S., M.S., and Ph.D. degrees from Columbia University. For nine years he was on the faculty at Yale University, and he is currently Professor of Chemistry at Boston College. While at Yale University, he and his students developed an experimental technique that provided the first accurate measurements of cross sections for the gas-phase reactions of alkali atoms with halogen molecules. Also jointly with colleagues, he developed the first operational confocal laser microscope and presented the basic theories applicable to the technique. At Boston College, Prof. Davidovits, together with graduate students and colleagues from Aerodyne Research, Inc., invented techniques to study gas−particle interactions and used these techniques to study gas−liquid interactions for more than 40 gas-phase species. He is a fellow of the American Physical Society and the American Association for the Advancement of Science. Together with R. Minsky and D. Egger, he is a recipient of the Year 2000 R. W. Wood Prize "for seminal contributions to confocal microscopy". In 2001 he received the Boston College Distinguished Senior Research Award, and in 2003 he received the Alpha Sigma Nu Annual Book Award.

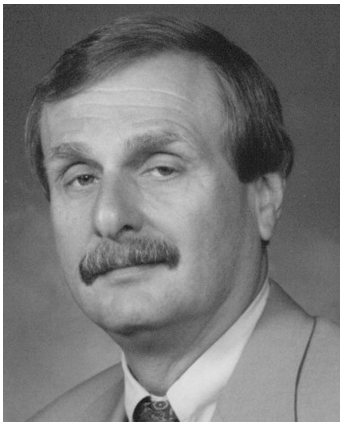

Charles E. Kolb received his S.B. from the Massachusetts Institute of Technology and his M.A. and Ph.D. from Princeton University. Dr. Kolb is the President and Chief Executive Officer of Aerodyne Research, Inc. He joined Aerodyne as a Senior Research Scientist in 1971. At Aerodyne, his personal areas of research have included atmospheric and environmental chemistry, combustion chemistry, chemical lasers, materials chemistry, and the chemical physics of rocket and aircraft exhaust plumes. In the area of atmospheric and environmental chemistry, Dr. Kolb initiated Aerodyne's programs for the identification and quantification of sources and sinks of trace atmospheric gases and aerosols involved in regional and global pollution problems. He has also motivated and designed chemical kinetic and molecular spectroscopy laboratory programs which provide gas-phase and gas/surface kinetic rate parameters for atmospheric modeling and quantitative spectroscopic parameters needed to design in situ measurements of trace species important in tropospheric, stratospheric, and mesospheric photochemistry. Dr. Kolb has been a member of numerous government and National Academy of Sciences/National Research Council committees dealing with atmospheric and environmental chemistry issues and was recognized as a National Associate of the National Academies in 2003. He received the 1997 Award for Creative Advances in Environmental Science and Technology from the American Chemical Society. He has been elected a fellow of the American Physical Society, the Optical Society of America, the American Geophysical Union, and the American Association for the Advancement of Science.

Leah R. Williams received her B.A. from Carleton College and her Ph.D. from the Massachusetts Institute of Technology. Dr. Williams joined Aerodyne Research, Inc., in 1999 as a Principal Research Scientist. Her research interests include measuring heterogeneous uptake and reaction rates on liquid and solid surfaces using a variety of experimental techniques. From 1991 to 1999, she headed the Atmospheric Chemistry Group in the Molecular Physics Laboratory at SRI International, Menlo Park, CA. There, she performed laboratory measurements of heterogeneous reaction rates on sulfuric acid surfaces representative of stratospheric sulfate aerosol particles and on soot surfaces. She also has performed experiments in the areas of laser spectroscopy of small molecules and ultrafast laser spectroscopy in condensed phases.

dx.doi.org/10.1021/cr100360b Chem. Rev. 2011, 111, PR76 - PR109

John T. Jayne received his B.S. from Hofstra University and his Ph.D. from Boston College. Dr. Jayne joined Aerodyne Research, Inc., as a Senior Research Scientist in 1993. In 1997 he was promoted to Principal Research Scientist. His research interests and experience include homogeneous and heterogeneous gas-phase kinetic studies utilizing optical and mass spectrometric detection techniques. Much of Dr. Jayne's graduate thesis work and subsequent efforts at Aerodyne have focused on mass accommodation coefficient measurements for tropospheric trace gas species. One of the main features of his work highlighted the fact that certain reactions can occur more readily on the surface of water droplets than in the bulk liquid phase. Currently, Dr. Jayne's work at Aerodyne is focused on developing an aerosol mass spectrometer for real-time size-resolved measurement of aerosol composition for micrometer and submicrometer size particles. This instrument has been developed for both laboratory and field applications. In 2004, Dr. Jayne, jointly with Dr. Worsnop, received the Benjamin Y. H. Liu Award from the American Association for Aerosol Research for "outstanding contributions to aerosol instrumentation and techniques".

Douglas R. Worsnop received his B.A. from Hope College and his Ph.D. from Harvard University. Dr. Worsnop joined Aerodyne Research, Inc., in 1985 and in 1988 was promoted to Principal Research Scientist. In 1997 he was named Director of the Center for Aerosol and Cloud Chemistry. Since 1992 he has also been an Adjunct Professor in the Chemistry Department of Boston College. His research interests include gas-phase chemical kinetics, atmospheric chemistry, heterogeneous chemistry, molecular spectroscopy, aerosol diagnostics, and mass spectrometry. In collaboration with Boston College, gas uptake rates are measured using a monodisperse stream of liquid droplets that provides a continuously renewed liquid surface area that is coupled to a low pressure flow tube. Results for over 40 atmospheric gases have led to the development of kinetic models for mass accommodation, reaction, and surface processes in liquids. More recently, a novel aerosol mass spectrometer has been developed for size-resolved composition measurements of submicrometer aerosol particles. In 2004, Dr. Worsnop, jointly with Dr. Jayne, received the Benjamin Y. H. Liu Award from the American Association for Aerosol Research for "outstanding contributions to aerosol instrumentation and techniques". Dr. Worsnop is a fellow of the American Association for the Advancement of Science.

ACKNOWLEDGMENT

The authors gratefully acknowledge the contributions of students and colleagues, including Y. G. Adewuyi, J. L. Cheung, W. J. De Bruyn, S. X. Duan, J. A. Gardner, M. Gershenzon, J. H. Hu, Y. Q. Li, J. Morris, M. Mozurkewich, O. V. Rattigan, D. V. Robinson, G. R. Robinson, Q. Shi, X. Shi, J. A. Shorter, J. Slowik, E. Swartz, I. Tchertkov, J. M. Van Doren, L. R. Watson, M. S. Zahniser, and H. Z. Zhang. Helpful discussions with B. Garrett, P. Jungwirth, M. Kulmala, A. Morita, D. Tobias, T. Vesala, J. Vieceli, and P. Wagner on the nature of vapor/liquid mass accommodation and molecular dynamics simulation of liquid water/vapor surfaces are gratefully acknowledged. Valuable discussions with B. Finlayson-Pitts, D. Hanson, and G. Nathanson on experimental techniques and results are also appreciated. Funding was provided by the NASA Upper Atmosphere Research Program, Contract NAG2-1462, by the Atmospheric Chemistry Program of the National Science Foundation, Grants ATM-0212464, ATM-0525355, and ATM 0854916, and by the Office of Biological and Environmental Research of the Department of Energy, Grants DE-FG02-98ER62581 and DE-FG02-05ER63995.

REFERENCES

(1) Finlayson-Pitts, B. J.; Pitts, J. N. *Chemistry of the Upper and Lower Atmosphere*; Academic Press: San Diego, CA, 2000.

(2) Sander, S. P.; Friedl, R. R.; Golden, D. M.; Kurulo, M. J.; Huie, R. E.; Orkin, V. L.; Moortgat, G. K.; Keller-Rudek, H.; Ravishankara, A. R.; Kolb, C. E.; Molina, M. J.; Finlayson-Pitts, B. J.; Wine, P. *Chemical Kinetics and Photochemical Data for Use In Atmospheric Studies, Evaluation No. 15*; JPL Publication 05-X; http://jpldataeval.jpl.nasa.gov, Jet Propulsion Laboratory: 2005.

(3) Atkinson, R.; Baulch, D. L.; Cox, R. A.; Crowley, J. N.; Hampson, R. F.; Hynes, R. G.; Jenkin, M. E.; Rossi, M. J.; Troe, J. *Atmos. Chem. Phys.* **2004**, *4*, 1461.

(4) Danckwerts, P. V. *Trans. Faraday Soc.* **1951**, *47*, 1014.

(5) Sherwood, T. K.; Pigford, R. L.; White, C. R. *Mass Transfer*; McGraw-Hill: New York, 1975.

(6) Chameides, W. L. *J. Geophys. Res.* **1984**, *89*, 4739.

(7) Kolb, C. E.; Worsnop, D. R.; Zahniser, M. S.; Davidovits, P.; Keyser, L. F.; Leu, M.-T.; Molina, M. J.; Hanson, D. R.; Ravishankara, A. R.; Williams, L. R.; Tolbert, M. A. In *Progress and Problems in Atmospheric Chemistry*; Barker, J. R., Ed.; World Scientific Publishing Co.: 1995.

(8) Molina, M. J.; Molina, L. T.; Kolb, C. E. *Annu. Rev. Phys. Chem.* **1996**, *47*, 327.

(9) Kolb, C. E.; Davidovits, P.; Jayne, J. T.; Shi, Q.; Worsnop, D. R. *Prog. React. Kinet. Mech.* **2002**, *27*, 1.

(10) Fogg, P. G. T.; Sangster, J. M. *Chemicals in the Atmosphere: Solubility, Sources and Reactivity*; John Wiley & Sons: London, U.K., 2003.

(11) Reid, J. P.; Sayer, R. M. *Chem. Soc. Rev.* **2003**, *32*, 70.

(12) Nathanson, G. M.; Davidovits, P.; Worsnop, D. R.; Kolb, C. E. *J. Phys. Chem.* **1996**, *100*, 13007.

(13) (a) Fogg, P. G. T. In *Chemicals in the Atmosphere: Solubility, Sources and Reactivity*; Fogg, P. G. T., Sangster, J. M., Eds.; John Wiley & Sons: London, U.K., 2003. (b) Kolb, C. E.; Cox, R. A.; Abbatt, J. P. D.; Ammann, M.; Davis, E. J.; Donaldson, D. J.; Garrett, B. C.; George, C.; Griffiths, P. T.; Hanson, D. R.; Kulmala, M.; McFiggans, G.; Pöschl, U.; Riipinen, I.; Rossi, M. J.; Rudich, Y.; Wagner, P. E.; Winkler, P. M.; Worsnop, D. R.; O'Dowd, C. D. *Atmos. Chem. Phys.* **2010**, *10*, 10561. (c) NASA: Chemical Kinetics and Photochemical Data for Use in Atmospheric Studies, JPL Publication No. 06-2; http://jpldataeval.jpl.nasa.gov/; Jet Propulsion Laboratory, National Aeronautics and Space Administration: Pasadena, CA, 2006.

(14) *Gas Transfer at Water Surfaces*; Donelan, M. A., Drennan, W. M., Saltzman, E. S., Wanninkhof, R., Eds.; Caplus: 2002; Vol. 127.

(15) (a) Rudich, Y. *Chem. Rev.* **2003**, *103*, 5097. (b) Garrett, B. C.; Schenter, G. K.; Morita, A. *Chem. Rev.* **2006**, *106*, 1355.

(16) Danckwerts, P. V. *Gas—liquid reactions*; McGraw-Hill: New York, 1970.
(17) Schwartz, S. E. In *Chemistry of Multiphase Atmospheric Systems*; Jaeschke, W., Ed.; NATO: Brussels, 1986; Vol. G6.
(18) Worsnop, D. R.; Zahniser, M. S.; Kolb, C. E.; Gardner, J. A.; Watson, L. R.; Doren, J. M. V.; Jayne, J. T.; Davidovits, P. *J. Phys. Chem.* **1989**, *93*, 1159.
(19) Shi, Q.; Davidovits, P.; Jayne, J. T.; Worsnop, D. R.; Kolb, C. E. *J. Phys. Chem. A* **1999**, *103*, 8812.
(20) Hanson, D. R.; Ravishankara, A. R. *J. Phys. Chem.* **1993**, *97*, 12309.
(21) Fuchs, N. A.; Sutugin, A. G. *Highly Dispersed Aerosols*; Ann Arbor Science Publishers: Newton, MA, 1970.
(22) Widmann, J. F.; Davis, E. J. *J. Aerosol Sci.* **1997**, *28*, 87.
(23) Hanson, D. R.; Ravishankara, A. R.; Lovejoy, E. R. *J. Geophys. Res.* **1996**, *101*, 9063.
(24) Pöschl, U.; Rudich, Y.; Ammann, M. *Atmos. Chem. Phys. Discuss.* **2007**, *7*, 5989.
(25) Jayne, J. T.; Duan, S. X.; Davidovits, P.; Worsnop, D. R.; Zahniser, M. S.; Kolb, C. E. *J. Phys. Chem.* **1991**, *95*, 6329.
(26) Hanson, D. R. *J. Phys. Chem. B* **1997**, *101*, 4998.
(27) Worsnop, D. R.; Morris, J.; Shi, Q.; Davidovits, P.; Kolb, C. E. *Geophys. Res. Lett.* **2002**, *29*, 10.1029/2002GL015542.
(28) Hanson, D. R.; Lovejoy, E. R. *Science* **1995**, *267*, 1326.
(29) Smith, G. D.; Woods, E. I.; DeForest, C. L.; Baer, T.; Miller, R. E. *J. Phys. Chem.* **2002**, *106*, 8085.
(30) Hu, J. H.; Shi, Q.; Davidovits, P.; Worsnop, D. R.; Zahniser, M. S.; Kolb, C. E. *J. Phys. Chem.* **1995**, *99*, 8768.
(31) Hanson, D. R.; Ravishankara, A. R. *J. Phys. Chem.* **1994**, *98*, 5728.
(32) Boniface, J.; Shi, Q.; Li, Y. Q.; Cheung, J. L.; Rattigan, O. V.; Davidovits, P.; Worsnop, D. R.; Jayne, J. T.; Kolb, C. E. *J. Phys. Chem. A* **2000**, *104*, 7502.
(33) Knipping, E. M.; Lakin, M. J.; Foster, K. L.; Jungwirth, P.; Tobias, D. J.; Gerber, R. B.; Dabdub, D.; Finlayson-Pitts, B. J. *Science* **2000**, *288*, 301.
(34) Shi, Q.; Li, Y. Q.; Davidovits, P.; Jayne, J. T.; Worsnop, D. R.; Mozurkewich, M.; Kolb, C. E. *J. Phys. Chem. B* **1999**, *103*, 2417.
(35) Ammann, M.; Pöschl, U. *Atmos. Chem. Phys.* **2007**, 6025.
(36) Worsnop, D. R.; Shi, Q.; Jayne, J. T.; Kolb, C. E.; Swartz, E.; Davidovits, P. *J. Aerosol Sci.* **2001**, *32*, 877.
(37) Morita, A.; Sugiyama, M.; Koda, S. *J. Phys. Chem. A* **2003**, *107*, 1749.
(38) Worsnop, D. R.; Williams, L. R.; Kolb, C. E.; Mozurkewich, M.; Gershenzon, M.; Davidovits, P. *J. Phys. Chem. A* **2004**, *108*, 8542.
(39) Morita, A.; Sugiyama, M.; Kameda, H.; Koda, S.; Hanson, D. R. *J. Phys. Chem. B* **2004**, *108*, 9111.
(40) Davidovits, P.; Worsnop, D. R.; Williams, L. R.; Kolb, C. E.; Gershenzon, M. *J. Phys. Chem. B* **2005**, *109*, 14742.
(41) Morita, A.; Sugiyama, M.; Koda, S.; Hanson, D. R. *J. Phys. Chem. B* **2005**, *109*, 14747.
(42) Ponche, J. L.; George, C.; Mirabel, P. *J. Atmos. Chem.* **1993**, *16*, 1.
(43) Gatherer, R. D. B.; Reid, J. P. *Chem. Phys. Lett.* **2002**, *357*, 153.
(44) Gatherer, R. D. B.; Sayer, R. M.; Reid, J. P. *Chem. Phys. Lett.* **2002**, *366*, 34–41.
(45) Swartz, E.; Boniface, J.; Tchertkov, I.; Rattigan, O. V.; Robinson, D. V.; Davidovits, P.; Worsnop, D. R.; Jayne, J. T.; Kolb, C. E. *Environ. Sci. Technol.* **1997**, *31*, 2634.
(46) Shorter, J. A.; De Bruyn, W. J.; Hu, J. H.; Swartz, E.; Davidovits, P.; Worsnop, D. R.; Zahniser, M. S.; Kolb, C. E. *Environ. Sci. Technol.* **1995**, *29*, 1171.
(47) Nozière, B.; Riemer, D. D. *Atmos. Environ.* **2003**, *37*, 841.
(48) Betterton, E. A. *Atmos. Environ.* **1991**, *25A*, 1473.
(49) Utter, R. G.; Burkholder, J. B.; Howard, C. J.; Ravishankara, A. R. *J. Phys. Chem.* **1992**, *96*, 4973.
(50) Hanson, D. R.; Burkholder, J. B.; Howard, C. J.; Ravishankara, A. R. *J. Phys. Chem.* **1992**, *96*, 4979.
(51) Thornberry, T.; Abbatt, J. P. D. *Phys. Chem. Chem. Phys.* **2004**, *6*, 84.
(52) Lovejoy, E. R.; Huey, L. G.; Hanson, D. R. *J. Geophys. Res.* **1995**, *100*, 18775.
(53) (a) Brown, R. L. *J. Res. Natl. Bur. Stand.* **1978**, *83*, 1. (b) Davis, E. J. *J. Phys. Chem. A* **2008**, *112*, 1922.
(54) Golden, D. M.; Spokes, G. N.; Benson, S. W. *Angew. Chem., Int. Ed. Engl.* **1973**, *12*, 534.
(55) Fenter, F. F.; Caloz, F.; Rossi, M. J. *J. Phys. Chem.* **1994**, *98*, 9801.
(56) Iraci, L. T.; Tolbert, M. A. *J. Geophys. Res.* **1997**, *102*, 16099.
(57) Klassen, J. K.; Lynton, J.; Golden, D. M.; Williams, L. R. *J. Geophys. Res.* **1999**, *104*, 26355.
(58) Michelsen, R. R.; Ashbourn, S. F. M.; Iraci, L. T. *J. Geophys. Res.* **2004**, *109*, doi: 10.1029/2004JD005041.
(59) Lovejoy, E. R.; Hanson, D. R. *J. Phys. Chem.* **1995**, *99*, 2080.
(60) Kane, S. M.; Caloz, F.; Leu, M. T. *J. Phys. Chem. A* **2001**, *105*, 6465.
(61) Hu, J. H.; Abbatt, J. P. D. *J. Phys. Chem. A* **1997**, *101*, 871.
(62) Mozurkewich, M.; McMurry, P. H.; Gupta, A.; Calvert, J. G. *J. Geophys. Res.* **1987**, *92*, 4163.
(63) McMurry, P. H.; Takano, H.; Anderson, G. R. *Environ. Sci. Technol.* **1983**, *17*, 347.
(64) Morris, J. W.; Davidovits, P.; Jayne, J. T.; Jimenez, J. L.; Shi, Q.; Kolb, C. E.; Worsnop, D. R.; Barney, W. S.; Cass, G. R. *Geophys. Res. Lett.* **2002**, *29*, doi: 10.1029/2002GL014692.
(65) Tolocka, M. P.; Saul, T. D.; Johnston, M. V. *J. Phys. Chem. A* **2004**, *108*, 2659.
(66) Mentel, T. F.; Sohn, M.; Wahner, A. *Phys. Chem. Chem. Phys.* **1999**, *1*, 5451.
(67) Hunt, S. W.; Roeselová, M.; Wang, W.; Wingen, L. M.; Knipping, E. M.; Tobias, D. J.; Dabdub, D.; Finlayson-Pitts, B. J. *J. Phys. Chem. A* **2004**, *108*, 11559.
(68) Rudolf, R.; Vrtala, A.; Kulmala, M.; Vesala, T.; Viisanen, Y.; Wagner, P. E. *J. Aerosol Sci.* **2001**, *32*, 913.
(69) (a) Winkler, P.; Vrtala, A.; Wagner, P. E.; Kulmala, M.; Lehtinen, K. E. J.; Vesala, T. *Phys. Rev. Lett.* **2004**, *93*, doi: 10.1103/Phys.Rev.Lett93.075701. (b) Winkler, P. M.; Vrtala, A.; Rudolf, R.; Wagner, P. E.; Riipinen, I.; Vesala, T.; Lehitnen, K. E. J.; Viisanen, Y.; Kulmala, M. *J. Geophys. Res.* **2006**, *111*, D19202, doi: 10.1029/2006JD007194.
(70) Kirchner, W.; Welter, F.; Bongartz, A.; Kames, J.; Schweighoefer, S.; Schurath, U. *J. Atmos. Chem.* **1990**, *10*, 427.
(71) Bongartz, A.; Schweighoefer, S.; Roose, C.; Schurath, U. *J. Atmos. Chem.* **1995**, *20*, 35.
(72) Kondow, T.; Mafuné, F. *Annu. Rev. Phys. Chem.* **2000**, *51*, 731.
(73) Tang, I. N.; Munkelwitz, H. R. *J. Geophys. Res.* **1994**, *99*, 18801.
(74) Schwell, M.; Baumgärtel, H.; Weidinger, I.; Krämer, B.; Vortisch, H.; Wöste, L.; Leisner, T.; Rühl, E. *J. Phys. Chem. A* **2000**, *104*, 6726.
(75) Shaw, R. A.; Lamb, D. *J. Chem. Phys.* **1999**, *111*, 10659.
(76) King, M. D.; Thompson, K. C.; Ward, A. D. *J. Am. Chem. Soc.* **2004**, *126*, 16710.
(77) Schütze, M.; Herrmann, H. *Phys. Chem. Chem. Phys.* **2002**, *4*, 60.
(78) Schütze, M.; Herrmann, H. *Phys. Chem. Chem. Phys.* **2004**, *6*, 965.
(79) Shimono, A.; Koda, S. *J. Chem. Eng. Jpn.* **1995**, *28*, 779.
(80) (a) Takami, A.; Kato, S.; Shimono, A.; Koda, S. *Chem. Phys.* **1998**, *231*, 215. (b) Laskin, A.; Wang, H.; Robertson, W. H.; Cowin, J. P.; Ezell, M. J.; Finlayson-Pitts, B. J. *J. Phys. Chem. A* **2006**, *110*, 10619.
(81) (a) Nathanson, G. M. *Annu. Rev. Phys. Chem.* **2004**, *55*, 231. (b) Enami, S.; Vecitis, C. D.; Cheng, J.; Hoffmann, M. R.; Colussi, A. J. *J. Phys. Chem. A* **2007**, *111*, 13032. (c) Enami, S.; Vecitis, C. D.; Cheng, J.; Hoffmann, M. R.; Colussi, A. J. *J. Phys. Chem. A* **2007**, *111*, 8749. (d) Enami, S.; Hoffmann, M. R.; Colussi, A. J. *Proc. Natl. Acad. Sci. U. S. A.* **2008**, *105*, 7365. (e) Enami, S.; Hoffmann, M. R.; Colussi, A. J. *J. Phys. Chem. A* **2009**, *113*, 7002. (f) Enami, S.; Hoffmann, M. R.; Colussi, A. J. *J. Phys. Chem. Lett.* **2010**, *1*, 1599.

(82) Van Doren, J. M.; Watson, L. R.; Davidovits, P.; Worsnop, D. R.; Zahniser, M. S.; Kolb, C. E. *J. Phys. Chem.* **1990**, *94*, 3265.
(83) Schweitzer, F.; Mirabel, P.; George, C. *J. Phys. Chem. A* **2000**, *104*, 72.
(84) De Bruyn, W. J.; Shorter, J. A.; Davidovits, P.; Worsnop, D. R.; Zahniser, M. S.; Kolb, C. E. *J. Geophys. Res.* **1994**, *99*, 16927.
(85) Schweitzer, F.; Magi, L.; Mirabel, P.; George, C. *J. Phys. Chem. A* **1998**, *102*, 593.
(86) Katrib, Y.; Mirabel, P.; Le Calvé, S.; Weck, G.; Kochanski, E. *J. Phys. Chem. B* **2002**, *106*, 7237.
(87) Li, Y. Q.; Zhang, H. Z.; Davidovits, P.; Jayne, J. T.; Kolb, C. E.; Worsnop, D. R. *J. Phys. Chem. A* **2002**, *106*, 1220.
(88) Zhang, H. Z.; Li, Y. Q.; Xia, J.-R.; Davidovits, P.; Williams, L. R.; Jayne, J. T.; Kolb, C. E.; Worsnop, D. R. *J. Phys. Chem. A* **2003**, *107*, 6398.
(89) Carstens, T.; Wunderlich, C.; Schurath, U. In *Proceedings EUROTRAC Symposium '96*; Borrell, P. M., Cvitas, T., Kelly, K., Seiler, W., Eds.; Computational Mechanics: Southampton, U.K., 1996.
(90) Worsnop, D. R.; Williams, L. R.; Kolb, C. E.; Mozurkewich, M.; Gershenzon, M.; Davidovits, P. *J. Phys. Chem. A* **2004**, *108*, 8546.
(91) Schurath, U.; Bongartz, A.; Kames, J.; Wunderlich, C.; Carstens, T. In *Heterogeneous and Liquid-Phase Processes. Transport and Chemical Transformation of Pollutants in the Troposphere*; Warneck, P., Ed.; Springer-Verlag: Berlin, 1996.
(92) Shimono, A.; Koda, S. *J. Phys. Chem.* **1996**, *100*, 10.
(93) Heal, M. R.; Pilling, M. J.; Titcombe, P. E.; Whitaker, B. J. *Geophys. Res. Lett.* **1995**, *22*, 3043.
(94) Müller, M.; Heal, M. R. *J. Phys. Chem. A* **2002**, *106*, 5120.
(95) (a) Duan, S. X.; Jayne, J. T.; Davidovits, P.; Worsnop, D. R.; Zahniser, M. S.; Kolb, C. E. *J. Phys. Chem.* **1993**, *97*, 2284. (b) Diévart, P.; Allou, L.; Louis, F.; Le Calvé, S. *Phys. Chem. Chem. Phys.* **2006**, *8*, 1714.
(96) Guimbaud, C.; Arens, F.; Gutzwiller, L.; Gäggeler, H. W.; Ammann, M. *Atmos. Chem. Phys.* **2002**, *2*, 249.
(97) Marek, R.; Straub, J. *Int. J. Heat Mass Transfer* **2001**, *44*, 39.
(98) Mozurkewich, M. *Aerosol Sci. Technol.* **1986**, *5*, 223.
(99) Li, Y. Q.; Davidovits, P.; Shi, Q.; Jayne, J. T.; Kolb, C. E.; Worsnop, D. R. *J. Phys. Chem. A* **2001**, *105*, 10627.
(100) Davidovits, P.; Worsnop, D. R.; Jayne, J. T.; Kolb, C. E.; Winkle, P.; Vrtala, A.; Wagner, P. E.; Kulmala, M.; Lehtinen, K. E. J.; Vesala, T.; Mozurkewich, M. *Geophys. Res. Lett.* **2004**, *31*, L22111, doi: 10.1029/2004GRL020835.
(101) Laaksonen, A.; Vesala, T.; Kulmala, M.; Winkler, P. M.; Wagner, P. E. *Atmos. Chem. Phys.* **2005**, *5*, 461.
(102) (a) Cappa, D. C.; Drisdell, W.; Smith, J. D.; Saykally, R. J.; Cohen, R. C. *J. Phys. Chem. A* **2005**, *109*, 24391. (b) Smith, J. D.; Cappa, C. D.; Drisdell, W. S.; Cohen, R. C.; Saykally, R. J. *J. Am. Chem. Soc.* **2006**, *128*, 12892. (c) Drisdell, W. S.; Cappa, C. D.; Smith, J. D.; Saykally, R. J.; Cohen, R. C. *Atmos. Chem. Phys.* **2008**, *8*, 6699. (d) Drisdell, W. S.; Saykally, R. J.; Cohen, R. C. *Proc. Natl. Acad. Sci. U.S.A.* **2009**, *106*, 18897. (e) Cappa, C. D.; Smith, J. D.; Drisdell, W. S.; Saykally, R. J.; Cohen, R. C. *J. Phys. Chem. C* **2007**, *111*, 7011. (f) Voigtländer, J.; Stratmann, F.; Niedermeier, D.; Wex, H.; Kiselev, A. *J. Geophys. Res.* **2007**, *112*, D2028. (g) Zientara, M.; Jakubczyk, D.; Kolwas, K.; Kolwas, M. *J. Phys. Chem. A* **2008**, *112*, 5152. (h) Fukuta, N.; Myers, M. N. *J. Atmos. Sci.* **2007**, *64*, 955.
(103) Jayne, J. T.; Davidovits, P.; Worsnop, D. R.; Zahniser, M. S.; Kolb, C. E. *J. Phys. Chem.* **1990**, *94*, 6041.
(104) Jayne, J. T.; Duan, S. X.; Davidovits, P.; Worsnop, D. R.; Zahniser, M. S.; Kolb, C. E. *J. Phys. Chem.* **1992**, *96*, 5452.
(105) Jayne, J. T.; Worsnop, D. R.; Kolb, C. E.; Swartz, E.; Davidovits, P. *J. Phys. Chem.* **1996**, *100*, 8015.
(106) Kolb, C. E.; Jayne, J. T.; Worsnop, D. R.; Davidovits, P. *Pure Appl. Chem.* **1997**, *69*, 959.
(107) Katrib, Y.; Deiber, G.; Schweitzer, F.; Mirabel, P.; George, C. *J. Aerosol Sci.* **2001**, *32*, 893.
(108) Takami, A.; Kondo, T.; Kado, A.; Koda, S. *J. Atmos. Chem.* **2001**, *39*, 139.
(109) Magi, L.; Schweitzer, F.; Pallares, C.; Cherif, C.; Mirabel, P.; George, C. *J. Phys. Chem. A* **1997**, *101*, 4943.
(110) Müller, B.; Heal, M. R. *Phys. Chem. Chem. Phys.* **2002**, *4*, 3365.
(111) Deiber, G.; George, C.; Le Calve, S.; Schweitzer, F.; Mirabel, P. *Atmos. Chem. Phys.* **2004**, *4*, 1291.
(112) Wachsmuth, M.; Gäggeler, H. W.; von Glasow, R.; Ammann, M. *Atmos. Chem. Phys.* **2002**, *2*, 121.
(113) Liu, D.; Ma, G.; Levering, L.; Allen, H. C. *J. Phys. Chem. B* **2004**, *108*, 2252.
(114) Petersen, P. B.; Johnson, J. C.; Knutsen, K. P.; Saykally, R. J. *Chem. Phys. Lett.* **2004**, *397*, 46.
(115) (a) Ghosal, S.; Hemminger, J. C.; Bluhm, H.; Mun, B. S.; Hebenstreit, E. L. D.; Ketteler, G.; Ogletree, D. F.; Requejo, F. G.; Salmeron, M. *Science* **2005**, *307*, 563. (b) Jungwirth, P.; Tobias, D. J. *Chem. Rev.* **2006**, *106*, 1259. (c) Gopalakrishnan, S.; Liu, D. F.; Allen, H. C.; Kuo, M.; Shultz, M. J. *Chem. Rev.* **2006**, *106*, 1155. (d) Petersen, P. B.; Saykally, R. J. *Annu. Rev. Phys. Chem.* **2006**, *57*, 333. (e) Jungwirth, P.; Winter, B. *Annu. Rev. Phys. Chem.* **2008**, *59*, 343. (f) Allen, H. C.; Casillas-Ituarte, N. N.; Sierra-Hernández, M. R.; Chen, X.; Cheng, Y.; Tang, C. Y. *Phys. Chem. Chem. Phys.* **2009**, *11*, 5538.
(116) (a) Thornton, J.; Abbatt, J. P. D. *J. Geophys. Res.* **2005**, *110*, D0830910.1029/2004JD005402. (b) Taketani, F.; Kanaya, Y.; Akimoto, H. *J. Phys. Chem. A* **2008**, *112*, 2370. (c) Taketani, F.; Kanaya, Y.; Akimoto, H. *Atmos. Environ.* **2009**, *43*, 1660.
(117) Rudich, Y.; Talukdar, R. K.; Ravishankara, A. R.; Fox, R. W. *J. Geophys. Res.* **1996**, *101*, 21023.
(118) Schütze, M.; Herrmann, H. *Atmos. Chem.* **2005**, *52*, 1.
(119) Thomas, K.; Volz-Thomas, A.; Mihelcic, D.; Smit, H. G. T.; Kley, D. *Atmos. Chem.* **1998**, *292*, 17.
(120) (a) Van Doren, J. M.; Watson, L. R.; Davidovits, P.; Worsnop, D. R.; Zahniser, M. S.; Kolb, C. E. *J. Phys. Chem.* **1991**, *95*, 1684. (b) Guimbaud, C.; Arens, F.; Gutzwiller, L.; Gaggeler, H. W.; Ammann, M. *Atmos. Chem. Phys.* **2002**, *2*, 249. (c) Saul, T. D.; Tolocka, M. P.; Johnston, M. V. *J. Phys. Chem. A* **2006**, *110*, 7614.
(121) George, C.; Ponche, J. L.; Mirabel, P.; Behnke, W.; Sheer, V.; Zetzsch, C. *J. Phys. Chem.* **1994**, *98*, 8780.
(122) Schweitzer, F.; Mirabel, P.; George, C. *J. Phys. Chem. A* **1998**, *102*, 3942.
(123) Mozurkewich, M.; Calvert, J. *J. Geophys. Res.* **1988**, *93*, 15882.
(124) Thornton, J. A.; Abbatt, J. P. D. *J. Phys. Chem. A* **2005**, *109*, 10004.
(125) Wahner, A.; Mentel, T. F.; Sohn, M.; Stier, J. *J. Geophys. Res.* **1998**, *103*, 31103.
(126) Bongartz, A.; Kames, J.; Schurath, U.; George, C.; Mirabel, P.; Ponche, J. L. *J. Atmos. Chem.* **1994**, *18*, 149.
(127) Mertes, S.; Wahner, A. *J. Phys. Chem.* **1995**, *99*, 14000.
(128) Harrison, R. M.; Collins, G. M. *J. Atmos. Chem.* **1998**, *30*, 397.
(129) Rossi, M. J. *Chem. Rev.* **2003**, *103*, 4823.
(130) Behnke, W.; George, C.; Scheer, V.; Zetsch, C. *J. Geophys. Res.* **1997**, *102*, 3795.
(131) George, C.; Behnke, W.; Scheer, V.; Zetzsch, C.; Magi, L.; Ponche, J. L.; Mirabel, P. *Geophys. Res. Lett.* **1995**, *22*, 1505.
(132) Frenzel, A.; Scheer, V.; Sikorski, R.; George, C.; Behnke, W.; Zetsch, C. *J. Phys. Chem. A* **1998**, *102*, 1329.
(133) Schweitzer, F.; Mirabel, P.; George, C. *J. Atmos. Chem.* **1999**, *34*, 101.
(134) Scheer, V.; Frenzel, A.; Behnke, W.; Zetsch, C.; Magi, L.; George, C.; Mirabel, P. *J. Phys. Chem. A* **1997**, *101*, 9359.
(135) De Bruyn, W. J.; Duan, S. X.; Shi, X. Q.; Davidovits, P.; Worsnop, D. R.; Zahniser, M. S.; Kolb, C. E. *Geophys. Res. Lett.* **1992**, *19*, 1939.
(136) George, C.; Lagrange, J.; Lagrange, P.; Mirabel, P.; Pallares, C.; Ponche, J. L. *J. Geopyhs. Res.* **1994**, *99*, 1255.
(137) George, C.; Saison, J. Y.; Ponche, J. L.; Mirabel, P. *J. Phys. Chem.* **1994**, *98*, 10857.
(138) Robinson, G. N.; Worsnop, D. R.; Jayne, J. T.; Kolb, C. E.; Swartz, E.; Davidovits, P. *J. Geophys. Res.* **1998**, *103*, 25371.
(139) De Bruyn, W. J.; Shorter, J. A.; Davidovits, P.; Worsnop, D. R.; Zahniser, M. S.; Kolb, C. E. *Environ. Sci. Technol.* **1995**, *29*, 1179.
(140) Manogue, W.; Pigford, G. L. *AIChE J.* **1960**, *6*, 494.

(141) Mertens, R.; von Sonntag, C.; Lind, J.; Merenyi, G. *Angew. Chem., Int. Ed. Engl.* **1994**, *33*, 1259.
(142) Wild, O.; Rattigan, O.; Jones, R. L.; Pyle, J. A.; Cox, A. *J. Atmos. Chem.* **1996**, *25*, 167.
(143) Martin, J. W.; Maybury, S. A.; Wong, S. A.; Noventa, F.; Solomon, K. R.; Alaee, M.; Muir, D. C. G. *Environ. Sci. Technol.* **2003**, *37*, 2889.
(144) Watson, L. R.; Doren, J. M. V.; Davidovits, P.; Worsnop, D. R.; Zahniser, M. S.; Kolb, C. E. *J. Geophys. Res.* **1990**, *95*, 5631.
(145) Hanson, D. R.; Lovejoy, E. R. *J. Phys. Chem.* **1996**, *100*, 6397.
(146) Shi, Q.; Jayne, J. T.; Kolb, C. E.; Worsnop, D. R.; Davidovits, P. *J. Geophys. Res.* **2001**, *106*, 24259.
(147) Robinson, G. N.; Worsnop, D. R.; Jayne, J. T.; Kolb, C. E.; Davidovits, P. *J. Geophys. Res.* **1997**, *102*, 3583.
(148) Wagner, R.; Naumann, K.-H.; Mangold, A.; Möhler, O.; Saathoff, H.; Schurath, U. *J. Phys. Chem. A* **2005**, *109*, 8140.
(149) Hanson, D. R.; Ravishankara, A. R. *Geophys. Res. Lett.* **1995**, *22*, 385.
(150) Hanson, D. R. *J. Geophys. Res.* **2003**, *108*, doi: 10.1029/2002JD002519.
(151) Waschewsky, G. C. G.; Abbatt, J. P. D. *J. Phys. Chem.* **1999**, *103*, 5312.
(152) Robbins, R. C.; Cadle, R. D. *J. Phys. Chem.* **1958**, *62*, 469.
(153) Huntzicker, J. J.; Cary, R. A.; Ling, C.-S. *Environ. Sci. Technol.* **1980**, *14*, 819.
(154) Daumer, B.; Nissner, R.; Klockow, D. *J. Aerosol Sci.* **1992**, *23*, 315.
(155) Hanson, D. R.; Kosciuch, E. *J. Phys. Chem. A* **2003**, *107*, 2199.
(156) Swartz, E.; Shi, Q.; Davidovits, P.; Jayne, J. T.; Worsnop, D. R.; Kolb, C. E. *J. Phys. Chem. A* **1999**, *103*, 8824.
(157) Hanson, D. R.; Kosciuch, E. *J. Phys. Chem. A* **2004**, *108*, 8549.
(158) Gershenzon, M.; Davidovits, P.; Williams, L. R.; Shi, Q.; Jayne, J. T.; Kolb, C. E.; Worsnop, D. R. *J. Phys. Chem. A* **2004**, *108*, 1567.
(159) Pöschl, U.; Canagaratna, M.; Jayne, J. T.; Molina, L. T.; Worsnop, D. R.; Kolb, C. E.; Molina, M. J. *J. Phys. Chem. A* **1998**, *102*, 10082.
(160) Hanson, D. R. *J. Phys. Chem. A* **2005**, *109*, 6919.
(161) Jefferson, A.; Eisele, F. L.; Ziemann, P. J.; Weber, R. J.; Marti, J. J.; McMurry, P. H. *J. Geophys. Res.* **1997**, *102*, 19021.
(162) Van Dingenen, R.; Raes, F. *Aerosol Sci. Technol.* **1991**, *15*, 93.
(163) Jayne, J. T.; Pöschl, U.; Chen, Y.; Dai, D.; Molina, L. T.; Worsnop, D. R.; Kolb, C. E.; Molina, M. J. *J. Phys. Chem. A* **1997**, *101*, 10000.
(164) Tolbert, M. A.; Praff, J.; Jayaweera, I.; Prather, M. J. *J. Geophys. Res.* **1993**, *98*, 2957.
(165) Cooper, P. L.; Abbatt, J. P. D. *J. Phys. Chem.* **1996**, *100*, 2249.
(166) Gershenzon, Y. M.; Ivanov, A. V.; Kucheryavyi, S. I.; Rozenshtein, V. B. *Kinet. Katal.* **1986**, *27*, 1069.
(167) Gershenzon, Y. M.; Grigorieva, V. M.; Ivanov, A. V.; Remorov, R. G. *Faraday Discuss.* **1995**, *100*, 83.
(168) Martin, L. R.; Judeikis, H. S.; Wun, M. *J. Geophys. Res.* **1980**, *85*, 5511.
(169) Abbatt, J. P. D. *Geophys. Res. Lett.* **1996**, *23*, 1681.
(170) Jayne, J. T.; Gardner, J. A.; Davidovits, P.; Worsnop, D. R.; Zahniser, M. S.; Kolb, C. E. *J. Geophys. Res.* **1990**, *95*, 20559.
(171) Donaldson, D. J.; Guest, J. A.; Goh, M. C. *J. Phys. Chem.* **1995**, *99*, 9313.
(172) (a) Petersen, M. K.; Iyengar, S. S.; Day, T. J. F.; Voth, G. A. *J. Phys. Chem. B* **2004**, *108*, 14804. (b) Buch, V.; Milet, A.; Vacha, R.; Jungwirth, P.; Devlin, J. P. *Proc. Natl. Acad. Sci. U.S.A.* **2007**, *104*, 7342. (c) Iuchi, S.; Chen, H.; Francesco, P.; Voth, G. A. *J. Phys. Chem. B* **2009**, *113*, 4017.
(173) Jungwirth, P.; Tobias, D. J. *J. Phys. Chem. B* **2002**, *106*, 6361.
(174) Dang, L. X.; Chang, T. M. *J. Phys. Chem. B* **2002**, *106*, 235.
(175) Hanson, D. R.; Sugiyama, M.; Morita, A. *J. Phys. Chem. A* **2004**, *108*, 3739.
(176) Kolb, C. E.; Worsnop, D. R.; Zahniser, M. S.; Davidovits, P. *J. Geophys. Res.* **1996**, *101*, 23039.
(177) Yamaguchi, S.; Kudoh, S.; Okada, Y.; Orii, T.; Takeuchi, K. *Chem. Phys. Lett.* **2002**, *359*, 480.
(178) Saxena, P.; Hildemann, L. M. *J. Atmos. Chem.* **1996**, *24*, 57.
(179) Jacobson, M. C.; Hansson, K. J.; Charlson, R. J. *Rev. Geophys.* **2000**, *38*, 267.
(180) Novakov, T.; Penner, J. E. *Nature* **1993**, *365*, 823.
(181) Rudich, Y.; Benjamin, I.; Naaman, R.; Thomas, E.; Trakhtenberg, S.; Ussyshkin, R. *J. Phys. Chem. A* **2000**, *104*, 5238.
(182) Demou, E.; Visram, H.; Donaldson, D. J.; Mazkar, P. A. *Atmos. Environ.* **2003**, *37*, 3529.
(183) Asad, A.; Mmereki, B. T.; Donaldson, D. J. *Atmos. Chem. Phys.* **2004**, *4*, 2083.
(184) Prenni, A. J.; DeMott, P. J.; Kreidenweis, S. M.; Sherman, D. E.; Russell, L. M.; Ming, Y. *J. Phys. Chem. A* **2001**, *105*, 11240.
(185) Kumar, P. P.; Broekhuizen, K.; Abbatt, J. P. D. *Atmos. Chem. Phys.* **2003**, *3*, 509.
(186) Raymond, T. M.; Pandis, S. N. *J. Geophys. Res.* **2002**, *107*, 4787, doi: 10.1029/2002JD002159.
(187) Broekhuizen, K. E.; Thornberry, T.; Kumar, P. P.; Abbatt, J. P. D. *J. Geophys. Res.* **2004**, *109*, doi: 10.1029/2004JD005298.
(188) Turpin, B. J.; Saxena, P.; Andrews, E. *Atmos. Environ.* **2000**, *34*, 2983.
(189) Moise, T.; Rudich, Y. *J. Geophys. Res.* **2000**, *105*, 14667.
(190) Zhang, H. Z.; Li, Y. Q.; Xia, J.-R.; Davidovits, P.; Williams, L. R.; Jayne, J. T.; Kolb, C. E.; Worsnop, D. R. *J. Phys. Chem. A* **2003**, *107*, 6388.
(191) Zhang, H. Z.; Davidovits, P.; Williams, L. R.; Jayne, J. T.; Kolb, C. E.; Worsnop, D. R. *J. Phys. Chem. A* **2005**, *109*, 3941.
(192) Gill, P. S.; Graedel, T. E.; Weschler, C. J. *Rev. Geophys.* **1983**, *21*, 903.
(193) Ellison, G. B.; Tuck, A. F.; Vaida, V. *J. Geophys. Res.* **1999**, *104*, 11633.
(194) Rubel, G. O.; Gentry, J. W. *J. Phys. Chem.* **1984**, *88*, 3142.
(195) Rubel, G. O.; Gentry, J. W. *J. Aerosol Sci.* **1984**, *15*, 661.
(196) Lawrence, J. R.; Glass, S. V.; Nathanson, G. M. *J. Phys. Chem. A* **2005**, *109*, 7449.
(197) Lawrence, J. R.; Glass, S. V.; Park, S.-C.; Nathanson, G. M. *J. Phys. Chem. A* **2005**, *109*, 7458.
(198) Mmereki, B. T.; Chaudhuri, S. R.; Donaldson, D. J. *J. Phys. Chem. A* **2003**, *107*, 2264.
(199) Mmereki, B. T.; Donaldson, D. J. *J. Phys. Chem. A* **2003**, *107*, 11038.
(200) Mmereki, B. T.; Donaldson, D. J.; Gilman, J. B.; Eliason, T. L.; Vaida, V. *Atmos. Environ.* **2004**, *38*, 6091.
(201) Donaldson, D. J.; Mmereki, B. T.; Chaudhuri, S. R.; Handley, S.; Oh, M. *Faraday Discuss.* **2005**, *130*, 227.
(202) (a) Raja, S.; Valsaraj, K. T. *J. Air Waste Manage. Assoc.* **2005**, *55*, 1345. (b) Donaldson, D. J.; Vaida, V. *Chem. Rev.* **2006**, *106*, 1445. (c) Donaldson, D. J.; Valsaraj, K. T. *Environ. Sci. Technol.* **2010**, *44*, 865. (d) Buajarern, J.; Mitchem, L. P.; Reid, J. P. *J. Phys. Chem. A* **2007**, *111*, 9054. (e) Badger, C. L.; George, I.; Griffiths, P. T.; Abbatt, J. P. D.; Cox, R. A. *J. Phys. Chem. A* **2006**, *110*, 6986. (f) McNeill, V. F.; Patterson, J.; Wolfe, G. M.; Thornton, J. A. *Atmos. Chem. Phys.* **2006**, *6*, 1635. (g) Park, S.-C.; Burden, D. K.; Nathanson, G. M. *J. Phys. Chem. A* **2007**, *111*, 2921. (h) Clifford, D.; Bartels-Rausch, T.; Donaldson, D. J. *Phys. Chem. Chem. Phys.* **2007**, *9*, 1362. (i) Ardura, D.; Donaldson, D. J. *Phys. Chem. Chem. Phys.* **2009**, *11*, 857.
(203) Davidovits, P.; Jayne, J. T.; Duan, S. X.; Worsnop, D. R.; Zahniser, M. S.; Kolb, C. E. *J. Phys. Chem.* **1991**, *95*, 6337.
(204) Pollack, G. L. *Science* **1991**, *251*, 1323.
(205) Davidovits, P.; Hu, J. H.; Worsnop, D. R.; Zahniser, M. S.; Kolb, C. E. *Faraday Discuss.* **1995**, *100*, 65.
(206) Braslau, A.; Deutsch, M.; Pershan, P. S.; Weiss, A. H.; Als-Nielsen, J.; Bohr, J. *Phys. Rev. Lett.* **1985**, *54*, 114.
(207) Braslau, A.; Pershan, P. S.; Swislow, G.; Ocko, B. M.; Als-Nielsen, J. *Phys. Rev. A* **1988**, *38*, 2457.
(208) Daillant, J.; Mora, S.; Fradin, C.; Alba, M.; Braslau, A.; Luzet, D. *Appl. Surf. Sci.* **2001**, *182*, 223.

(209) Mora, S.; Daillant, J.; Mecke, K.; Luzet, D.; Braslau, A.; Alba, M.; Struth, B. *Phys. Rev. Lett.* **2003**, *90*, 216101/1.
(210) Matsumoto, M.; Kataoka, Y. *J. Chem. Phys.* **1988**, *88*, 3233.
(211) Wilson, M. A.; Pohorille, A.; Pratt, L. R. *J. Phys. Chem.* **1987**, *91*, 4873.
(212) Townsend, R. M.; Rice, S. A. *J. Chem. Phys.* **1991**, *94*, 2207.
(213) Besseling, N. A. M.; Lyklema, J. *J. Phys. Chem.* **1994**, *98*, 11610.
(214) Taylor, R. S.; Dang, L. X.; Garrett, B. C. *J. Phys. Chem.* **1996**, *100*, 11720.
(215) Somasundaram, T.; Lynden-Bell, R. M.; Patterson, C. H. *Phys. Chem. Chem. Phys.* **1999**, *1*, 143.
(216) Du, Q.; Freysz, E.; Shen, Y. R. *Science* **1994**, *264*, 826.
(217) Wilson, K. R.; Rude, B. S.; Catalano, T.; Schaller, R. D.; Tobin, J. G.; Co, D. T.; Saykally, R. J. *J. Phys. Chem. B* **2001**, *105*, 3346.
(218) Liu, P.; Harder, E.; Berne, B. J. *J. Phys. Chem. B* **2005**, *109*, 2949.
(219) Donaldson, D. J. *J. Phys. Chem. A* **1999**, *103*, 62.
(220) Donaldson, D. J.; Anderson, D. *J. Phys. Chem. A* **1999**, *103*, 871.
(221) Mmereki, B. T.; Hicks, J. M.; Donaldson, D. J. *J. Phys. Chem. A* **2000**, *104*, 10789.
(222) Dabkowski, J.; Zargorska, L.; Dabkowska, M.; Koczorowski, Z.; Trasatti, S. *J. Chem. Soc., Faraday Trans.* **1996**, *92*, 3873.
(223) Karpovich, D. S.; Ray, D. *J. Phys. Chem. B* **1998**, *102*, 649.
(224) Allen, H. C.; Gragson, D. E.; Richmond, G. L. *J. Phys. Chem. B* **1999**, *103*, 660.
(225) Allen, H. C.; Raymond, E. A.; Richmond, G. L. *J. Phys. Chem. B* **2001**, *105*, 660.
(226) Remorov, R. G.; Bardwell, M. W. *Surf. Sci.* **2005**, *585*, 59.
(227) Buff, F. P.; Lovett, R. A.; Stillinger, R. H. *Phys. Rev. Lett.* **1965**, *15*, 621.
(228) Knox, C. J. H.; Phillips, L. F. *J. Phys. Chem. B* **1998**, *102*, 8469.
(229) Phillips, L. F. *Acc. Chem. Res.* **2004**, *37*, 982.
(230) Phillips, L. F. *J. Phys. Chem. B* **2004**, *108*, 1986.
(231) Phillips, L. F. *Chem. Phys. Lett.* **1997**, *266*, 161.
(232) Phillips, L. F. *Chem. Phys. Lett.* **2005**, *407*, 249.
(233) Wilson, M. A.; Pohorille, A. *J. Phys. Chem. B* **1997**, *101*, 3130.
(234) (a) Taylor, R. S.; Garrett, B. C. *J. Phys. Chem. B* **1999**, *103*, 844. (b) Canneaux, S.; Soetens, J. C.; Henon, E.; Bohr, F. *Chem. Phys.* **2006**, *327*, 512.
(235) Ishiyama, T.; Takeru, Y.; Fujikawa, S. *Phys. Fluids* **2004**, *16*, 4714.
(236) Tsuruta, T.; Nagayama, G. *J. Phys. Chem. B* **2004**, *108*, 1736.
(237) Vieceli, J.; Roeselová, M.; Tobias, D. J. *Chem. Phys. Lett.* **2004**, *393*, 249.
(238) Vieceli, J.; Roeselová, M.; Potter, N.; Dang, L. X.; Garrett, B. C.; Tobias, D. J. *J. Phys. Chem. B* **2005**, *109*, 15876.
(239) Morita, A.; Kanaya, Y.; Francisco, J. S. *J. Geophys. Res.* **2004**, *109*, D09201/1.
(240) Roeselová, M.; Jungwirth, P.; Tobias, D. J.; Gerber, R. B. *J. Phys. Chem. B* **2003**, *107*, 12690.
(241) Roeselová, M.; Vieceli, J.; Dang, L. X.; Garrett, B. C.; Tobias, D. J. *J. Am. Chem. Soc.* **2004**, *126*, 16308.
(242) Kathmann, S. M.; Schenter, G. K.; Garrett, B. C. *J. Chem. Phys.* **2002**, *116*, 5046.
(243) Dang, L. X.; Chang, T. M. *J. Chem. Phys.* **1997**, *106*, 8149.
(244) Jorgensen, W. L.; Chandrasekhar, J.; Madura, J. D.; Impey, R. W.; Klein, M. L. *J. Chem. Phys.* **1983**, *79*, 926.
(245) Merikanto, J.; Vehkamaki, H.; Zapadinsky, E. *J. Chem. Phys.* **2004**, *121*, 914.
(246) Wernet, P.; Nordlund, D.; Bergmann, U.; Cavalleri, M.; Odelius, M.; Ogasawara, H.; Naslund, L. A.; Hirsch, T. K.; Ojamae, L.; Glatzel, P.; Pettersson, L. G. M.; Nilsson, A. *Science* **2004**, *304*, 995.
(247) Zubavicus, Y.; Grunze, M. *Science* **2004**, *304*, 974.
(248) Wilson, K. R.; Schaller, R. D.; Co, D. T.; Saykally, R. J.; Rude, B. S.; Catalano, T.; Bozek, J. D. *J. Chem. Phys.* **2002**, *117*, 7738.
(249) Wilson, K. R.; Cavalleri, M.; Rude, B. S.; Schaller, R. D.; Nilsson, A.; Pettersson, L. G. M.; Goldman, N.; Catalano, T.; Bozek, J. D.; Saykally, R. J. *J. Phys.: Condens. Matter* **2002**, *14*, L221.
(250) Raymond, E. A.; Tarbuck, T. L.; Brown, M. G.; Richmond, G. L. *J. Phys. Chem. B* **2003**, *107*, 546.
(251) Wilson, K. R.; Rude, B. S.; Smith, J.; Cappa, C.; Co, D. T.; Schaller, R. D.; Larsson, M.; Catalano, T.; Saykally, R. J. *Rev. Sci. Instrum.* **2004**, *75*, 725.
(252) Morita, A.; Hynes, J. T. *J. Phys. Chem. B* **2002**, *106*, 673.
(253) Phillips, L. F. *J. Phys. Chem. B* **2000**, *104*, 2534.
(254) Carignano, M. A.; Jacob, M. M.; Avila, E. E. *J. Phys. Chem. A* **2008**, *112*, 3676.
(255) Wilson, E. K. *C&EN News* **2010**, *88*, 35.
(256) Beattie, J. K.; Djerdjev, A. M.; Warr, G. G. *Faraday Discuss.* **2009**, *141*, 31.